Title

Arabian Sea Monsoon: Deep sea drilling in the Arabian Sea: Constraining tectonic-monsoon interactions in South Asia

Authors

Pandey, DK
Clift, PD
Kulhanek, DK
et al.

Publication Date

2015-07-01

Peer reviewed

International Ocean Discovery Program Expedition 355 Preliminary Report

Arabian Sea Monsoon

Deep sea drilling in the Arabian Sea: constraining tectonic-monsoon interactions in South Asia

31 March–31 May 2015

D.K. Pandey, P.D. Clift, D.K. Kulhanek, S. Andò, J.A.P. Bendle, S. Bratenkov, E.M. Griffith, G.P. Gurumurthy, A. Hahn, M. Iwai, B.-K. Khim, A. Kumar, A.G. Kumar, H.M. Liddy, H. Lu., M.W. Lyle, R. Mishra, T. Radhakrishna, C.M. Routledge, R. Saraswat, R. Saxena, G. Scardia, G.K. Sharma, A.D. Singh, S. Steinke, K. Suzuki, L. Tauxe, M. Tiwari, Z. Xu, and Z. Yu

IODP
INTERNATIONAL OCEAN DISCOVERY PROGRAM

Publisher's notes

Core samples and the wider set of data from the science program covered in this report are under moratorium and accessible only to Science Party members until 29 August 2016.

This publication was prepared by the International Ocean Discovery Program *JOIDES Resolution* Science Operator (IODP JRSO) as an account of work performed under the International Ocean Discovery Program. Funding for the program is provided by the following implementing organizations and international partners:

National Science Foundation (NSF), United States
Ministry of Education, Culture, Sports, Science and Technology (MEXT), Japan
European Consortium for Ocean Research Drilling (ECORD)
Ministry of Science and Technology (MOST), People's Republic of China
Korea Institute of Geoscience and Mineral Resources (KIGAM)
Australia-New Zealand IODP Consortium (ANZIC)
Ministry of Earth Sciences (MoES), India
Coordination for Improvement of Higher Education Personnel (CAPES), Brazil

Disclaimer

Any opinions, findings, and conclusions or recommendations expressed in this publication are those of the author(s) and do not necessarily reflect the views of the participating agencies, Texas A&M University, or Texas A&M Research Foundation.

Portions of this work may have been published in whole or in part in other International Ocean Discovery Program documents or publications.

Copyright

Citation:

Pandey, D.K., Clift, P.D., Kulhanek, D.K., Andò, S., Bendle, J.A.P., Bratenkov, S., Griffith, E.M., Gurumurthy, G.P., Hahn, A., Iwai, M., Khim, B.-K., Kumar, A., Kumar, A.G., Liddy, H.M., Lu., H., Lyle, M.W., Mishra, R., Radhakrishna, T., Routledge, C.M., Saraswat, R., Saxena, R., Scardia, G., Sharma, G.K., Singh, A.D., Steinke, S., Suzuki, K., Tauxe, L., Tiwari, M., Xu, Z., and Yu, Z., 2015. *Expedition 355 Preliminary Report: Arabian Sea Monsoon.* International Ocean Discovery Program. http://dx.doi.org/10.14379/iodp.pr.355.2015

ISSN

World Wide Web: 2372-9562

July 2015

Expedition 355 participants

Expedition 355 scientists

Dhananjai K. Pandey
Co-Chief Scientist
Department of Marine Geophysics
National Centre for Antarctic and Ocean Research (NCAOR)
Vasco da Gama
Goa 403804
India
dhananjai@gmail.com

Peter D. Clift
Co-Chief Scientist
Department of Geology and Geophysics
Louisiana State University
E253 Howe-Russell-Kniffen Geoscience Complex
Baton Rouge LA 70803
USA
pclift@lsu.edu

Denise K. Kulhanek
Expedition Project Manager/ Staff Scientist
International Ocean Discovery Program
Texas A&M University
1000 Discovery Drive
College Station TX 77845
USA
kulhanek@iodp.tamu.edu

Sergio Andò
Sedimentologist
Department of Earth and Environmental Sciences
University of Milano Bicocca
Piazza della Scienza 4
20126 Milan
Italy
sergio.ando@unimib.it

James A.P. Bendle
Organic Geochemist
School of Geography, Earth and Environmental Sciences
University of Birmingham
Edgbaston
Birmingham B15 2TT
United Kingdom
j.bendle@bham.ac.uk

Sophia Bratenkov
Organic Geochemist
Department of Earth and Planetary Sciences
Faculty of Science and Engineering
Macquarie University
Level 2, The Australian Hearing Hub
16 University Avenue
Sydney NSW 2109
Australia
sophia.aharonovich@gmail.com

Elizabeth M. Griffith
Downhole Measurements/Physical Properties Specialist
Department of Earth and Environmental Sciences
University of Texas at Arlington
Geosciences Building, Room 107
500 Yates Street
Arlington TX 76019
USA
lgriff@uta.edu

Gundiga P. Gurumurthy
Inorganic Geochemist
Manipal Centre for Natural Sciences
Manipal University
Dr. T.M.A. Pai Planetarium Building
Manipal 576104
India
gurumurthy.gp@manipal.edu

Annette Hahn
Physical Properties Specialist
MARUM
University of Bremen
Leobener Strasse
28359 Bremen
Germany
ahahn@marum.de

Masao Iwai
Paleontologist (diatoms)
Department of Natural Science
Faculty of Science
Kochi University
2-5-1 Akebono-cho
Kochi 780-8520
Japan
iwaim@kochi-u.ac.jp

Boo-Keun Khim
Sedimentologist
Departmnet of Oceanography
Pusan National University
63 Beongil 2, Busandaehag-ro
Busan 609-735
Republic of Korea
bkkhim@pusan.ac.kr

Anil Kumar
Sedimentologist
Department of Science and Technology
Wadia Institute of Himalayan Geology, Dehradun
33 GMS Road, Dehradun
Uttrakhand 248001
India
anilgeo@wihg.res.in

A. Ganesh Kumar
Microbiologist
Marine Biotechnology Department
National Institute of Ocean Technology
Velachery-Tambaram Main Road
Pallikaranai, Chennai 600100
India
microganesh@yahoo.com

Hannah M. Liddy
Organic Geochemist
Department of Earth Sciences
University of Southern California
3651 Trousdale Parkway
Los Angeles CA 90089
USA
liddy@usc.edu

Huayu Lu
Sedimentologist
School of Geographical and Oceanographical Sciences
Nanjing University
163 Xianlin Avenue
Nanjing 210023
China
huayulu@nju.edu.cn

Mitchell W. Lyle
Sedimentologist/Stratigraphic Correlator
College of Earth, Ocean and Atmospheric Sciences
Oregon State University
104 CEOAS Adiministration Building
Corvallis OR 97331
USA
mlyle@coas.oregonstate.edu

Ravi Mishra
Sedimentologist
IODP-India
National Centre for Antarctic and Ocean Research (NCAOR)
Vasco da Gama
Goa 403804
India
ravismishra@rediffmail.com

Tallavajhala Radhakrishna
Paleomagnetist/Petrologist
Geosciences Division
National Centre for Earth Science Studies
Aakkulam Trivandrum 695031
India
tradha1@rediffmail.com

Claire M. Routledge
Paleontologist (nannofossils)
Department of Earth, Ocean and Atmospheric Sciences
Florida State University
Carraway Building
909 Antarctic Way
Tallahassee FL 32306
USA
cmrouty@gmail.com

Rajeev Saraswat
Physical Properties Specialist
Geological Oceanography Division
National Institute of Oceanography
Dona Paula
Goa 403004
India
rsaraswat@nio.org

Rakesh Saxena
Downhole Measurements/Physical Properties Specialist
ONGC
11 High, Bandra-Sion Link Road
Mumbai 400017
India
saxena_rakesh@ongc.co.in

Giancarlo Scardia
Paleomagnetist/Stratigraphic Correlator
Instituto de Geociências e Ciências Exatas
Universidade Estadual Paulista
1515 Avenida 24-A
Rio Claro SP 13506-900
Brazil
scardia@rc.unesp.br

Girish K. Sharma
Paleontologist (radiolarians)
Deparment of Geology
Kumaun University
Nainital 263002
India
gksharma61@yahoo.com

Arun D. Singh
Paleontologist (foraminifers)
Department of Geology
Banaras Hindu University
Varanasi Uttar Pradesh 221005
India
arundeosingh@yahoo.com

Stephan Steinke
Paleontologist (foraminifers)
MARUM – Center for Marine Environmental Sciences
University of Bremen
Leobener Strasse
28359 Bremen
Germany
ssteinke@uni-bremen.de

Kenta Suzuki
Sedimentologist
Graduate School of Environmental Science
Hokkaido University
N10W5, Kita-ku
Sapporo 060-0810
Japan
kenta.suzuki@ees.hokudai.ac.jp

Lisa Tauxe
Paleomagnetist
Scripps Institution of Oceanography
9500 Gilman Drive
La Jolla CA 92093-0220
USA
ltauxe@ucsd.edu

Manish Tiwari
Inorganic Geochemist
National Centre for Antarctic and Ocean Research (NCAOR)
Vasco da Gama
Goa 403804
India
manish.ncaor@gmail.com

Zhaokai Xu
Sedimentologist
Key Laboratory of Marine Geology and Environment
Institute of Oceanology
Chinese Academy of Sciences
7 Nanhai Road
Qingdao Shandong 266071
China
zhaokaixu@qdio.ac.cn

Zhaojie Yu
Inorganic Geochemist
Laboratoire Géosciences Paris-Sud (GEOPS, UMR8148-CNRS)
Université de Paris-Sud (Orsay)
Bâtiment 504
91405 Orsay Cedex
France
yuzhj1988@gmail.com

Siem Offshore AS Officials

Terry Skinner
Master of the Drilling Vessel

Sam McLelland
Offshore Installation Manager

Technical support

Susan Boehm
X-Ray Laboratory

Adam Bogus
Underway Geophysics Laboratory

Chad Broyles
Curatorial Specialist

Etienne Claassen
Marine Instrumentation Specialist

Bill Crawford
Senior Imaging Specialist

Aaron de Loach
Physical Properties Laboratory

Keith Dupuis
Publications Specialist

David Fackler
Applications Developer

Edwin Garrett
Paleomagnetics Laboratory

Thomas Gorgas
Core Laboratory

Margaret Hastedt
Core Laboratory

Michael Hodge
Marine Computer Specialist

David Houpt
Core Laboratory

Jan Jurie Kotze
Marine Instrumentation Specialist

Aaron Mechler
Thin Section Laboratory

Erik Moortgat
Chemistry Laboratory

Vincent Percuoco
Chemistry Laboratory

Chieh Ping
Laboratory Officer

Michael Storms
Operations Superintendent

Kerry Swain
Logging Engineer

Steven Thomas
Marine Computer Specialist

Rui Wang
Applications Developer

Abstract

The Indian (southwest) summer monsoon is one of the most intense climatic phenomena on Earth. Its long-term development has been linked to the growth of high topography in South and Central Asia. The Indian continental margin, adjoining the Arabian Sea, offers a unique opportunity to investigate tectonic–climatic interactions and the net impact of these processes on weathering and erosion of the western Himalaya. During International Ocean Discovery Program Expedition 355, two sites (U1456 and U1457) were drilled in Laxmi Basin in the eastern Arabian Sea to document the coevolution of mountain building, weathering, erosion, and climate over a range of timescales. In addition, recovering basement from the eastern Arabian Sea provides constraints on the early rifting history of the western continental margin of India with special emphasis on continental breakup between India and the Seychelles and its relationship to the plume-related volcanism of the Deccan Plateau.

Drilling and coring operations during Expedition 355 recovered sediment from Sites U1456 and U1457 in the Laxmi Basin, penetrating 1109.4 and 1108.6 m below seafloor (mbsf), respectively. Drilling reached sediment dated to 13.5–17.7 Ma (late early to early middle Miocene) at Site U1456, although with a large hiatus between the lowermost sediment and overlying deposits dated to <10.9 Ma. At Site U1457, a much longer hiatus occurs near the base of the cored section, spanning from 10.9 to ~62 Ma. At both sites, hiatuses span ~8.2–9.2 and ~3.6–5.6 Ma, with a possible condensed section spanning ~2.0–2.6 Ma, although the total duration for each hiatus is slightly different between the two sites.

A major submarine fan draining the western Himalaya and Karakoram must have been supplying sediment to the eastern Arabian Sea since at least ~17 Ma. Sand mineral assemblages indicate that the Greater Himalayan Crystalline Sequence was fully exposed to the surface by this time. Most of the recovered sediment appears to be derived from the Indus River and includes minerals that are unique to the Indus Suture Zone, in particular glaucophane and hypersthene, most likely originating from the structural base of the Kohistan arc. Pliocene sandy intervals at Site U1456 were deposited in lower fan "sheet lobe" settings, with intervals of basin plain turbidites separated by hemipelagic muddy sections deposited during the Miocene. Site U1457 is more distal in facies, reflecting its more marginal setting. No major active lobe appears to have affected the Laxmi Basin since the Middle Pleistocene (~1.2 Ma).

We succeeded in recovering sections spanning the 8 Ma climatic transition, when monsoon intensity is believed to have changed strongly, although the nature of this change awaits postcruise analysis. We also recovered sediment from a large mass transport deposit measuring ~330 and ~190 m thick at Sites U1456 and U1457, respectively. This section includes an upper sequence of slump-folded muddy and silty rocks, as well as underlying calcarenites and limestone breccias, together with smaller amounts of volcanic clasts, all of which are likely derived from the western Indian continental shelf. Identification of similar facies on the regional seismic lines in Laxmi Basin suggests that these deposits form parts of one of the world's largest mass transport deposits.

Coring of igneous basement was successful at Site U1457. Recovery of massive basalt and associated volcaniclastic sediment at this site should address the key questions related to rifting and volcanism associated with formation of Laxmi Basin. Geochemical analysis is required to understand the petrogenesis and thus the tectonic setting of volcanism that will reveal whether it is oceanic basalt or volcanic rock contaminated by underlying continental crust or continental flood basalt. However, the fact that the lavas are massive and have few vesicles implies water depths of eruption likely deeper than 2000 m. This precludes opening of the basin in the presence of a major mantle thermal anomaly, such as that associated with the Deccan Large Igneous Province. Other observations made at the two sites during Expedition 355 provide vital constraints on the rift history of this margin. Heat flow measurements at the two drill sites were calculated to be ~57 and ~60 mW/m^2. Such heat flow values are compatible with those observed in average oceanic crust of 63–84 Ma age, as well as with the presence of highly extended continental crust. Postcruise analyses of the more than ~1722 m of core will provide further information about the nature of tectonic–climatic interactions in this global type area for such studies.

Introduction

The theory of plate tectonics established that the solid Earth's lithosphere interacts intimately with the underlying, circulating asthenosphere. However, more recently the geoscience community has started to recognize that the lithosphere also has significant interactions with the atmosphere and oceans. Such interactions can influence circulation patterns and thereby control Earth's climate by changing the distribution of heat across the planet. Furthermore, feedbacks from the atmosphere to the lithosphere provide a new vision of how orogenic belts and even passive margins evolve under the stress of surface processes. Interactions between the solid Earth and the climate system can occur in at least two different ways. The opening and closure of deep-ocean gateways are believed to have caused large-scale climate changes by affecting heat transport between ocean basins or between polar and tropical regions (e.g., Haug and Tiedemann, 1998; Cane and Molnar, 2001; von der Heydt and Dijkstra, 2006). Alternatively, mountain building may perturb planetary-scale atmospheric circulation, influencing continental environments and oceanography of the surrounding basins as mountain barriers divert air streams and affect continental temperatures and humidity (e.g., Huber and Goldner, 2012). Furthermore, changes in continental erosion can profoundly impact Earth's carbon and biogeochemical cycles (e.g., Berner et al., 1983). These various pathways for interaction occurred throughout the Cenozoic with the closure of the Tethys Ocean by the northward motion of Africa, Arabia, India, and a host of smaller continental fragments that caused the uplift of the Alpine-Himalayan mountain belt.

The suggestion that mountain building in Asia has intensified monsoon strength in the Indian subcontinent is the most dramatic proposed example of lithospheric-atmospheric interactions (Prell and Kutzbach, 1992; Molnar et al., 1993; An et al., 2001). This is partly a reflection of the scale of the tectonism and the resultant mountains. Nonetheless, there is increasing recognition that other factors, such as the retreat of shallow seas in Central Asia, may have also played a role in controlling monsoon intensity (Ramstein et al., 1997). Asia is the only continent that experiences such a strong monsoon, which is partly a reflection of landmass size but is also linked to its tectonic history and anomalously high altitude across a broad region. Understanding what controls monsoon intensity is of great scientific interest and has substantive societal as well as economic importance considering the large number of people whose livelihood depends on the monsoon and who would be affected if it varied significantly.

Quantifying the various processes that control monsoon intensity over geologic timescales will improve the context for shorter term modeling of how future climate change may affect the densely

populated environments of Asia. Specifically, we aim to answer the question of what the links between the monsoon and the building of high topography in Asia are, and whether climatic feedbacks have influenced the tectonic evolution of the western Himalaya and Karakoram.

The Arabian Sea in the northern Indian Ocean (Figure **F1**) preserves regional sedimentary records of rifting, tectonic subsidence, and paleoceanographic history, and also provides archives of long-term erosion of the Himalaya since the start of collision between India and Eurasia. Although the timing is controversial (Aitchison et al., 2007; DeCelles et al., 2014; Wu et al., 2014), it is thought that collision probably began in the Eocene (Garzanti et al., 1987; Rowley, 1996; Najman et al., 2010). Scientific drilling in the Arabian Sea was designed to reconstruct the evolution of erosion and weathering in the western Himalaya and Karakoram, as well as the environmental conditions in the flood plains of the Indus Basin through the Cenozoic. This was done in an area where the Indian monsoon evolution is already partly reconstructed (Kroon et al., 1991; Prell et al., 1992). Thus erosion, tectonism, and climate can be directly compared to one another.

In addition to being a repository of information about past climate and mountain building, the Arabian Sea also holds potentially illuminating records of continental rifting and breakup tectonics dating from the time of Gondwana fragmentation in the Cretaceous (Heine et al., 2004). Paleogeographic reconstructions based on magnetic anomalies, as well as similarities in structural/tectonic elements, suggest a conjugate relationship between the western continental margin of India and the eastern continental margin of Madagascar and the Seychelles (Storey et al., 1995; Collier et al., 2008). In-depth studies of the conjugate margins in this region offer new data to complement our knowledge from other well-studied conjugate margins, such as the Iberia-Newfoundland and Greenland-Norway pairs of the Atlantic Ocean. The nature of the continent/ocean boundary is controversial in the Arabian Sea, especially with regard to Laxmi Ridge, an enigmatic block located offshore of the western Indian coast (Figure **F1**).

The widely held view among geoscientists is that Laxmi Ridge is a continental sliver rifted away from India (Naini and Talwani, 1983); however, contrary views have also emerged that suggest it could be stretched/oceanic crust (Bhattacharyya et al., 1994; Miles et al., 1998; Talwani and Reif, 1998). The proximity of this margin to the volcanic Deccan Traps makes this potentially a classic margin for investigating plume-rift interactions. However, links are presently only conjectural because the nature of the breakup, including the style of strain accommodation, and the timing of the extension in relation to the Deccan volcanic event are unconstrained and require physical sampling of the basement on the continental margin.

An international workshop on scientific drilling in the Indian Ocean was organized in Goa, India, in October 2011 at which understanding the evolution of the Asian monsoon was highlighted as a crucial theme. Following this workshop, several proposals related to the evolution of the Asian monsoon were developed. International Ocean Discovery Program (IODP) Expedition 355 is based on drilling Proposal 793-CPP2. The primary objectives of this expedition can be summarized under two major themes, "Climate and Ocean Change" and "Earth Connections", which are described in the IODP Science Plan (available at **http://www.iodp.org/science-plan-for-2013-2023**). Specific goals of this proposal include

1. Testing whether the timing of the exhumation of the Greater Himalaya correlates with enhanced erosional flux and intense chemical weathering at ~23 Ma;
2. Determining the amplitude and direction of environmental change at ~8 Ma and other times of major climatic variation during the Cenozoic;
3. Dating the age of the base of the fan to constrain the timing of India/Eurasia collision and subsequent uplift of the Himalaya and Tibetan Plateau; and
4. Deciphering the nature of the crust in Laxmi Basin (eastern Arabian Sea), which has a significant bearing on paleogeographic reconstructions along conjugate margins in the Arabian Sea and models of continental breakup on rifted volcanic margins.

Background

Geological setting

The eastern Arabian Sea presents an intriguing case for the study of continental breakup between India and Madagascar, differing in important ways from both the classic nonvolcanic Iberia-Newfoundland conjugate (Boillot et al., 1995; Whitmarsh et al., 2001) and the volcanic Norway-Greenland margin (Skogseid et al., 2000; Hopper et al., 2003). The northern Arabian Sea is characterized by the presence of large structural blocks located between the western continental shelf of India and the deep seafloor of the Arabian Basin. Laxmi Ridge is presumed by most geoscientists to be mostly continental (Talwani and Reif, 1998), and is separated from the western Indian margin by Laxmi Basin (Figure **F2**). There are isolated highs east of Laxmi Ridge, namely Wadia Guyot, and Panikkar and Raman Seamounts, which are collectively referred to as Panikkar Ridge (Karlapati, 2004; Krishna et al., 2006; Bhattacharya et al., 2009; Mishra et al., 2015). The oldest seafloor spreading–related magnetic anomalies identified in this region are Anomalies 27n (62.2–62.5 Ma) and 28n (63.5–64.7 Ma), located southwest of Laxmi Ridge in the Arabian Basin and north of the Seychelles, respectively (Chaubey et al., 2002; Royer et al., 2002) (Figures **F1**, **F2**). Magnetic anomalies in Laxmi Basin itself are rather erratic, and whereas some researchers have argued that these correspond to seafloor spreading (Bhattacharyya et al., 1994; Mishra et al., 2012), it is possible that instead these could have been caused by dikes intruded within a hyperextended continental crust (e.g., Talwani and Reif, 1998; Krishna et al., 2006).

Previous studies using magnetic anomalies from the oceanic crust describe the juxtaposition of India and the Seychelles immediately before the onset of extensional tectonics (Chaubey et al., 1998; Royer et al., 2002). However, most plate tectonic reconstruction models for this region suggest a wide deepwater offshore region (Laxmi Basin, Gop Rift, and offshore Indus Basin) of ~300 km width between the Seychelles and the Indian subcontinent before the onset of seafloor spreading (Chaubey et al., 2002; Royer et al., 2002). The tectonic complexity in this region is further increased when considering the massive Deccan volcanic event at ~65 Ma. It is not yet convincingly known whether eruption of the Deccan flood basalt predates the rifting in Laxmi Basin or otherwise. Lack of geochronological data from Laxmi Basin makes it difficult to correlate the opening of the basin to the Deccan volcanism in the Late Cretaceous. Numerous geophysical studies to investigate the nature of crust in Laxmi Basin remain inconclusive, with some authors favor-

ing the presence of rifted continental crust (Naini, 1980; Naini and Talwani, 1983; Kolla and Coumes, 1990; Miles and Roest, 1993; Miles et al., 1998; Radha Krishna et al., 2002; Krishna et al., 2006; Minshull et al., 2008), whereas others argue for oceanic crust (Biswas and Singh, 1988; Bhattacharyya et al., 1994; Malod et al., 1997; Talwani and Reif, 1998; Singh, 1999; Bernard and Munschy, 2000). Testing of these competing models, largely based on indirect geophysical data, requires direct sampling of rocks from the basement of Laxmi Ridge and Laxmi Basin.

Significant sediment cover overlies the basement of Laxmi Basin, with the oldest parts representing a rifted passive margin sequence. Since the onset of the India/Eurasia collision, the Indus River and its associated tributaries have been the primary source of clastic sediment in the Arabian Sea (Clift et al., 2001), and this Indus-derived sediment likely accounts for most of the postrift sedimentary section targeted during Expedition 355. Far lesser amounts are discharged into the Arabian Sea from mostly small rivers on the steep western margin of India; however, these may have been important sediment sources prior to the India/Eurasia collision and during phases when Indus Fan sediment was being fed to lobes on the western side of the Arabian Basin. The substantial run-off from the Narmada River in central western India (Figure **F1**) is likely to have been buffered by the wide and gently sloping shelf near the margin. This is evident from the thick hydrocarbon-rich sedimentary sequences under the Indian shelf (Biswas, 1987; Gombos et al., 1995).

Much of the present Indus River discharge represents runoff during the summer monsoon rains, enhanced with the seasonal melting of Karakoram and Himalayan glaciers (Garzanti et al., 2005). The Indus Fan covers more than one million square kilometers, stretching ~1500 km into the Arabian Sea from the present delta front. It is the second largest submarine fan in the world and is >10 km thick at the northernmost part (Clift et al., 2002). As the proto-Indus Fan prograded southward, characteristic sediment eroded from the Indus drainage began to accumulate on the distal parts, as observed at Deep Sea Drilling Project (DSDP) Site 221 (Shipboard Scientific Party, 1974; Kolla and Coumes, 1987). The Indus River may have experienced major drainage capture during the Miocene (Clift and Blusztajn, 2005) but has otherwise been stable within the Indus Suture Zone and western syntaxis of the Himalaya since the Eocene.

Drilling can provide erosion records through analyses of the sediment cores, as well as by providing age control for the regional seismic stratigraphy. It is only by quantifying the volume of sediment deposited in the fan that we will be able to mass balance the volume of bedrock eroded from the mountains, constrained by thermochronology, with the volume of eroded rock deposited in the offshore and in the foreland basin.

Stratigraphic framework

The general stratigraphy of the Indus Fan has already been defined by seismic surveying of the drilling region and the more proximal part of the fan (Figures **F3**, **F4**, **F5**). The youngest unit is characterized by strongly reflective sequences that show small internal onlapping relationships in the vicinity of Laxmi Basin. Complex "cut-and-fill" channel bodies are also visible in this thick uppermost sequence. Closer to the Indus Delta, this sequence is dominated by channel-levee complexes that are typical of deepwater turbidite sequences (Kolla and Coumes, 1987; Clift et al., 2002). Sedimentation was active in such bodies during the Last Glacial Maximum, but the fan has been largely dormant since the start of the Holocene (Kenyon et al., 1995; Prins et al., 2000). This uppermost unit is interpreted to be dominated by siliciclastic turbidites fed from the Indus Delta and interbedded with occasional pelagic carbonate deposits associated with sea level highstands when sediment was trapped on the shelf. This sequence was termed the "Indus Fan Megasequence" by Droz and Bellaiche (1991). In the area targeted by Expedition 355, additional sediment may also be derived from the Narmada River and other smaller basins on the west coast of India, as well as even some wind-blown dust from the deserts of Arabia (Figure **F1**).

Toward the northeast, the Indus Fan Megasequence overlies a series of less reflective bedded units that are presumed to represent distal muddy fan deposits. However, in Laxmi Basin, strongly reflective sediment overlies an acoustically transparent unit that thins from north to south and from east to west across Laxmi Basin (Figure **F3**) and is inferred to have been derived from the Indian continental margin. This sequence is interpreted as a large mass transport deposit shed from the shelf edge, likely around the middle to late Miocene boundary (Calvés et al., submitted). It is unclear if the unit significantly eroded the underlying deposits, but its top is rugged in places and inclined so that the Indus Fan Megasequence disconformably overlies it, progressively onlapping over the submarine topography generated by the mass transport deposit as the basin filled. The transparent unit itself has very little in the way of internal patterns or structure but is bounded by very prominent reflectors at the top and base.

The underlying unit is not well bedded or clearly reflective but is also not transparent like the succeeding sequence. This unit, tentatively dated as being Eocene–Oligocene in age before drilling, is interpreted as shales and siltstones forming the early, distal Indus Fan. Regional considerations argue that the base of the fan may lie close to the base of the Eocene, below which lies a highly variable, weakly bedded Paleocene unit that infills the rugged basement topography. The unit between the rift onset and breakup unconformities can be clearly identified on the seismic images. This basal unit represents sedimentation during and after rifting along the western continental margin of India. The Paleogene unit thins from east to west and reaches a maximum of ~0.4 s two-way traveltime (TWT) in the central Laxmi Basin just to the east of Site U1456 (Figure **F3**), although it is thinner further north and west near Site U1457 (Figure **F4**). Further west, between Site U1456 and Laxmi Ridge this unit is disrupted by a late-stage igneous intrusion that penetrates well up into the Neogene and Quaternary section. The Paleogene, and indeed much of the younger cover, onlaps against and is cut out entirely against the side of Laxmi Ridge (Figures **F3**, **F4**). The Paleocene is thought to predate fan sedimentation and probably the onset of India/Eurasia collision, although there is no seismic evidence indicating the base of the fan, implying that the lithologic change may be quite subtle. The source of sediment in the Paleocene is inferred to be dominantly either rift related or from peninsular India to the east.

The lowermost Paleocene section thickens toward the east with a maximum thickness of ~0.4 s TWT near parts of the Panikkar Ridge (Figure **F3**), especially where the ridge is very large. This Paleocene section is ponded away from the basement high underlying the drilled section at Site U1456 and onlaps the basement to the west. The seismic signatures exhibited by this lower Paleocene unit are slightly more seismically reflective than the upper Paleocene section and are associated with early rifting in Laxmi Basin. Although it is difficult to infer its composition, the reflective character compared to the overlying distal Indus Fan sediment and hemipel-

agic units suggests that it may be composed of coarser grained clastic sedimentary rocks, and possibly volcaniclastic sedimentary rocks, linked to Laxmi Ridge and neighboring seamounts along Panikkar Ridge.

Seismic studies/site survey data

Extensive 2-D multichannel seismic data from the eastern Arabian Sea (Figures **F5**, **F6**) were utilized to develop a seismic stratigraphic framework. The regional seismic lines run in east–west (coast perpendicular) and northwest–southeast (coast parallel) directions (Figure **F6**). The seismic images exhibit major reflective surfaces from the shelf through the deep Arabian Basin. We identified seismic units through correlation to available lithologic data from industrial boreholes in the vicinity, located on the Indian continental shelf. A high-resolution multibeam bathymetric survey was carried out to map seafloor morphology before selection of the drill sites (Figure **F7**), all of which were located on relatively smooth, muddy seafloor. Three primary and three alternate sites were proposed to meet planned scientific objectives of this expedition, and we ultimately cored at two of these sites, U1456 and U1457 (Figures **F1**, **F2**). A broad seismic network provides good general control on the sediment thickness in the area.

Scientific objectives

Expedition 355 was designed to drill deep into the Indus submarine fan and to sample the underlying basement at two of the sites. The primary objective is to better understand the erosional and weathering response of the western Himalaya, Karakoram, and Hindu Kush to the changing intensity of the southwest Asian monsoon since the onset of the India/Eurasia collision in the early Paleogene. Such interactions lie at the heart of many popular models for Himalayan tectonic evolution, such as the "channel flow" model in which focused erosion, driven by climate (i.e., monsoon), controls the exhumation of deeply buried igneous and metamorphic rocks (Figure **F8**) (Beaumont et al., 2001; Hodges, 2006; Whipple, 2009). If such models are correct, then there should be close coupling among structural evolution of the mountains, climate change, and sedimentation in the Arabian Sea (Clift et al., 2008; Whipple, 2009); however, testing this on shore is impossible because of the large Oligocene unconformity in the foreland that removed most of that record (Najman, 2006). Only in the offshore can continuous erosion records be found. One goal of this expedition is to understand what feedbacks exist among climatic evolution, mountain building, and surface processes in the global-type area for these processes.

In addition, coring the basement of Laxmi Basin will allow us to date the age of continental breakup and constrain the style of strain accommodation between Laxmi Ridge and the western margin of India. Proximity to the Deccan Traps suggests that this margin could be a volcanic passive margin; however, this depends on the relative timing of rifting and magmatism (Minshull et al., 2008). The role that mantle thermal anomalies, most notably the Réunion Plume, have played in the breakup and subsequent formation of the Indian Ocean and emplacement of the Deccan Traps is crucial. This particular event has implications for biotic mass extinction events, as well as for continental margin tectonics (Courtillot et al., 1988, 1999). Specifically, our objectives are to:

1. *Reconstruct long-term changes in erosion and weathering rates at submillennial to millennial timescales in order to compare with existing records of high-frequency climatic variability.*

Neogene sedimentary sections from the Indus Fan are expected to record the erosional and weathering responses of the Indus drainage basin to changing climate, which has been reconstructed using speleothem (Fleitmann et al., 2003), eolian dust (DeMenocal et al., 1991; Clemens and Prell, 2003), and upwelling/productivity records (Kroon et al., 1991; Prell et al., 1992), largely from the Oman margin on the western side of the Arabian Sea. However, these records mostly do not extend back in time before 18 Ma. Links between climate and erosion on short timescales would be expected if those proposed on longer timescales are correct. Attempts to understand the erosional response of landscape to climate change in southwest Asia have largely been limited to the last glacial cycle (Bookhagen et al., 2005; Dortch et al., 2009; Giosan et al., 2012; Blöthe et al., 2014); however, our sediment cores may permit us to examine the changes spanning many such cycles. Specific questions include whether monsoon intensification causes less or more erosion, and whether this erosion occurs in the Himalaya or other mountainous regions. Does a strengthening monsoon result in more grassland (C4) or woodland (C3) flora? Are phases of increased productivity in the Arabian Sea paralleled by changes in the continental environments onshore, both driven by change in monsoon wind intensity? What role does the westerly jet play in controlling continental environments within the Indus Basin? Could the intensity of chemical weathering linked to monsoon intensity have a role in controlling glacial cycles in the Northern Hemisphere?

Weathering intensity will be reconstructed using bulk sediment geochemical analysis, selected isotope systems (such as Sr), and clay mineralogy. These measurements must be performed in concert with provenance work to establish whether any of the chemical changes could be driven by changes in source composition or drainage capture rather than weathering intensity. Bulk sediment and single-grain provenance methods, including heavy mineral studies, U-Pb dating of detrital zircons, Ar-Ar dating of detrital mica grains, Nd isotopes, and apatite fission track represent some of the methods known to be effective in this drainage system that will allow tracking of changing patterns of erosion caused by waxing and waning of the monsoon (Clift et al., 2004; Garzanti et al., 2005; Alizai et al., 2011).

Age control will be central to the success of this objective, especially if we are to estimate the lag times between climate change and the sediment record of the deep basin. This will be achieved using a combination of biostratigraphy and magnetostratigraphy. Oxygen isotope stratigraphy is also intended to build a high-resolution age model that contributes toward the proposed objectives. Palynology, carbon isotopes, and leaf-wax organic geochemical studies will provide further information on the evolving onshore landscape, as they are known to be effective in this region (Budziak et al., 2000; Ponton et al., 2012). The data from our expedition can then be correlated with existing climate records to determine links between erosion and climate on shorter timescales.

2. *Reconstruct changes in erosion and weathering intensity over tectonic timescales and assess whether any changes occurred at ~23, 15, and 10–8 Ma to test earlier hypotheses that invoke changes in monsoon intensity at those times.*

Competing hypotheses exist for the timing of initial monsoon intensification based on a variety of proxies from across Asia, with some invoking the growth of the Tibetan Plateau (Molnar et al., 1993), the rising of the Greater Himalaya (Boos and Kuang, 2010), or the retreat of shallow seas from Central Asia (Ramstein et al.,

1997). Unfortunately, most of the existing climate reconstructions do not span tectonic timescales, especially the critical start of Greater Himalayan exhumation and movement along the Main Central Thrust at ~23 Ma (Catlos et al., 2001; Godin et al., 2006; Tobgay et al., 2012). Without a long-term reconstruction of the erosion history, it is impossible to judge which surface processes might control tectonic processes. At the same time, erosion of older sediment from the flood plain, as opposed to directly from the Himalaya, implies that the deep-sea fan sediment can be used to constrain environmental conditions in the drainage basin. These in turn can be used to infer the age of monsoon intensification and test the assumption that stronger monsoon rains change the flora and likely increase rates of chemical weathering, which in turn should result in delivery of more altered sediment to the ocean.

Improved understanding of how the monsoon and erosion/weathering interact on short timescales (Objective 1) will allow us to better use the long-term erosion and weathering record to reconstruct monsoon intensity through the Cenozoic. Upper Miocene to recent proxy records of monsoon intensity can be compared to weathering and environmental proxies so that the relationship between the monsoon and weathering can be established. For the period before ~18 Ma we have no independent climate record, and the monsoon intensity for that time will likely be constrained from weathering and erosion records whose interpretation will be ground-truthed in the younger section where both types of reconstruction exist. Many tectonic models for the Himalaya link intensified erosion, driven by stronger summer monsoon rains, to the start of Greater Himalaya exhumation (Hodges, 2006; Harris, 2007; Clift et al., 2008); however, currently no well-dated, high-resolution erosion record spans this critical interval. Available records provide only subepoch resolution (Rea, 1992; Métivier et al., 1999; Clift, 2006), so these models remain untested. Correlating changes in Himalayan-Tibetan tectonics with the marine record of erosion and weathering is the key test for these mechanisms.

Changes in sediment provenance tracked by a variety of bulk and single-grain proxies are needed to identify the focused erosion that is predicted during Greater Himalayan exhumation. The timing of the final unroofing of the Greater Himalaya is also poorly defined (White et al., 2002; Bernet et al., 2006; Najman, 2006; Szulc et al., 2006) and should be indicated by influxes of high-grade metamorphic minerals into the Indus Fan. Seeing whether the arrival of this material from the Greater Himalaya coincides with, or likely follows, intensification of the summer monsoon rains would be a critical test of the channel flow and competing orogenic wedge models. Comparison of detrital mineral cooling ages with depositional ages will allow us to assess changing rates of exhumation in Himalaya source regions in order to see how these are linked to climate change. Combining biostratigraphic and magnetostratigraphic studies to generate an integrated high-resolution chronostratigraphy will allow the age of these provenance and thermochronologic changes to be fixed.

Determining the age of the base of the Indus Fan is a key objective, as this is only known in distal (and therefore young) locations at present (e.g., Site 221) (Shipboard Scientific Party, 1974). Provenance methods and mass accumulation rates are expected to show when the first detritus sourced from the northern side of the Indus Suture Zone arrived in the Arabian Sea, beyond the tentative finding of before 45 Ma inferred from sediment cored on the Owen Ridge at DSDP Site 224 (Clift et al., 2001). This age would provide an important constraint on the much debated timing of India/Eurasia collision (Aitchison et al., 2007; Najman et al., 2010; Wu et al., 2014). This age is of broader significance to Himalayan tectonics than simple local paleogeographic reconstruction because it constrains how much Indian continental crust has been underthrust into the collision zone, since the rate of convergence is well known. Simple comparison of that volume with the size of the Tibetan Plateau will allow us to assess whether horizontal compression can explain all of the strain accommodation since the onset of collision (England and Houseman, 1986; Dewey et al., 1989), or if major "extrusion" of crust as rigid blocks along major strike-slip faults is needed to accommodate the impact of Greater India (Molnar and Tapponnier, 1975; Replumaz and Tapponnier, 2003).

3. *Decipher the nature of basement rocks in Laxmi Basin and constrain the timing of early seafloor spreading and its relationship to the emplacement of Deccan Flood Basalts. Does mantle plume initiation predate or postdate rifting and early spreading?*

We planned penetration of 50–100 m of basement at two sites in order to determine the nature of basement rocks and the age of their formation. Although biostratigraphic and magnetostratigraphic analyses conducted during the expedition will provide an age for the oldest sediment overlying the basement, postcruise radiometric dating, using methods such as $^{40}Ar/^{39}Ar$, will be employed to constrain the age of formation. Because the Deccan Traps have been very precisely dated onshore (Baksi, 1994; Courtillot et al., 2000; Chenet et al., 2008), the relationship between opening of Laxmi Basin and emplacement of the Deccan Traps will be revealed if the basin crust can be dated. This would further improve our knowledge of whether or not and how far Deccan Flood Basalts extend offshore (Pandey et al., 2010, 2011). The potential cause behind the failure of rifting in Laxmi Basin shortly after the opening in the more clearly oceanic Gop Basin (Yatheesh et al., 2009; Chatterjee et al., 2013) is also not yet fully understood.

Because the precise timing of rifting in Laxmi Basin is unknown (Minshull et al., 2008), the indistinct nature of the magnetic anomalies in the basin leaves open the possibility that it is floored by either slow-spreading oceanic crust (Bhattacharyya et al., 1994; Misra et al., 2015) or hyperextended continental crust (Krishna et al., 2006). Geochemical analyses will allow the composition of the volcanic rocks to be compared with Deccan Flood Basalts, rift volcanic rocks, and mid-ocean-ridge basalts (MORB) that would have no linkage to a deep-seated mantle plume or other mantle compositional anomalies. Sediment overlying the basement may potentially allow reconstruction of the margin subsidence, which can further be used to look at the thermal state of the mantle under Laxmi Basin during its rifting because positive thermal anomalies drive surface uplift. Many rifted volcanic margins are characterized by subaerial eruption and rapid subsidence (Calvés et al., 2008). The petrography and geochemistry of sediments, as well as igneous basement rocks, would enable us to build the syn- and postrift history of the Laxmi Basin. If the volcanic sequences of Laxmi Basin are linked to the Deccan Traps, then this would add significantly to their volume and thus to their potential environmental impact and role in the biotic mass extinctions at the Cretaceous/Paleogene boundary (Courtillot et al., 1988; Self et al., 2008). The timing of rifting and bathymetric evolution of Laxmi Basin also has significant implications for precise paleogeographic reconstructions of the Arabian Sea during the Paleogene (Chaubey et al., 2002; Royer et al., 2002).

Principal results

Site U1456

Background and objectives

Site U1456 (proposed Site IND-03C), the first drill site during Expedition 355, lies within Laxmi Basin in the eastern Arabian Sea (16°37.28′N, 68°50.33′E) in 3640 m of water (Figure F2). The site is situated ~475 km west of the Indian coast and ~820 km south from the modern mouth of the Indus River, which is presumed to be the primary source of sediment to the area, at least since the Neogene and likely since the Eocene (Clift et al., 2001).

Laxmi Basin is flanked to the west by Laxmi Ridge and to the east by the Indian continental shelf (Figures F1, F2). The nature of the crust in Laxmi Basin has been the subject of vigorous debate. Some workers have proposed that it is stretched continental crust (Miles et al., 1998; Todal and Edholm, 1998; Krishna et al., 2006) based on the reduced crustal thickness in Laxmi Basin (~6–7 km) compared to the neighboring thicker crust on either side (as thick as 17 km under Laxmi Ridge [Misra et al., 2015] and ~40 km under peninsular India [Singh et al., 2015]). In this model, Laxmi Ridge would be a continental fragment rifted from peninsular India (Naini and Talwani, 1983; Talwani and Reif, 1998; Minshull et al., 2008). In contrast, some workers interpret Laxmi Basin to be of oceanic affinity based on asymmetrical magnetic anomalies within the basin (Figure F2). Such a model relates these magnetic anomalies to the early phases of seafloor spreading in the Arabian Sea (Bhattacharyya et al., 1994; Pandey et al., 1995), which removed a microcontinental Laxmi Ridge block from mainland peninsular India. In this case, Laxmi Basin would be more similar to its along-strike equivalent in the Gop Rift to the northwest.

Since the time of continental breakup at the end of the Cretaceous to earliest Paleocene, Laxmi Basin has been largely tectonically inactive as seafloor spreading has migrated away toward the southwest of Laxmi Ridge (Royer et al., 2002). The seismic data from this region suggest that the process of gradual postrift thermal subsidence has been interrupted by the emplacement of localized magmatic intrusions, but there has been no strong deformation of the basin since the end of extension, estimated to be prior to ~65 Ma based on magnetic anomalies within the basin (Bhattacharyya et al., 1994) or before 63 Ma based on the timing of onset of seafloor spreading west of Laxmi Basin (Chaubey et al., 2002). Although Laxmi Basin is separated from the main Arabian Sea by the topographic high of Laxmi Ridge, it has nevertheless been supplied by sediment from the Indus River and forms the easternmost part of the Indus submarine fan, the second largest such sediment body in the modern oceans. Proximity to peninsular India means that the basin has been the recipient of some sediment discharged from rivers flowing to the west coast of the subcontinent, most notably the Narmada and Tapti Rivers (Figure F1), although their discharge is much less than that seen in the Indus River. Milliman and Syvitski (1992) estimated 125×10^6 and 250×10^6 ton/y for the modern Narmada and the Indus Rivers, respectively, whereas others argue for even higher values for the Indus River (Ali and de Boer, 2008).

Site U1456 is the focus of a number of scientific objectives central to Expedition 355. Sampling and dating the base of the Indus Fan is a primary objective of this expedition. The proposed deep penetration at Site U1456 was aimed at revealing the Cenozoic evolution of the Indus Fan with the intention of reconstructing the weathering and erosion history of the western Himalaya. Sediment recovered at this site should allow us to reconstruct patterns and rates of erosion, as well as to constrain how and when continental environmental conditions changed (e.g., humidity and vegetation patterns) in the Indus drainage since the onset of the India/Eurasia collision. In particular, we aimed to test the hypothesis that the exhumation of the Himalaya was driven by the changing strength of the summer monsoon precipitation. For instance, increased erosion along the southern flank of the Tibetan Plateau in response to a stronger monsoon rainfall allowed the Greater Himalaya to be exhumed (Clift et al., 2008). Direct coupling of erosion rates and exhumation is a prediction of the popular channel flow model for Himalaya evolution (Beaumont et al., 2001; Hodges, 2006). Such coupling would also be applicable to some tectonic wedge models for structural evolution (Robinson et al., 2006) and is not unique to the Himalaya (Willett, 1999). Because Site U1456 is located in the distal fan and we estimated reasonably high sedimentation rates based on seismic ties to industrial wells with age control on the outer western continental shelf of India, the site was also designed to document high-resolution changes in weathering, erosion, and paleoenvironment during the Quaternary that can be related to millennial-scale monsoonal changes linked to insolation and ice sheet–related forcing.

In addition to the objectives related to Cenozoic evolution of the Indus Fan, Site U1456 was also planned to address questions pertaining to the nature of the basement of Laxmi Basin. In order to test the hypotheses of whether Laxmi Basin is oceanic or continental, we need to directly sample the basement underlying the basin. The result of this has significant implications for the breakup history of India and the Seychelles. In addition, analyses of sediment retrieved from Laxmi Basin will allow us to constrain depositional conditions in a rifted basin. Such sediment may be used to reconstruct vertical tectonic motions and so determine the response of the lithosphere to the syn- and postrift tectonic stresses associated with continental breakup.

At Site U1456, we planned to core to ~100 m into basement through the base of the Indus Fan to address the primary expedition objectives. However, because of technical difficulties encountered when drilling the complex lithologies within a mass transport deposit emplaced in the basin during the Miocene, we were forced to terminate coring in the deepest hole of this site at ~1109 mbsf (Figure F9), well above the target depth of ~1590 mbsf. The cored interval at Site U1456 includes an expanded section of upper Miocene to recent strata punctuated by several hiatuses (Figure F10). Nonetheless, using the samples and data generated at this site, we will be able to address the questions related to changes in the monsoon at ~8 Ma, as well as how monsoon intensity varied after the onset of Northern Hemisphere Glaciation. In addition, we cored through ~350 m of mass transport deposit that likely represents the largest known deposit of this type in the geological record (Calvès et al., submitted). Studies focused on this interval will help to identify the source of these deposits, as well as examine how such large deposits are emplaced, and may help us to understand the mechanism through which they are formed.

Operations

After a 941 nm transit from Colombo, Sri Lanka, the vessel stabilized over Site U1456 at 1054 h (UTC + 5.5 h) on 9 April 2015. We cored five holes at Site U1456. The original operations plan called for three holes: the first to advanced piston corer (APC) refusal, followed by a second APC hole with extended core barrel (XCB) coring to ~650 mbsf. The third hole was a planned reentry of the hole including 650 m of casing, followed by coring to a total depth of ~1590 mbsf, which included 100 m of basement. The plan was

modified to include a short APC hole for high-resolution microbiological and geochemical sampling of the upper ~30 m of section (Table **T1**).

When APC refusal was reached at a much shallower depth than anticipated (~140 mbsf), we opted to deepen Hole U1456A using the half-length APC (HLAPC). Because of good hole conditions, we continued coring in Hole U1456A with the XCB to 426.6 mbsf when the XCB cutting shoe detached and was left in the hole, forcing us to abandon the hole. Hole U1456B was cored with the APC to 29.1 mbsf. We then cored Hole U1456C with the APC and HLAPC to 221.6 mbsf, drilled ahead without coring to 408.0 mbsf, and then continued coring with the XCB to 465.2 mbsf. We terminated coring operations in Hole U1456C when we determined that the lithology at 465.2 mbsf would be ideal for the base of the casing for our deep hole. After conditioning the hole for logging, we conducted three logging runs in Hole U1456C. The triple combo tool string was run first without the radioactive source to 465 m wireline depth below seafloor (WSF), and then the Formation MicroScanner (FMS)-sonic tool string was run to 465 m WSF with two upward passes. The last logging run was made with the triple combo tool string with the radioactive source after the hole was determined to be in good condition.

In Hole U1456D, we drilled-in a 10¾ inch casing string to 458.8 mbsf and then began coring with the rotary core barrel (RCB) coring assembly. When we reached 1024.2 mbsf, we pulled out of the hole for a bit change; however, we encountered difficulties reentering the hole. The drill string became stuck in the open hole below the casing and ultimately had to be severed, effectively terminating the hole. We then decided to install a longer 10¾ inch casing string to 748.2 mbsf in Hole U1456E, drilled without coring to 970 mbsf, and then continued to RCB core to 1109.4 mbsf. We pulled out of the hole for a bit change and again encountered difficulties trying to trip the drill string back to the bottom of the hole. After little progress was made to advance the bit over a 12 h period and several instances of the drill string getting temporarily stuck, we decided to terminate the hole and end operations at Site U1456. The total time spent on Site U1456 was 885 h (36.9 days).

A total of 197 cores were collected at this site. The APC coring system was deployed 35 times, recovering 276.91 m of core over 301.9 m of penetration (92% recovery). The HLAPC was deployed 72 times, recovering 287.55 m of core over 334.8 m of penetration (86% recovery). The XCB coring system was deployed 13 times, recovering 44.58 m of core over 94.3 m of penetration (47% recovery). The RCB coring system was deployed 77 times, recovering 401.63 m of core over 705.0 m of penetration (57% recovery).

Principal results

The cored section at Site U1456 is divided into four lithologic units based on a compilation of Holes U1456A through U1456E (Figure **F9**). Lithologic Unit I consists of an ~121 m thick sequence of Pleistocene light brown to light greenish nannofossil ooze and foraminifer-rich nannofossil ooze interbedded with clay, silt, and sand. The sand layers show normal grading and sharp erosive bases and are interpreted as distal basin plain turbidites. The hemipelagic nannofossil ooze and nannofossil-rich clay show intense bioturbation and also include common pyrite concretions. Quartz, feldspar, and mica grains are common in Unit I, whereas heavy minerals are rare in abundance, but when they are seen these include hornblende, kyanite, tourmaline, augitic clinopyroxene, apatite, and glauconite.

Lithologic Unit II is ~240 m thick and is dated to the late Pliocene to early Pleistocene. The unit consists mainly of massive dark grayish to blackish sand and silt interbedded with thinly bedded nannofossil-rich clay. This sediment also shows normal grading and common sharp erosive bases, which are interpreted as a series of turbidites, likely deposited in a sheet lobe setting. Unit II contains similar sets of light and heavy minerals as Unit I, although the heavy minerals are more abundant in this unit. The presence of diagnostic high-pressure sodic amphiboles (glaucophane) and pink-green hypersthene is distinctive of Unit II and indicative of erosion from the Indus Suture Zone. The only known source of glaucophane is from blueschists exposed along the Main Mantle Thrust in the suture zone in Kohistan (Anczkiewicz et al., 2000) and these would have to be delivered to the main stream by the Swat and Kabul Rivers from the west.

Upper Miocene to upper Pliocene lithologic Unit III is ~370 m thick and mainly consists of semi-indurated to indurated light brown to dark green clay/claystone, light brown to dark gray sand/sandstone, light greenish nannofossil chalk, and light to dark greenish gray nannofossil-rich claystone. Clay/claystone and sand/sandstone cycles of sedimentation are separated by intervals dominated by nannofossil chalk and nannofossil-rich claystone. Sand layers typically have sharp erosive bases and normal grading into the clay-rich intervals. Low recovery in this unit makes it harder to assign a depositional setting, but the turbidites may have been deposited in a sheet lobe. The lower part of Unit III contains common wood-rich layers (as thick as ~1 cm). Bioturbation is mostly limited to intervals of nannofossil chalk and nannofossil-rich claystone. The mineral assemblage of the silt fraction observed under the microscope is similar to that of Unit II, but heavy mineral abundances are different in the clay fraction. The assemblage is typical of erosion from the Greater Himalaya (Garzanti et al., 2005), but glaucophane is not observed.

Miocene lithologic Unit IV is ~380 m thick and consists of a mixture of interbedded lithologies dominated by dark gray massive claystone, light greenish massive calcarenite and calcilutite, and conglomerate/breccia, with minor amounts of limestone, especially toward the base of the unit (Figure **F9**). A variety of deformation structures including microfaults, soft-sediment folds, slickensides, and tilted to vertical bedding are observed in this unit. The most common minerals in Unit IV are quartz and micas, with trace to very rare occurrences of heavy minerals. Clasts of vesicular volcanic rock and shallow-water limestone in the breccia point to a source on the Indian continental shelf (Biswas, 1987; Whiting et al., 1994), with possible erosion from the Deccan Plateau province. No significant sediment supply from the Indus River is found in this unit, except for a 2 m thick sandstone and claystone bed below the base of the mass transport deposit. This suggests that an early to middle Miocene Indus submarine fan was active in the area at that time.

Calcareous and siliceous microfossils recovered at Site U1456 are typical of subtropical to tropical assemblages. Diatoms and radiolarians are only found in the mudline and uppermost cores from this site, whereas calcareous nannofossils and planktonic foraminifers occur in varying numbers throughout the succession. Diatoms in the mudline samples are well preserved and consist mainly of coastal species, whereas these taxa are absent in the cored sediment. Diatoms are sparse and moderately preserved in the uppermost 10 mbsf, and the assemblage includes benthic and freshwater taxa that indicate transport to the site. Radiolarians are very rare but well preserved in the upper 120 mbsf and absent below. Abun-

dance and preservation of calcareous nannofossils and planktonic foraminifers depends on lithology. In general, calcareous nannofossils are moderately to well preserved throughout Site U1456, whereas planktonic foraminifer preservation varies from poor to good. Both groups are common to abundant in Unit I. Nannofossils are sparse and foraminifers are usually absent in the coarse-grained intervals of Units II and III. Reworked Cretaceous and Paleogene nannofossils are common through Units I–III. In lithologic Unit IV, nannofossil and foraminifer abundance varies significantly, from absent to abundant, and the assemblage is characterized by mixed Paleogene to early Neogene taxa that hamper age interpretation.

The age model for Site U1456 is based on calcareous nannofossil and planktonic foraminifer biostratigraphy, together with magnetostratigraphy (Figure **F10**). The succession of bioevents indicates that Site U1456 spans the lower to middle Miocene to recent but is punctuated by several hiatuses of varying duration. The Indus submarine fan sediment at the base of the succession below the mass transport deposit contains a nannofossil assemblage characteristic of the early to middle Miocene. The mass transport deposit of Unit IV appears to have been rapidly emplaced in the late Miocene based on the presence of late Miocene nannofossils within two short hemipelagic intervals within the transported unit. After deposition of the mass transport deposit, the sedimentation rate appears to have been relatively consistent in the late Miocene at ~10 cm/ky, although deposition was interrupted for ~0.5 million years between ~8 and 9 Ma. Another hiatus spanning ~2 million years encompasses the Miocene/Pliocene boundary. The sedimentation rate in the late Pliocene to early Pleistocene was again ~10 cm/ky. After a 0.45 million year hiatus, sedimentation rates in the early Pleistocene are much higher (~45 cm/ky) during deposition of Unit II. The sedimentation rate decreased in the late early Pleistocene to recent, averaging ~12 cm/ky.

Geochemical measurements at Site U1456 were designed to characterize the distribution of hydrocarbon gases, sediment geochemistry (including carbon, nitrogen, sulfur, and carbonate contents), and interstitial water compositions. Sulfate concentration in the interstitial water decreases sharply in the uppermost 60 mbsf, indicating anaerobic sulfate reduction. Below the sulfate reduction zone, methanogenesis becomes an important process, which is reflected by an increase in methane concentrations between 60 and 120 mbsf. Methane concentrations decrease to ~2000 ppmv near the boundary between Units I and II (~120 mbsf) and then reach maximum values within Unit II at ~360 mbsf. This pattern could be controlled by lithology, with gas accumulating in the relatively porous silty sand and silt with sand layers in Unit II, which are capped by the nannofossil-rich clay of Unit I.

Alkalinity, ammonia, and phosphate in interstitial water are produced as byproducts of organic matter degradation in the upper 60 mbsf within the sulfate reduction zone. Increased alkalinity in this interval causes calcium and magnesium to precipitate as carbonate, resulting in a decrease in calcium and magnesium concentrations. Manganese concentrations in the interstitial water also decline sharply in the uppermost 70 mbsf within the sulfate reduction zone, where hydrogen sulfide is produced. Total dissolved iron is consistently low over this interval and may be removed, together with manganese, by metal sulfide formation under anaerobic conditions. The boron concentration in the interstitial water shows an inverse relationship with that of manganese, suggesting that the adsorption/desorption reaction is the primary control over the boron concentration. Dissolved silica concentrations are higher (300–520 μM) in the uppermost 120 mbsf, which may be caused by its release during the dissolution of biogenic silica, consistent with the near-absence of siliceous microfossils over this interval. Barium concentrations in the interstitial water increase from 250 to 450 mbsf, which could suggest high organic matter diagenesis through this interval. Alternatively, barium could also be released through dissolution of barite under low sulfate conditions or through leaching of lithogenous minerals.

Total carbon and $CaCO_3$ contents are variable at this site and show similar variations, indicating that most of the carbon is present as $CaCO_3$. Carbonate content is generally higher in Unit I, particularly in the nannofossil ooze and nannofossil-rich clay (60–80 wt%). Carbonate content is lower (10–30 wt%) in the silt and sand-rich intervals of Unit I and throughout most of Units II and III, which are dominantly siliciclastic. Very high carbonate content (70–90 wt%) deeper than 975 mbsf in Unit IV corresponds to the presence of calcarenite, calcilutite, and limestone. Total organic carbon (TOC) values at Site U1456 mostly vary between 0 and 2 wt%, with a few higher values in Unit IV. We report TOC/total nitrogen (TN) as a preliminary estimate for the source of organic material. In general, the TOC/TN separates predominantly marine (TOC/TN < 8) from predominantly terrestrial (TOC/TN > 12) organic input according to Müller and Mathesius, 1999; however, a simple model of the factors influencing TOC/TN ratios is not always applicable. High TOC/TN ratios atypical for algal source organic matter have been measured in organic-rich Mediterranean sapropel layers, upper Neogene sediment from the Benguela upwelling region, Eocene horizons from the Arctic Ocean, and Cenomanian–Turonian black shales (Meyers, 1990; Stein and MacDonald, 2004; Stein et al., 2006; Twichell et al., 2002). In Unit I, three distinct intervals with high TOC/TN (>20), suggestive of terrestrial sources, correspond to beds of silty sand with nannofossils and silt with sand; however, the dominantly hemipelagic nature of these lithologies precludes confident assignment of the organic matter to terrestrial input. Meyers (1997) suggests that in organic-rich marine sediment these high TOC/TN ratios are explained by the fact that (1) algae are able to synthesize lipid-rich organic carbon during times of abundant nutrient supply and/or (2) during sinking, partial degradation of algal organic carbon may selectively diminish nitrogen-rich proteinaceous components and the TOC/TN ratio. In Units II and III, low TOC/TN values suggest primarily marine to mixed sources of organic matter. Unit IV is characterized by high variability, with very high values within the 930–1018 mbsf interval suggesting strong terrestrial input of organic matter. Correlation between TOC and total sulfur provides a further general estimation of the source of organic matter in marine sediment (Berner and Raiswell, 1983) and is consistent with the interpretations based on TOC/TN.

A total of 72 whole-round samples (5–10 cm long) were collected at Site U1456 for microbiological studies. These samples were taken adjacent to interstitial water whole-round samples for comparison with interstitial water chemistry. Samples were mostly preserved for postcruise characterization of the microbial population using DNA/RNA, as well as lipid and cultivation-based studies. Fluorescent microspheres were added to the core catcher sub before the core barrel was deployed during APC coring to use as a contamination tracer. Samples were collected from the exterior, interior, and an intermediate position from each of the whole-round samples to determine the potential extent of contamination. Examination of the microsphere content of these samples was carried out on board and indicates that samples from the exterior contain higher concentrations of microspheres than those from the intermediate position. Microspheres were completely absent in samples from the interior

of the cores, indicating no apparent contamination of the interiors of these cores. Some samples were also analyzed for new microbial community structures. The subsurface sediment (0–27 mbsf) in Hole U1456B contains many specimens of eukaryotic species (fungi) and deep-marine invertebrates (meiofauna). Additional analyses are required to pinpoint the phylogenetic positions of these new taxa, which will be addressed during postcruise research.

Paleomagnetic analyses of Site U1456 cores produced a magnetic polarity stratigraphy defined on the basis of inclination data as core orientation attempts met with mixed success. A composite polarity log was constructed from detailed demagnetization experiments on discrete samples from Holes U1456A, U1456C, and U1456D (Figure **F10**). The polarity log was correlated with some confidence to the geomagnetic polarity timescale with a total of 12 tie points ranging from the Brunhes (Chron C1n; beginning at 0.781 Ma) to the top of Chron C5n (9.786 Ma). In collaboration with biostratigraphic results, we identified three substantial hiatuses. The youngest spanned from within Chron C2n to the top of Chron C2An.1n. The second spanned all of Chron C3n to the top of Chron C3An, and the third eliminated Chron C4n through part of Chron C4r.

Rock magnetic studies were carried out on samples from Holes U1456A and U1456D and point to a complex array of magnetic minerals including iron sulfides (greigite) and iron oxides (magnetite, maghemite, and hematite). No behavior indicative of goethite was observed. Further study is necessary to determine which minerals are likely detrital (with the potential of constraining weathering on the continent) and which formed during diagenesis.

The physical property data collected for Site U1456 includes *P*-wave velocity, bulk density, magnetic susceptibility, and natural gamma radiation (NGR) on whole-round cores from Holes U1456A–U1456E and additional measurements on split cores and discrete samples including thermal conductivity; shear strength; *P*-wave velocity; porosity; and bulk, dry, and grain densities (Figure **F9**). Acquired data correlate with lithology, composition, and induration of the recovered section. Bulk density, *P*-wave velocity, shear strength, and thermal conductivity generally increase with depth from 0.8 to 2.4 g/cm^3, 1500 to 3400 m/s, 10 to 220 kPa (at ~360 mbsf), and 0.8 to 2.0 W/(m·K), respectively, whereas porosity decreases from nearly 80% to 50% at 150 mbsf, and then to ~20% at the base of the recovered section. This indicates that sediment compaction plays a significant role in physical property variations.

Lithologic changes are apparent in variations in NGR and magnetic susceptibility, which range from 10 to 80 counts/s and 0 to 400 SI units, respectively. Carbonate sediment has low NGR activity (10–35 counts/s average) and low magnetic susceptibility (0–20 SI units) and is dominant in Unit I and the lower part of Unit IV (deeper than ~975 mbsf) (Figure **F9**). Detrital sediments (such as sand, silt, and clay, or their lithified equivalents) that are abundant in Unit II have much higher average NGR activity (50–80 counts/s), magnetic susceptibility (50–150 SI units), and bulk density (1.8–2.0 g/cm^3) than the sediments of Unit IV. Unit III and the upper part of Unit IV show variable NGR but generally lower and less variable magnetic susceptibility than the other units (Figure **F9**). Grain density varies between 2.75 and 3.0 g/cm^3 with no visible downcore trend except for characteristically low and consistent values of 2.7 g/cm^3 in the lower part of Unit IV. Shear strength indicates that sediment ranges from soft (0–50 kPa) above 200 mbsf to stiff (150–220 kPa) from 200 to 360 mbsf, below which core material has a shear strength >220 kPa.

Two downhole logging tool strings were run in Hole U1456C, the triple combo (NGR, porosity, density, electrical resistivity, and magnetic susceptibility) and the FMS-sonic (NGR, sonic velocity, and electrical resistivity images) (Figure **F9**). All runs reached the total depth of the hole at 465 m WSF. Borehole log quality was affected by an enlarged borehole above 200 m wireline matched depth below seafloor (WMSF) and large and rapid variations in borehole size were found between 370 and 200 m WMSF. Below 370 m WMSF, the hole diameter was mostly in gauge, with few washed-out zones. Lithologic variations are apparent in the NGR, bulk density, porosity, and magnetic susceptibility logs, and these correlate well with measurements made on the recovered cores from Holes U1456A and U1456C. Density and sonic velocity increases from the top of the logs at ~80 m WMSF to the bottom of the hole are due largely to compaction and cementation with depth (Figure **F9**). A large increase in NGR and bulk density occurs between logging Units 2 and 3, which correlates to an increase in grain size from clay to silt and sand. Formation temperature measurements made with the advanced piston corer temperature tool (APCT-3) on Cores 355-U1456A-7H, 10H, and 13H indicate a geothermal gradient of ~57°C/km for the upper ~120 mbsf.

Distinctive changes in color, magnetic susceptibility, NGR, and gamma ray attenuation (GRA) bulk density were used to make hole-to-hole correlations between the sediment from Holes U1456A–U1456C. We constructed a spliced section for Site U1456 from the seafloor to ~142 m core composite depth below seafloor (CCSF). This spliced interval includes the Upper Pleistocene (~1.3 Ma) to recent.

We were also able to correlate core data from Holes U1456A and U1456C to wireline logging data collected in Hole U1456C. The NGR signal was sufficiently high that we could make unambiguous correlations between the core data and logs in the interval logged through pipe (0–81 mbsf). Distinctive magnetic susceptibility signals were very useful for correlating cores to the logs between 150 and 450 mbsf.

Site U1457

Background and objectives

Site U1457 (proposed Site IND-06B), the second drill site of Expedition 355, lies within Laxmi Basin in the eastern Arabian Sea (17°9.95′N, 67°55.80′E) in 3534 m water depth (Figures **F1**, **F2**). The site is ~490 km west of the Indian coast and ~760 km south from the present-day mouth of the Indus River, which is presumed to be the primary source of sediment to the area, at least since the Neogene and likely since the Eocene (Clift et al., 2001).

Laxmi Basin is flanked to the west by Laxmi Ridge and to the east by the Indian continental shelf (Figures **F1**, **F2**). Site U1457 lies on the western side of the basin at the foot of the slope leading to Laxmi Ridge. The seafloor appears to be relatively flat in the vicinity of Site U1457 (Figure **F2**); however, seismic reflection data show that the basement depth gradually increases to the east away from the site (Figure **F4**). The nature of the crust in Laxmi Basin is an enigma. Some workers have proposed that it is stretched continental crust (Miles et al., 1998; Todal and Edholm, 1998; Krishna et al., 2006) based on the reduced crustal thickness in Laxmi Basin (~6–7 km) compared to the neighboring thicker crust on either side (as thick as 17 km under Laxmi Ridge [Misra et al., 2015] and ~40 km under peninsular India [Singh et al., 2015]). In this model, Laxmi Ridge would be a continental fragment rifted from peninsular India (Naini and Talwani, 1983; Talwani and Reif, 1998; Minshull et al.,

2008). In contrast, some workers interpret Laxmi Basin to be of oceanic affinity based on magnetic anomalies reported within the basin. This latter model relates these magnetic anomalies to the early phases of seafloor spreading in the Arabian Sea (Bhattacharyya et al., 1994; Pandey et al., 1995), which removed a microcontinental Laxmi Ridge block from mainland peninsular India. In this scenario, Laxmi Basin would be analogous to its along-strike equivalent in Gop Rift to the northwest and Site U1457 would lie seaward of the oldest magnetic anomaly, requiring Laxmi Basin to be floored by oceanic crust.

Since the time of continental breakup at the end of the Cretaceous, Laxmi Basin has for the most part been tectonically inactive as seafloor spreading jumped to the west of Laxmi Ridge after ~62 Ma (Royer et al., 2002) so that the active extension is now far to the southwest. Seismic data from this region suggest that the process of postrift thermal subsidence has been interrupted by localized magmatic intrusions, but there has been no strong deformation of the basin since the end of extension, estimated to be prior to ~65 Ma based on magnetic anomalies within the basin (Bhattacharyya et al., 1994) or before 63 Ma based on the timing of the onset of seafloor spreading west of Laxmi Basin (Chaubey et al., 2002).

Although Laxmi Basin is separated from the main basin of the Arabian Sea by the topographic high of Laxmi Ridge, it has nevertheless been supplied by sediment from the Indus River and forms the easternmost part of the Indus Fan, the second largest such sediment body in the modern oceans. Proximity to peninsular India means that the basin must have been the recipient of some sediment discharge from rivers flowing to the west coast of the subcontinent, most notably the Narmada and Tapti Rivers (Figure **F1**), although their discharge is much less than that seen from the Indus River. Milliman and Syvitski (1992) estimated recent loads of 125 × 10^6 and 250 × 10^6 ton/y for the Narmada and the Indus Rivers, respectively, although some studies estimate Indus discharge as high as 675 × 10^6 ton/y (Ali and de Boer, 2008). Much of the flux from the Narmada and Tapti Rivers would tend to be ponded on the eastern side or in the central part of the basin rather than at or around Site U1457.

Site U1457 was originally proposed as an alternate site for meeting our basement objectives. The proposed deep penetration at Site U1457 aimed to reveal the Cenozoic evolution of the Indus Fan with the intention of reconstructing the weathering and erosion history of the western Himalaya. However, predrilling seismic interpretation suggested that this record would be truncated compared to that at Site U1456. Nonetheless, sediment recovered at this site should allow reconstruction of patterns and rates of erosion, as well as constrain how and when continental environmental conditions changed (e.g., humidity and vegetation patterns) in the Indus drainage since the late Miocene. In particular, we aim to test the hypothesis that major changes in the structural evolution of the Himalaya were driven by the changing strength of summer monsoon precipitation. For instance, the southward migration of the main thrust detachment fault to the location of the Main Boundary Thrust after 10 Ma may have accelerated the unroofing of the Lesser Himalayan Duplex and may be linked to the change in monsoon strength at ~8 Ma (Huyghe et al., 2001; Bollinger et al., 2004). Because Site U1457 is located in the distal fan and we estimated reasonably high sedimentation rates based on seismic ties to industrial wells with age control on the outer western continental shelf of India, the site was also designed to document high-resolution changes in weathering, erosion, and paleoenvironment during the Quaternary that can be related to millennial-scale monsoonal changes linked to solar and ice sheet–related forcing.

Because we were unable to sample the older sediment section and basement at Site U1456, Site U1457 was specifically planned to address questions pertaining to the nature of the basement in Laxmi Basin. In order to test the hypotheses of whether Laxmi Basin is oceanic or continental, we needed to directly sample the basement underlying the basin, which has significant implications for the breakup history of India and the Seychelles. In addition, analyses of sediment retrieved from Laxmi Basin will allow us to constrain depositional conditions in the basin, which may be used to reconstruct vertical tectonic motions and so determine the response of the lithosphere to the syn- and postrift tectonic stresses associated with continental breakup.

At Site U1457, we planned to core ~50 m into basement after penetrating a series of submarine fan sediments, as well as the large mass transport deposit encountered at Site U1456. Drilling was successful in reaching the basement, although we had time to penetrate only 16.27 m of basement below the sedimentary cover, recovering 8.72 m of basalt (Figure **F11**). The cored section at Site U1457 includes expanded upper Miocene to recent strata punctuated by some hiatuses or condensed sections (Figure **F12**), as well as lower Paleocene sediment that directly overlies the basement. A long hiatus separates the Paleocene sediment below from the Miocene sediment above. Nonetheless, using the samples and data generated at this site, we should be able to address questions related to changes in the monsoon at ~8 Ma, as well as how monsoon intensity varied after the onset of Northern Hemisphere Glaciation in response to this forcing. This is despite the moderate hiatus that occurs close to this time. In addition, we cored through ~190 m of mass transport deposit that likely represents the largest known deposit of this type in the geological record (Calvès et al., submitted). Studies focused on this interval and comparisons with the thicker section sampled at Site U1456 will help to identify the source of these deposits, as well as examine how such large deposits are emplaced, and may help us to understand the causes of this major event.

Operations

After a 62 nm transit from Site U1456, the vessel stabilized over Site U1457 at 1330 h (UTC + 5.5 h) on 16 May 2015. The original operations plan called for three holes: the first to APC refusal, followed by a second APC hole with XCB coring to ~500 mbsf. The third hole was planned as a single-bit RCB hole to 50 m into basement, which was estimated at ~970 mbsf. We ultimately cored three holes at Site U1457, although the second hole was cored to a shallower depth than originally planned (Table **T1**).

We reached APC refusal at ~110 mbsf. In order to deepen the hole more quickly, we opted to core a 4.7 m interval with the HLAPC, followed by a 4.7 m advance without coring. In the interest of time, we terminated the hole after reaching 144.8 mbsf. We then cored Hole U1457B for stratigraphic correlation purposes in the upper ~110 mbsf. After reaching APC refusal, we continued with the HLAPC using the coring by advance method to 204.7 mbsf, where we terminated the hole to preserve enough time to reach our objective in the deep hole. Hole U1457C was drilled without coring to 191.6 mbsf and then cored using the RCB to 1108.6 mbsf, which included ~16 m of basement penetration. Hole U1457C was terminated when time allotted for the expedition expired.

A total of 136 cores were collected at this site. The APC coring system was deployed 24 times, recovering 202.73 m of core over

218.9 m of penetration (93% recovery). The HLAPC system was deployed 15 times, recovering 71.22 m of core over 70.9 m of penetration (101% recovery). The RCB coring system was deployed 97 times, recovering 436.96 m of core over 917.0 m of penetration (48% recovery).

Principal results

The cored section at Site U1457 is divided into five lithologic units based on Holes U1457A–U1457C (Figure **F11**). Lithologic Unit I consists of a ~74 m sequence of Pleistocene light brown to light greenish nannofossil ooze including foraminifer-rich nannofossil ooze and nannofossil-rich clay, interbedded with silty clay and silty sand. Unit I here is similar to Unit I at Site U1456 in being mostly muddy and carbonate rich. The silty sand layers show normal grading and sharp erosive bases and are interpreted as turbidities. The hemipelagic nannofossil ooze and nannofossil-rich clay show intense burrowing and also include common pyrite nodules and veins. Quartz, feldspar, and mica grains are common in Unit I, whereas heavy minerals (hornblende, clinopyroxene, epidote, garnet, and augite) are rare.

Lithologic Unit II is ~311 m thick and is dated to the early Pleistocene. The unit consists mainly of light brownish gray to dark gray silty clay and dark gray sandy silt. Silty clay layers are typically massive and interbedded with very thin gray sandy silt layers, which are interpreted as turbidites. Unit II at Site U1457 is similar in age to Unit II at Site U1456, but the sediment is much finer grained. Light and heavy silt- to sand-sized mineral grains are more abundant in Unit II compared to Unit I.

Unit III is ~450 m thick and consists of upper Pliocene to upper Miocene semi-indurated to indurated light brown to dark green silty claystone, light brown to dark gray silty sandstone, light greenish nannofossil chalk, and light to dark greenish gray nannofossil-rich claystone. Nannofossil chalk and nannofossil-rich claystone cycles of sedimentation are separated by intervals dominated by clay/claystone and sand/sandstone deposition. Strong bioturbation is mostly observed in the nannofossil chalk and nannofossil-rich claystone. Silty sandstone layers are characterized by sharp erosive bases and grade upward into silty claystone intervals. The silty sandstone and silty claystone of Unit III occasionally have very thin (<1 cm) wood-rich layers, as well as large numbers of tiny wood particles. Unit III contains abundant light minerals with variable amounts of heavy minerals.

Miocene Unit IV is ~225 m thick and consists of a mixture of interbedded lithologies dominated by dark gray to greenish gray massive claystone, light greenish massive calcarenite and calcilutite, breccia, and limestone, particularly toward the base of the unit. Deformation structures are widespread throughout this unit, including microfaults, soft-sediment folds, slickensides, and tilted to vertical bedding, which are indicative of a mass transport deposit. Light minerals are abundant in Unit IV, whereas heavy minerals are only present in trace amounts. Clasts of vesicular volcanic rock and shallow-water limestone in the breccia point to a source from the Indian continental shelf, with possible erosion from the Deccan Plateau province.

The ~30 m thick Paleocene Unit V consists mostly of dark brown to dark greenish gray claystone and dark gray to black volcaniclastic sediment that overlies the basaltic basement. There is a major hiatus between Units IV and V determined from biostratigraphy, as well as the change in facies between debris-flow breccia above and mudstone underneath. The dark brown massive claystone shows very small amounts of interbedded dark greenish gray silty claystone. The thick dark greenish gray claystone contains black, discontinuous manganese layers and nodules, as well as small (1 to 3 cm) gray inclusions and rare parallel bands that are identified as carbonate-cemented nodules. Unit V contains abundant glass particles, trace amounts of light minerals, and no heavy minerals.

Core catcher samples and additional samples from split core sections at Site U1457 were analyzed for calcareous nannofossils, planktonic foraminifers, diatoms, and radiolarians. Microfossil assemblages are typical of subtropical to tropical water masses. Diatoms and radiolarians are found in the mudline sample in Hole U1457B, where they are well preserved. Diatoms in the mudline sample consist of mainly coastal species that have been transported to the site location. Diatom abundance decreases rapidly downcore, with specimens mostly restricted to the uppermost ~50 cm at Site U1457. Radiolarians are very rare and poorly preserved in the uppermost cores and only occur sporadically below.

Preservation of calcareous nannofossils and planktonic foraminifers varies from poor to good throughout Site U1457. Both groups are abundant in Unit I. Nannofossils are sparse and planktonic foraminifers usually absent in the clay/claystone that dominates Unit II. In Unit III, nannofossils are common in abundance, whereas planktonic foraminifers are less abundant and vary from rare to common. Reworked Cretaceous and Paleogene nannofossils are common through Units I–III. Within Units IV and V, both nannofossils and foraminifers are moderately to poorly preserved, with varying abundances. There is also an interval characterized by mixed Paleogene to early Neogene taxa that hamper age interpretation within the lower part of Unit IV. Calcareous nannofossils and planktonic foraminifers are common in the uppermost part of Unit V but rapidly decrease in abundance downcore through this unit, which overlies the basement.

The chronostratigraphic framework for Site U1457 is based on calcareous nannofossil and planktonic foraminifer biostratigraphy, together with magnetostratigraphy (Figure **F12**). The succession of calcareous nannofossil and planktonic foraminifer events indicates that Site U1457 spans the early Paleocene through recent, albeit with a very long hiatus (~50 million years) between lower Paleocene and upper Miocene sediment. The biostratigraphic framework established at Site U1457 enabled identification of three unconformities and an interval of mass transport in the recovered Neogene section. Calculated sedimentation rates at Site U1457 suggest that the sedimentation rate appears to have been relatively consistent in the late Miocene at ~17 cm/ky, although deposition was interrupted for ~0.50 million years around 8 Ma. Sedimentation rates were somewhat lower after sedimentation resumed following this hiatus, averaging ~10 cm/ky during the remainder of the late Miocene. There is some evidence for a short interval dominated by slower, hemipelagic sedimentation between ~6 and 7.4 Ma. There is an ~2 million years hiatus that spans the Miocene/Pliocene boundary and early Pliocene. The sedimentation rate in the late Pliocene to early Pleistocene was ~4 cm/ky. After another ~0.45 million years hiatus in the early Pleistocene, sedimentation rates for the remainder of the early Pleistocene were much higher (~58 cm/ky) during deposition of Unit II. The sedimentation rate slowed down from the late early Pleistocene to present, averaging ~7 cm/ky).

We cored ~16.27 m into igneous basement at Site U1457, recovering 8.72 m of basalt. Texture ranges from aphyric to phyric. The aphyric material occurs in three intervals and consists mostly of altered glass. Phenocrysts vary from being absent to making up as much as 10% of the rock and are composed of clinopyroxene, plagioclase, and olivine. Phenocryst grain size ranges from 1 to 5 mm,

with a mode of ~3 mm. The groundmass is mostly aphyric and may contain mesostasis. The basalt is nonvesicular and massive and contains veins up to 3 mm in width and of variable lengths that are filled with calcite. These rocks are classified as clinopyroxene-plagioclase-phyric basalt and plagioclase-clinopyroxene-phyric basalt, with the former the more dominant lithology. The basalt is only slightly altered.

Geochemistry measurements at Site U1457 aimed to characterize the distribution of hydrocarbon gases, sediment geochemistry (including carbon, nitrogen, sulfur, and carbonate contents), and interstitial water composition. Sulfate concentration in the interstitial water decreases sharply in the upper 60 mbsf, indicating anaerobic sulfate reduction. Below the sulfate reduction zone, methanogenesis is likely active, reflected by a peak in methane concentrations between 65 and 200 mbsf. A second interval of methane increase is observed between 400 and 550 mbsf, which correlates with Unit III. Higher TOC values through this interval are indicative of lithologic control on the methane concentrations. Below 590 mbsf, methane levels do not exceed 10,000 ppmv and progressively decrease with depth.

Alkalinity, ammonia, and phosphate in interstitial water are produced as byproducts of organic matter degradation in the upper 60 mbsf, within the sulfate reduction zone. Increased alkalinity in this interval helps to precipitate calcium and magnesium in carbonate minerals, resulting in a decrease in calcium and magnesium concentrations. Manganese concentrations in the interstitial water also decline sharply in the uppermost 60 mbsf within the sulfate reduction zone, where hydrogen sulfide is being produced as a result of anaerobic organic oxidation reactions. Dissolved iron concentrations are low and decrease downhole, suggesting its removal from the interstitial water through metal sulfide formation under anaerobic conditions. Dissolved silica concentrations are high in the uppermost 110 mbsf, which may be caused by its release during the dissolution of biogenic silica, which is consistent with the near-absence of siliceous microfossils in this interval. Barium concentrations in the interstitial water increase somewhat between 600 and 850 mbsf, which could be a result of its release through barite dissolution under low-sulfate fluid conditions or through the leaching of aluminosilicate minerals.

Total carbon and $CaCO_3$ contents are highly variable at Site U1457 and are tightly coupled, indicating that most of the carbon is present as $CaCO_3$. Carbonate content is generally higher in Unit I, particularly in the nannofossil ooze and nannofossil-rich clay (20–75 wt%) intervals. A decrease in carbonate content between Units I and II reflects a transition to lithologies that are dominantly siliciclastic. Carbonate-rich intervals (33–47 wt%) in Unit III correspond to intervals of nannofossil ooze. TOC values at Site U1457 vary between 0.02 and 2.58 wt%. As with Site U1456, we report TOC/TN as a preliminary estimate for the source of organic material. Typically high values (TOC/TN > 12) in marginal basins are interpreted as an indicator of terrestrial organic input (Müller and Mathesius, 1999). However, an alternative model to explain high TOC/TN ratios, such as those observed in some organic carbon-rich marine sediments (e.g., sapropels and black shales), invokes marine algae synthesizing lipid-rich organic carbon during times of abundant nutrient supply and/or diagenetic factors (Meyers, 1997). In Unit I, three distinct intervals with high TOC/TN (>12), correspond to beds of carbonate ooze. The dominantly hemipelagic nature of this lithology precludes confident assignment of the high values to terrestrial input and awaits further shore-based analysis. Intermediate TOC/TN values (4.5–11.4) suggest mixed marine/terrestrial organic input in Unit II and the upper part of Unit III. Low TOC/TN values (0.3–8.7) in Unit IV suggest predominantly marine organic matter input. Due to time constraints, shipboard analysis of samples from Unit V and the igneous basement were not conducted.

A total of 12 whole-round samples (5 cm long) were collected for microbiological studies at Site U1457. All samples were collected adjacent to interstitial water whole-round samples for comparison to geochemical analyses. After collection, samples were immediately flushed with N_2 and processed for shipboard analysis or preserved for shore-based analyses. Fluorescent microspheres were used as tracers during APC operations to help determine contamination in microbiology samples. Microsphere samples were collected from the exterior and interior of each core, as well as a location in between. Microspheres were completely absent in samples from the interior of the cores, indicating no apparent contamination. Samples from intermediate positions contained a low concentration of microspheres and the presence of significant numbers of microspheres in exterior samples is a strong indication of surface contamination to the outside of the core during the coring process.

We analyzed some samples on board for microbial community structure. The direct microscopic observation of the core samples found different kinds of meiobenthos in sediment from Site U1457. Preliminary results of microbial community structure and enumeration show that fungal communities are present at very low concentrations in samples from 0 to 100 mbsf. These fungi living in the subsurface form diverse communities and interactions with other living organisms. While surveying for possible symbioses between fungi and meiobenthos, we found abundant assemblages in certain zones showing that these may follow trends related to the carbon, nitrogen, and sulfur cycles. Shore-based molecular studies are required to support the evidence of their relationship and to pinpoint exactly the phylogenetic positions of these new extremophiles.

At Site U1457 we performed paleomagnetic analyses on archive-half sections from Holes U1457A and U1457B and on discrete samples from all holes. Archive-half section measurements produced reliable results for the upper ~60 mbsf; results were more ambiguous in the deeper sections. Discrete samples were fully demagnetized by alternating field treatment and the inclination of the magnetization's stable component was used to define the magnetostratigraphy. A composite polarity log was constructed from the three holes and correlated with some confidence to the geomagnetic polarity timescale with at least 16 tie points, which range from the Brunhes (Chron C1n; beginning at 0.781 Ma) to the top of Chron C5n (9.786 Ma).

Using the combination of magnetostratigraphy and biostratigraphic data, we identified three substantial hiatuses or condensed sections. The early Matuyama (much of Chron C2r) and the top of the Gauss (Chron C2An) may be missing or are condensed. Chrons C3n and C4n are completely missing. Similar to Site U1456, there is an "extra" subchron that is not in the official timescale, which is located between the Cobb Mountain (Chron C1r.2n) and the Olduvai (Chron C2n). The identity of this subchron (which could be the Garder [1.472–1.48 Ma] or the Gilsa [1.567–1.575 Ma] according to Channell et al. [2002]) could help constrain the age model during this interval of very rapid sedimentation.

Paleomagnetic data from the lowermost sediment cores are well behaved, with an average inclination of 39°. If these are indeed Paleocene in age, they are reversely magnetized and translate to a

paleolatitude for the site of ~22°S, which is in reasonable agreement with a paleolatitude of between 16°S and 25°S for 60–65 Ma (Besse and Courtillot, 2002).

The physical property data collected for Site U1457 includes bulk density, *P*-wave velocity, magnetic susceptibility, and NGR on whole-round cores from Holes U1457A–U1457C and additional measurements on split cores and discrete samples including thermal conductivity; shear strength; *P*-wave velocity; porosity; and bulk, dry, and grain densities (Figure **F11**). Acquired data correlate with lithology, composition, and induration of the recovered section. Bulk density, *P*-wave velocity, and thermal conductivity generally increase with depth from 1.4 to 3.0 g/cm^3, 1500 to 5600 m/s, and 1 to 2.6 W/(m·K), respectively, whereas porosity decreases from ~80% to 50% in the upper 100 mbsf, and then to ~20% at the base of Unit IV. Shear strength varies between 10 and 70 kPa in the upper 150 mbsf, indicating that the sediment is soft and uncompacted.

Generally, the changes in physical properties are gradual, indicating that sediment compaction plays a significant role in physical property variations (Figure **F11**). However, shifts in porosity, bulk density, and thermal conductivity are seen between lithologic units, demonstrating the influence lithology has on physical properties. For example, between Units I and II, lithology changes from soft carbonate ooze and clay to detrital silt, clay, and sand, resulting in an increase in bulk density and thermal conductivity and a decrease in porosity. NGR also increases across this boundary (from ~30 to ~60 counts/s), whereas magnetic susceptibility becomes less variable and generally lower in Unit II compared with Unit I. At the base of Unit IV below 1000 mbsf, *P*-wave velocity abruptly increases to values up to 4300 m/s, reflecting the occurrence of high-density calcarenite and breccia, which contrasts with lower values for the overlying claystone (2000 m/s). NGR and magnetic susceptibility dramatically decrease over this same interval. A return to lower bulk density (~2.0 g/cm^3) and *P*-wave velocity (~2000 m/s) occurs within Unit V above the igneous rock at the base of Core 355-U1457A-96R. The recovered basalt has characteristically high bulk densities (~2.6 g/cm^3), magnetic susceptibility (~3000 instrument units), and *P*-wave velocities (4500 to 5500 m/s), but low NGR (~1 count/s). A geothermal gradient of 53°C k/m for the upper ~100 m was estimated from the APCT-3 measurements taken on Cores 355-U1457A-4H, 7H, and 10H.

Distinctive changes in color, magnetic susceptibility, NGR, and GRA bulk density were used to make hole-to-hole correlations between the sediment in Holes U1457A and U1457B. Correlations were limited to these two holes because there was minimal overlap with the cored section of Hole U1457C, and no opportunity for wireline logging. We constructed a spliced sediment section for Site U1457 from cores recovered from Holes U1457A and U1457B. The splice is good down to ~88 m CCSF or ~1.2 Ma. With appended cores, the Site U1457 splice was extended to 123.55 m CCSF. Profiles in the spliced section of Site U1457 of magnetic susceptibility change (clay content) and color change ($CaCO_3$ variations) are similar to those at Site U1456. Initial age correlations support the hypothesis that the variations can be used to make lithostratigraphic correlations between the two sites.

Expedition synthesis

Operations during Expedition 355 (31 March–31 May 2015) drilled two sites in the central and western parts of Laxmi Basin in the eastern Arabian Sea, Indian Ocean. Laxmi Basin separates the Indian continental shelf in the east from Laxmi Ridge in the west. Site U1456 lies within Laxmi Basin and was cored into the lower–middle Miocene. The second site, U1457, penetrated to igneous basement in the transition zone between Laxmi Basin and Laxmi Ridge. In total, we recovered 1712 m of sediment and sedimentary rock, as well as 8.72 m of igneous basement. We further collected downhole wireline logs at Site U1456 using the triple combo and FMS-sonic tool strings. We present here the initial findings of our analyses of these materials and data, which provide (1) an improved understanding of how the Indian Ocean first began to drift as India separated from the Seychelles and (2) partial constraints on erosion in the source regions that have supplied sediment into the Arabian Sea since that time. Much of the recovered sediment was derived from the Indus River, and this provides us with an opportunity to document the weathering and erosional responses of the western Himalaya to changes in monsoon strength during the recovered intervals, largely during the latter parts of the Neogene. We also collected sediment that provides information about erosion and mass transport from the continental margin of western India.

Rift tectonics in the eastern Arabian Sea

The eastern Arabian Sea evolved after the breakup of Madagascar and India in the mid-Cretaceous and between India and the Seychelles during the Late Cretaceous (Norton and Sclater, 1979; Courtillot et al., 1988). The rifting between India and the Seychelles is thought to have initiated in the Gop Rift, leading to final continental breakup. The rapid rifting (Royer et al., 2002) propagated southward into Laxmi Basin before aborting after a ridge jump at the time of Anomaly 28 to the west of Laxmi Ridge (Collier et al., 2008). The nature of crust in Laxmi Basin has been the subject of vigorous debate, and sampling the igneous basement to provide field-based constraint on the history of the rift tectonics was one of the primary scientific objectives of Expedition 355. In order to achieve this objective, we originally planned to core ~100 m into the basement at Site U1456 in Laxmi Basin. The sediment cover at this site was estimated at ~1470 m thick, so we planned a reentry system to improve our chances of success. We initially installed a casing string with reentry cone to ~455 mbsf in Hole U1456D and then continued to core to 1024.4 mbsf. After pulling out of the hole for a bit change, the drill string became stuck while trying to run back to the bottom of the hole. We ultimately had to sever the pipe and abandon Hole U1456D. Because we assumed that unconsolidated sands between ~500 and 720 mbsf had collapsed around the drill string while trying to reenter the hole, we decided to install a reentry system in a new hole (U1456E) to 750 mbsf, below the base of the sand. Coring continued to 1109.4 mbsf in Hole U1456E. After once again pulling out of the hole for a bit change, we encountered similar problems trying to work the bit back to the bottom of the hole. At this time it became apparent that swelling clays were binding the drill string and drill bit and we decided to abandon the site and attempt to achieve our deeper objectives (Paleogene and basement) at an alternate site (see **Operations**).

Although we were unable to core into basement at Site U1456, we did core through most of the postrift strata in Laxmi Basin at this site. Considering that surface processes (e.g., erosion) significantly control the dynamics of a rift basin by redefining the surface load distribution through infilling accommodation space, information collected at Sites U1456 and U1457 will be important for examining the postrift development of this basin and thus its origin. Physical and lithologic knowledge gathered from Site U1456 is equally important in determining the geometry and volumes of the sedimentary load. Wireline log data collected at Site U1456 should

allow for better regional stratigraphic correlation and precise determination of postrift sediment budget.

Because coring through the base of the fan into the basement was one of the primary objectives of this expedition, we opted to core at Site U1457, which was originally an alternate site for the basement objective. Site U1457 is located in the western Laxmi Basin, with a similar, if somewhat reduced (~1100 m), stratigraphy overlying the basement. We ultimately recovered 8.72 m of basalt, as well as associated volcaniclastic sediment, using a single RCB bit in an uncased hole. Because the igneous basement at Site U1457 was recovered at the end of the expedition, we only described the cores visually. Additional shore-based geochemical analysis after the end of the expedition is required to determine if this is a truly oceanic rock formed by seafloor spreading and melting of the upper mantle, or if it might be contaminated either by underlying continental crust or continental flood basalt related to the mantle hotspot of the Deccan Large Igneous Province.

Heat flow data measured at each site provides additional constraints to infer the rift history in Laxmi Basin. Average heat flow measured at Site U1456 is 57 mW/m^2, whereas heat flow at Site U1457 is 60 mW/m^2. Comparison with other data from the Arabian Sea (Figure **F13**) shows that Laxmi Basin is warmer than many parts of the Arabian Sea, in particular those regions close to the Indus Delta and the Murray Ridge (Calvés et al., 2010). Our sites also have higher heat flow than those in the eastern and northern sides of Laxmi Ridge. This could be attributed to the late-stage intrusion of volcanic features into the basin, west of Panikkar Ridge, as seen in Figure **F3**. Stein and Stein's (1992) compilation of oceanic crustal heat flow data indicates that the observed heat flow values at our sites are equivalent to oceanic crust of 76 and 84 Ma age. If the magnetic anomalies interpreted by Bhattacharyya et al. (1994) are considered to be a reliable estimate of the timing of extension, then rifting in Laxmi Basin would have occurred between 63 and 84 Ma (Anomalies 28–33). This age would be consistent with the measured heat flow values but requires that no later thermal rejuvenation occurred, yet late-stage intrusions are seen in the seismic profiles, making this assumption somewhat problematic. This is because if the heat flow at our drill sites is normal and oceanic then the lower values in the eastern and northern Laxmi Basin would be anomalous in that they are colder than oceanic crust of corresponding age. This in turn would imply either that the crust in those areas is not oceanic or that the measured locations are positioned in cooler than average regions related to local heat flow patterns. Heat flow tends to be normal or higher than average where oceanic basement is flat but depressed in the vicinity of seamounts, which themselves are elevated due to discharge of warm fluids where the sediment cover is thin or nonexistent (Villinger et al., 2002).

The measured heat flow values are also compatible with models that consider Laxmi Basin to be extended continental crust. The basin has significant water depths that imply large degrees of extension. This combined with the clear presence of volcanic seamounts in the basin, especially along Panikkar Ridge, implies at least 200% extension ($\beta > 3$) in order to explain melting in the ambient upper mantle (McKenzie and Bickle, 1988). Comparison with a pure shear rifting model (McKenzie, 1978) indicates that if $\beta > 3$, then heat flow should be >54 mW/m^2 (rifting finished at 63 Ma) or >48 mW/m^2 (rifting finished at 84 Ma). Because the younger age is more likely and extension could be somewhat more than $\beta = 3$, we conclude that our measured heat flow is also consistent with an extended continental origin for Laxmi Basin.

Therefore, in order to distinguish between the two plausible models as described above, geochemical analyses and radiometric age dating of basement rocks obtained at Site U1457 are essential. The precise radiometric dating of the recovered samples will establish the rifting age, whereas geochemical data will ascertain their continental or oceanic affinity.

Fan sedimentation

Drilling in Laxmi Basin at Site U1456 confirmed the presence of thick upper Miocene and younger strata (~700 m), as observed on the seismic profiles (Figures **F3** and **F14**). The presence of sandy channels within the upper Units I–III shows that the fan is built up by a series of overlapping lobes. Units I–III at Site U1456 and Unit III at Site U1457 form parts of the Indus submarine fan. Although the locations of both sites are ~800 km from the modern river mouth, the reflective character of the seismic image covering these units marks them as being part of the Indus Fan Megasequence of Droz and Bellaiche (1991). This means that they are lateral equivalents of sequences with clear channel-levee complexes in the proximal upper fan. In those more proximal areas the channels are accretionary, not erosive features. Smaller channel-levee complexes are better developed around Site U1457 (Figure **F15**), but in both locations the reflectors tend to be mostly parallel and with only modest onlapping relations between successive depositional packages. In contrast, the seismic images show that the strata are incised by channels that have cut and fill geometries, and at Site U1457 drilling passed through the side of one of these channels (Figure **F15**). Taken in this context, the units drilled at Site U1456 can be understood as representing not only records of weathering and erosion but also different parts of the fan architecture. Presently both sites lie within an area that would be considered "lower fan" under the simple classification scheme of Walker (1978).

Unit II at Site U1456 is by far the coarsest grained of the sequences recovered, although the low recovery in Unit III, which was only sampled by RCB coring through all but the top of this unit, may also be much sandier than is apparent from the recovery (Figure **F9**). RCB coring is inefficient at recovering unconsolidated sand, and this may lead to a bias in our documentation of the unit if the coring preferentially recovered clay and claystone. The sand of Unit II may represent a depositional lobe on the fan where turbidity currents dropped their suspended load as they decelerated after exiting an incised or leveed channel. Seismic evidence rules out this sequence being a channel complex, and there is also little seismic evidence for leveed channels in this area. Channel deposits are often stacked massive sandstone (Hartog Jager et al., 1993; McCaffrey et al., 2002), but Unit II does not show this type of sequence. Instead, it is characterized by common muddy interbeds between the sand beds that suggest the depositional character is more distal. The cores, in conjunction with seismic data, indicate that Unit II is a "sheet lobe" complex as defined by Mutti (1992), contrasting with the coarser grained "mounded lobes" of Normark et al. (1979). Sheet lobes tend to be more subdued in their bathymetry and are associated with muddier depositional systems, much like the Indus Fan. They are also associated with moderate to strong incised channeling, which is a feature of the sequence in the area of operations (Figure **F14**).

If Unit III at Site U1456 is really sand-rich below ~450 mbsf, then this sediment could also be a sheet lobe complex separated from Unit II by a ~75 m thick interval of more muddy sediment mixed with carbonate deposits that would correspond to overbank

or distal hemipelagic sediments (Figure F9). However, if the bulk of Unit III is basically similar to the material that was actually recovered, then this unit would be more like a sequence of basin plain sheet turbidites that represent the distal equivalent of the coarser, thicker bedded sheet lobes (Mutti, 1977; Reading and Richards, 1994). In this context we can imagine Laxmi Basin being the recipient of sediment as sheet-like turbidites during deposition of Unit III, and then being abandoned as the active lobe avulsed to other parts of the Arabian Sea, followed by another pulse of coarse sand sedimentation as an active lobe was reestablished east of Laxmi Ridge during deposition of Unit II. We emphasize that changes in grain size probably represent autocyclic processes of avulsion within a fan complex and do not necessarily represent changes in erosion rates onshore. Thus linear sedimentation rates at Site U1456 and U1457 are not proxies for rates of sediment supply to the fan on a regional scale.

Why is Unit I so muddy and carbonate rich when global estimates of terrestrial erosion and deltaic/fan sedimentation point to this being a time of very high erosion and sediment transport (Métivier et al., 1999; Zhang et al., 2001)? The Holocene of the Indus Fan is characterized as being a carbonate drape (Kolla and Coumes, 1984), which is interpreted to reflect cessation of deepwater sedimentation as a result of postglacial sea level rise (Prins et al., 2000) and subsequent sediment sequestration on the shelf and in the upper canyon (Clift et al., 2014). Such an explanation cannot answer the relative lack of clastic sedimentation through the entire lithologic Unit I because this covers the last ~1.2 million years, spanning much of the Pleistocene, during which time there have been many sea level cycles and plenty of opportunities for the accumulation of "lowstand" fan deposits. We speculate that since 1.2 Ma the active lobes of the Indus Fan have been located west of Laxmi Ridge, allowing a dominantly muddy and hemipelagic sequence to accumulate at our drill sites. It is possible that the higher carbonate content of Unit I could also reflect greater biogenic productivity and a deeper carbonate compensation depth (CCD) at that time. This is a sequence in which there is also some influence related to discharge from peninsular India (see below).

Sediment provenance

Reconstructing the erosion of the western Himalaya is a key goal of Expedition 355, and consequently we need to distinguish sediment delivered from the delta of the Indus River from that which might be a product of erosion in peninsular India. Some of this work requires shore-based geochemical work, but initial studies on board are able to pinpoint the influence of the Indus using traditional microscopy applied to heavy minerals. Sand and silt in Unit I at Site U1456 show the presence of abundant muscovite, a mineral that is particularly common in the modern Indus River (Garzanti et al., 2005) and in the Indus Delta since the Last Glacial Maximum (Clift et al., 2010), as well as quartz and feldspars. Furthermore, a strong link to the Indus River is demonstrated by the presence of tourmaline, epidote, and especially high-grade metamorphic minerals such as kyanite and sillimanite (Figure F16). Augite was also observed (Figure F16A). Although this phase is indicative of a volcanic source, this mineral could either point to erosion from the Deccan Flood Basalts exposed on the peninsula or the Kohistan arc within the Indus Suture Zone, making this a nonunique proxy. Evidence from combined Sr and Nd isotopes close to the Laccadive Ridge indicates variable sediment supply from the Indus River and peninsular India to sedimentary basins at the foot of the continental slope and even perhaps from the Bay of Bengal driven by monsoon-controlled currents (Goswami et al., 2012). We do not rule out sediment supply from peninsular India to Laxmi Basin; we only argue that the provenance indicates that this source is a minor portion of the flux for most time periods, at least at these drill sites.

Unit II at Site U1456 shows a similar heavy mineral assemblage, but the minerals are present in much greater abundance and with additional minerals including garnet, blue-green calcic amphibole, and clinopyroxene. Most significantly, microscopic analysis identified rare sodic amphiboles, such as glaucophane (Figure F16D) and hypersthene (Figure F16F), which require erosion from a source that experienced high-pressure, low-temperature metamorphism (blueschist facies) of a type normally associated with subduction complexes (Miyashiro, 1994). Few such sources are known in peninsular India. Proterozoic blueschists are known from the Delhi fold belt in Rajasthan (Sinha-Roy and Mohanty, 1988), but even those parts of this terrane that do drain into the Arabian Sea are not currently rapidly eroding and would not be expected to have undergone much exhumation during the Cenozoic. Instead, the presence of glaucophane and hypersthene strongly suggest erosion from the Indus Suture Zone where a series of subduction-related rocks are exposed. The best documented blueschist exposures within the Indus catchment lie along the Main Mantle Thrust in Kohistan in the Shangla area of that magmatic arc complex (Anczkiewicz et al., 2000). Other areas are known to have eclogites, associated with continental subduction, such as the Tso Morari Complex in Ladakh (Donaldson et al., 2013) and Kagan in Pakistan (Tonarini et al., 1993), but these do not yield large volumes of glaucophane, and in the case of Tso Morari, were likely not areas of rapid erosion since the late Miocene. Other suture zone blueschists are eroded into the Brahmaputra and are not relevant here (Chatterjee and Ghose, 2010). This provenance demonstrates a direct link between the main stream of the Indus River and the fan at Sites U1456 and U1457.

Unit III at Site U1456 also shows a dominant Indus-derived mineralogy, including blue-green hornblende, clinopyroxene, epidote, rare garnets, and trace amounts of kyanite, chloritoid, apatite, zircon, tourmaline, and rutile, but no glaucophane. This does not necessarily mean that the river was no longer draining the Shangla blueschists, but rather that erosion from that area was heavily diluted by flux from other areas of the hinterland, much as it is today (Garzanti et al., 2005). Additional dilution from peninsular sources is possible, but with current information there is no suggestion that this was volumetrically significant.

Much of Unit IV, which is interpreted largely as a mass transport deposit, has a different provenance from the overlying units. Heavy minerals found in this unit include hornblende, actinolite, epidote, and garnet, with traces of zircon, tourmaline, spinel, and rutile, but not the typical high-grade assemblage with abundant mica seen in the three shallower units (Figure F16). For example, tourmaline can be found in granitic or metamorphic rocks but is not unique to the Greater Himalaya. Breccia interbedded with the siltstone (discussed below) is dominated by large fragments of shallow-water limestone, as well as much lower volumes of pebbles of vesicular basaltic rock. Unit IV provenance points to derivation from the western coast and continental margin of India, where similar sediment is found, such as Eocene–Miocene carbonates in the western parts of the Bombay offshore (Whiting et al., 1994; Rao and Wagle, 1997).

The only exception to this otherwise uniform pattern for Unit IV is the final lower–middle Miocene sandstone-dominated core at the base of the unit in Hole U1456E. This shows a return to a different, Indus-like provenance with a heavy mineral assemblage con-

sisting of hornblende, with common epidote and garnet, and rare tourmaline, apatite, titanite, and chloritoid. These sediments represent the oldest evidence at Site U1456 for an active Indus River draining a Greater Himalayan source in the late early or early middle Miocene. With only 2.82 m recovered sediment it is not possible to define the depositional setting beyond this being a sandy fan turbidite, which is most similar to the sheet lobe deposits in the Pliocene–Pleistocene. There is a thin sequence of Paleocene brown and dark gray claystone at Site U1457 that underlies the mass transport deposit, but its origin and nature are even more obscure. Calcareous nannofossil and planktonic foraminifer assemblages date these deposits to ~62–63 Ma, which is a little older than most estimates of India/Eurasia collision (Najman et al., 2010; DeCelles et al., 2014). However, some reconstructions do predict collision even as early as 65 Ma (Jaeger et al., 1989; Beck et al., 1995) and a minimum age from the fan would be useful in assessing such end-members, if the Paleocene did prove to be derived from within or north of the Indus Suture Zone. The sediment itself is massive and muddy with modest amounts of silt. This could be a distal hemipelagic deposit to an early Indus Fan or base of slope deposits of the western Indian continental margin, two alternatives that can be tested by postcruise isotopic-based provenance analysis. The claystone becomes darker and interbedded with volcaniclastic sediment with manganese mineralization downcore, which includes coarse breccia of basaltic character, similar to the underlying basalt interpreted as proximal hyaloclastite deposited synchronous with the volcanism during extension of Laxmi Basin. The flows are massive and not vesicular, which implies that they were erupted in significant water depths, likely >2000 m (Moore, 1970), as deepwater vesicular flows are mostly limited to subduction settings where volatile content is high. Although these depths imply normal depths for a seafloor-spreading center, they also indicate that there was no significant mantle thermal anomaly under the basin at the time of emplacement. This in turn indicates that Laxmi Basin may have opened before the start of Deccan Plateau magmatism at 65 Ma (Courtillot et al., 1988).

Mass sediment transport

Drilling at both sites resulted in sampling of a large complex of mass transported sediment, which volumetrically is estimated to be ~19,000 km^3, making it the largest such deposit known in any ocean basin worldwide (Calvès et al., submitted). This deposit is substantially larger even than the Storegga Slide from the Norwegian margin that redeposited 3500 km^3 around 6200 years ago (Bünz et al., 2003). Prior to our operations, the age of this mass transport deposit was poorly constrained as being middle to early Miocene (Calvès et al., submitted). On the basis of nannofossil assemblages and magnetostratigraphy, we demonstrate that sediment lying immediately above and within the mass transport deposit is dated at <10.8 Ma, whereas sediment lying directly underneath the deposit at Site U1456 is dated as 13.5–17.7 Ma (Figure **F10**). The hiatus under the deposit at Site U1457 is too long to provide tight age control on the emplacement. Because the catastrophic emplacement of these deposits may have caused significant erosion of the sediment present in Laxmi Basin before sedimentation, we do not interpret these ages to indicate that mass transport continued for >3.5 million years. Instead, we conclude that the section reflects at least two major phases of mass transport, probably both of them occurring at ~10 Ma. A short interval of hemipelagic claystone was found separating two sequences within which there is abundant structural and sedimentary evidence for catastrophic redeposition (e.g., small slump folds, faults, and high dips). In contrast, the claystone shows a normal paleomagnetic signature coupled with a microfossil assemblage that does not indicate significant reworking of older microfossils, such as seen in the rest of the mass transport unit.

Much of the mass transport deposit comprises claystone and silty claystone, with soft-sediment deformation in the form of folds and small brittle reverse faulting structures, consistent with being in the toe region of a large-scale slump (Bovis, 2003). There are examples of larger faults with slickensides indicating brittle deformation at the base of the deposit, which is ~330 m thick at Site U1456 and ~190 m thick at Site U1457. Steeply dipping beds and contorted, folded geometries mark the upper part of the main deposit, which is draped by a subhorizontal muddy blanket likely deposited in the immediate aftermath of the event. There is no sharp lithologic change to distinguish mass transport from the hemipelagic sediment, which are both composed of claystone. However, the mass transport deposit itself, largely comprising lithologic Unit IV at both sites, contains sediment with a strongly reworked microfossil assemblage eroded from Paleogene to lower Neogene sources, whereas the drape has a coherent microfossil assemblage with little reworking.

The mass transport deposit comprises two types of sediment. The first type is composed of well-bedded materials, which have undergone soft-sediment plastic deformation. These were presumably originally deposited on the outer shelf or continental slope of western India and were then largely redeposited en masse into the deeper parts of Laxmi Basin. This sediment tends to occur in the upper part of the mass transport unit. The second type of sediment in the mass transport deposit is composed of breccia dominated by angular clasts of limestone whose composition and microfossil content indicates original sedimentation in a carbonate-dominated setting and which must have been broken into the clasts that constitute the breccia during the emplacement of the mass transport deposit. Massive calcarenite is also associated with the breccia toward the base of the deposit. Suitable source rocks are present on the western Indian Shelf (Rao and Wagle, 1997). At Site U1456, the breccia is separated by a claystone-dominated sequence (Figure **F9**). This internal structure supports the suggestion that the emplacement of the mass transport deposit took place in two major phases. The breccia is associated with thick-bedded calcarenite that also represents high-energy resedimentation of carbonate material. Although the calcarenite could have been deposited on the Indian continental shelf adjacent to a carbonate platform and then transported into the present position, its association with the breccia units suggests that it represents high-energy deposits linked to the mass transport process itself. Brittle deformation is associated with the base of the two breccia intervals, whereas soft-sediment deformation dominated in the overlying muddier sequences.

Each phase of mass transport could have been made up of smaller depositional episodes, but we do not anticipate these being separated in time by long periods because there are no other hemipelagic drapes identified within the cores. We think it unlikely that Unit IV at Site U1456 represents a collection of small debris flows. The source of the mass transport deposit must be the Indian continental margin because it preserves a suitable sequence of Cenozoic shallow-water and slope deposits (Biswas, 1987; Whiting et al., 1994). Even the Deccan volcanic rock clasts can be derived from mass transport offshore because the province is known to extend out under the continental shelf (Karisiddaiah and Iyer, 1991; Pandey et al., 2011). In any case, suitable sources are not present on any other topographic high adjacent to Laxmi Basin (i.e., Laxmi Ridge or Panikkar Ridge). Laxmi Ridge has local development of shallow-water carbonates that must have accumulated soon after its initial

formation when the ridge crest was still located close to sea level and not in the ~3 km of water as observed today. Laxmi Ridge does have a modest hemipelagic drape (on the order of a couple of hundred meters along seismic Profile W06; Figure **F3**) but would not be a suitable source of shallow-water material spanning such a long period or for the voluminous amounts of clay and siltstone observed.

Moreover, given the long transport (~400 km) from the potential source region (Calvès et al., submitted), it seems unlikely that this deposit could represent the product of numerous small events, which would lack the gravitational potential to travel such great distances. Even if the precise origin of the deposit were disputed, the seismic images indicate a single pulse that stretches almost 400 km along Laxmi Basin, mostly north of Site U1456, without major similar events before or after. The deposit we cored is therefore likely caused by one or two large collapses of the outer shelf and upper slope. Such a collapse would be required to explain such long runout and volume. In contrast to the Storegga Slide, whose emplacement is associated with gas hydrate dissociation during a time of climatic change (Bünz et al., 2003), we do not yet understand what might have triggered the large-scale collapse of the Indian continental margin.

Preliminary scientific assessment

Expedition 355 was designed to obtain sediment and igneous basement samples from the eastern Arabian Sea to address two broad categories of objectives as outlined in the *Scientific Prospectus* (Pandey et al., 2014). Through coring into the sediment and basement of Laxmi Basin during this expedition we addressed many of our primary objectives and also made some additional findings that have significant geodynamic implications. The principal objectives outlined for this expedition are enumerated as follows:

1. *Reconstruct long-term changes in erosion and weathering rates at submillennial to millennial timescales in order to compare with existing records of high frequency climatic variability.*

All planned sites of Expedition 355 were designed to drill through the fan sediment in the eastern Arabian Sea to examine the erosional and weathering response of the western Himalaya, Karakoram, and Hindu Kush to the changing intensity of the southwest Asian monsoon at millennial to submillennial scales. Successful coring with the APC and HLAPC, which provided very good recovery through the upper parts of the sections at both Sites U1456 and U1457, provides an opportunity to reconstruct and model orbital-scale variations in erosion, weathering, environment, and climate. The well-constrained spliced sections generated through coring multiple holes at both sites, in conjunction with a robust age model, provide a mostly continuous high-resolution record of weathering and erosion during much of the Pleistocene (since ~2.0 Ma). The recovered intervals may allow us to determine whether the intensity of Himalaya chemical weathering had a role in controlling glacial cycles in the Northern Hemisphere. Significant hiatuses and/or condensed sections at ~1.8–2.2 and 3.6–5.6 Ma mean that we cannot follow the entire Pliocene–Pleistocene climate variation in terms of its erosional and weathering impact, but because a large number of glacial cycles are spanned by a relatively well recovered and expanded section, the general pattern and response to monsoon change by these processes should be amenable to study. The expanded section represented by Unit II at both sites provides an especially good chance to look at the erosional response to monsoon changes at the millennial scale. The sandy character of Unit II at Site U1456 may represent an even shorter amount of time and be deposited in a small number of turbidite events.

2. *Reconstruct changes in erosion and weathering intensity over tectonic timescales and assess whether any changes occurred at ~23, 15, and 10–8 Ma to test earlier hypotheses that invoke changes in monsoon intensity at those times.*

Cenozoic sedimentary sections from the Indus Fan are expected to record the erosional and weathering responses of the Indus drainage basin to large-scale climatic changes. Deep penetration through the entire fan was intended to retrieve long-term continuous records. Site U1456 penetrated ~1110 m of sediment cover, whereas sediment penetration of ~1100 m was achieved at Site U1457. Both sites cover the ~10 Ma (late Miocene) and younger section, which will enable us to examine proposed hypotheses on tectonic scales. These include answers to questions such as whether monsoon intensification causes less or more erosion, and whether this erosion occurs in the monsoon-influenced Himalayas or other mountainous regions within the Indus catchment. Reasonably good age control and decent core recovery may allow us to ascertain if increased grassland (C4) and reduced woodland (C3) flora at ~8 Ma is related to strengthening or weakening of monsoon rainfall and what other environmental changes occurred through that time. For example, are phases of increased productivity in the Arabian Sea linked to changes in continental environments onshore, and are both driven by change in monsoon wind intensity? A moderate hiatus close to 8 Ma itself means that the record will not be continuous but the transition should still be resolvable. Shore-based analyses of core samples collected during Expedition 355 will further improve our understanding of sedimentation in Laxmi Basin and the provenance of this sediment during key intervals of climate change from the late Miocene to present.

Unfortunately, with effective recovery limited to the past ~10 million years, we will be unable to address whether monsoon intensification occurred at 15 Ma and in particular test whether Greater Himalaya exhumation is linked to heavier rainfall and faster erosion after ~23 Ma, as implied by tectonic models such as channel flow (Beaumont et al., 2001). Recent suggestions that the monsoon might have been active during the Eocene (Licht et al., 2014) are also beyond analysis by Expedition 355 cores. Inability to penetrate deep into the fan stratigraphy at either site further makes it impossible to date the start of fan sedimentation, which would have provided a minimum age to the controversial timing of initial India/Eurasia collision. The presence of a short section (~20 m) of Paleocene (62–63 Ma) sediment at Site U1457 should allow us to test whether India/Eurasia collision was before or after this time, and thus at least eliminate some of the more extreme early collision models.

3. *Decipher the nature of basement rocks in Laxmi Basin and constrain the timing of early seafloor spreading and its relationship to the emplacement of Deccan Flood Basalts. Does mantle plume initiation predate or postdate rifting and early spreading?*

Penetration to ~100 m into igneous basement after ~1470 m of sediment cover was planned at Site U1456. This site was designed to core through the base of the Indus Fan, in order to determine the nature of basement in Laxmi Basin and to constrain rifting history and its relationship to Deccan volcanism. We planned a reentry and casing system for this site because of the deep penetration and potential for unconsolidated coarse-grained sediment. Unfortunately, the complex lithologies encountered in the mass transport deposit ultimately resulted in us having to abandon two attempts to reach

basement at Site U1456. In both cases, we were unable to work the drill string back to the bottom of the hole after a bit change, likely because of swelling claystone within the mass transport deposit (see **Operations**). This unexpected development prevented us from coring the base of the fan, as well as the basement at Site U1456. A third attempt to core into the basement during Expedition 355 was successful at Site U1457 and resulted in recovery of ~8.72 m of massive basalt and associated volcaniclastic sediment. Geochemical analysis is expected to distinguish if these are truly oceanic basalt or whether they are contaminated by continental crust or continental flood basalt.

Our objectives linked to the origin of the basin were further advanced by being able to core through most of the postrift strata in Laxmi Basin at these locations. Because surface processes (e.g., erosion) significantly control the dynamics of rift basins by redefining the surface load distribution through infilling accommodation space, information collected at both sites will be significant for examining the postrift development of this basin and thus its origins. Physical and lithologic knowledge gathered from these sites is equally important in determining the geometry and volume of the sedimentary load. Wireline log data collected in Hole U1456C should allow better regional stratigraphic correlation and precise determination of postrift sediment budget.

As well as the planned objectives, Expedition 355 also confirmed the presence of a huge mass transport deposit along the western continental margin of India that had previously only been recognized seismically (Calvès et al., submitted). Prior to our expedition very little was known about the presence of this mass transport deposit, which is significantly larger than the well-known Storegga Slide of Norway (Bugge et al., 1988; Bryn et al., 2003). Coring during Expedition 355 now allows us to constrain the extent, timing, and volume generated by this large-scale catastrophic event with significant implications for geohazards on this and other margins.

Operations

Port call

Expedition 355, Arabian Sea Monsoon, officially began with the first line ashore at JCT Feeder Berth in Colombo, Sri Lanka, at 0842 h (UTC + 5.5 h) on 31 March 2015. This also officially ended IODP Expedition 354, Bengal Fan. Ultimately, the ship was asked to move to another pier (Bandaranaike West Quay [BQ-1]), and the vessel remained at this location for the remainder of the port call.

The first week of Expedition 355 consisted entirely of port call activities in Colombo. Logistical challenges were experienced throughout the port call, especially the first day. Oncoming IODP staff was supposed to board the vessel for crossover with the offgoing Expedition 354 staff the morning of 31 March. The first batch of IODP staff was eventually allowed to board the ship at 1500 h, and the last complement of staff finally boarded the ship at 2100 h. Clearance of the Expedition 354 scientists and IODP technical staff was so delayed that they were disembarked from the ship according to their flight departure time. The final group of offgoing personnel departed the vessel at 2300 h, finally arriving at the hotel at 0230 h on 1 April. Although the crossover of the Siem crew and arrival of the Expedition 355 science party was less eventful on the second day of port call (1 April), they were not without challenges and confusion.

Logistical operations during the port call included bunkering 850 metric tons of marine gas oil, 400 metric tons of drill/potable water, 80 metric tons of barite drilling mud from 1 ton bags, 100 metric tons of attapulgite sea gel drilling mud from 1 ton bags, 88 joints of 10¾ inch casing, two drilling motors, one underreamer, one standard reentry cone, two boxes of core liner, other miscellaneous operational hardware, three 40 ft containers of science supplies, and three 20 ft containers of frozen, refrigerated, and food/dry goods. The inbound hazardous material air shipment experienced several delays resulting in a new estimated arrival of 5 April, the estimated day of departure. Local acquisition of critical items prevented waiting for the shipment.

Siem was able to repair the X-band radar and also installed shims on the traveling block sheaves to remove excessive play, both of which could have been pacing items for departure.

Despite the logistical challenges experienced in all aspects of the port call, the ship departed only 13 h behind schedule because of the hard work and dedication of the Siem/Overseas Drilling Ltd. and IODP logistics personnel and crew. At 2136 h on 5 April, the last line was cast off, and the transit to the first site began.

Transit to Site U1456

The transit to Site U1456 was uneventful. The 941 nmi trip (including 2 mi under pilot) was made at an average speed of 11.1 kt. The sea voyage ended at 1054 h on 9 April 2015, and command of the vessel was switched from the bridge to dynamic positioning control.

Site U1456

Hole U1456A

After arriving on site and deploying the acoustic positioning beacon, initial operations included picking up drill collars from the forward main deck pipe rack, spacing out the APC/XCB coring systems, and measuring (strapping) and verifying the internal diameter (drifting) of all tubulars during the first pipe trip of the expedition. The bottom hole assembly (BHA) included two stands of 5½ inch drill pipe, a tapered drill collar, five 8¼ inch control length drill collars, a nonmagnetic drill collar, head sub, top sub, latch sub, seal bore drill collar (which serves as the outer core barrel for the coring system), bit sub with a lockable float valve, and a "used" 9⅞ inch Russian polycrystalline diamond compact (PDC) APC/XCB core bit.

A Falmouth Scientific positioning beacon was deployed at 1108 h on 9 April 2015. After pumping a drill string wiper plug, we deployed the APC, spudding Hole U1456A at 0210 h on 10 April after offsetting the ship 15 m to the west of the original prospectus coordinates for the drill site. We positioned the bit at a depth of 3645.0 meters below rig floor (mbrf) and the first APC core was on deck at 0235 h, recovering 4.54 m of sediment and establishing a seafloor depth to the rig floor of 3650.0 mbrf. This hole was originally planned as an APC/XCB hole to ~250 mbsf; however, because the hole conditions were better than anticipated we elected to continue coring to ~600 mbsf as was planned initially for Hole U1456C.

Oriented APC coring using nonmagnetic core barrels and Whirl-Pak bags for microbiology contamination testing continued through Core 355-U1456A-16H to 139.3 mbsf. The APCT-3 was deployed on Cores 4H (33.0 mbsf), 7H (61.5 mbsf), 10H (90.0 mbsf), and 13H (118.5 mbsf). The first deployment was unsuccessful due to flooding of the APC shoe pressure case. After two successive partial strokes on Cores 15H and 16H, with the latter returning only a small amount of sediment in the core catcher, we decided to switch to the HLAPC. Coring continued using the HLAPC from Core 17F through 40F to 249.3 mbsf.

Coring with the HLAPC continued in Hole U1456A through Core 70F to 389.5 mbsf. The coring system was changed to the XCB, and at 0615 h on 13 April, the first XCB core (71X) was on deck, recovering 7.10 m. Coring continued through Core 74X. When that core barrel was retrieved on deck, the XCB cutting shoe was missing. Further examination revealed that it had broken off at the last engaged thread of the inner barrel connection, terminating Hole U1456A at 426.6 mbsf. Although short of the planned depth of ~600 mbsf, discussions had been under way to possibly terminate the hole at a depth of 450 to 460 mbsf due to the consistently fine-grained lithologies encountered below 400 mbsf. We decided to defer wireline logging in Hole U1456A in favor of logging Hole U1456C, which would likely be deeper and open for a shorter period of time. The drill string was tripped back to the seafloor with the top drive in place in case any hole problems were encountered due to the unconsolidated sands. Although a fair amount of sand was evident in the cores, the driller did not experience any difficulty recovering the drill string. The bit cleared the seafloor at 1805 h, ending Hole U1456A and beginning Hole U1456B. A total of 4.3 days were spent in Hole U1456A.

Hole U1456A consisted of 16 APC cores recovering 121.18 m of core over 139.3 m of penetration (87% recovery), 54 HLAPC cores recovering 216.22 m of core over 250.2 m of penetration (86% recovery), and 4 XCB cores recovering 27.85 m of core over 37.1 m of penetration (75% recovery). The total depth of the hole was 426.6 mbsf.

Hole U1456B

The ship was offset 15 m to the east of the original site coordinates, with the bit positioned at 3647 mbrf, 2 m lower than for Hole U1456A. Hole U1456B was started at 1955 h on 13 April. A seafloor depth of 3655.8 mbrf (3645.0 meters below sea level [mbsl]) was established based on APC core recovery, which was ~7 m deeper than the previous hole 30 m west. Based on discussions with the coring technician on watch, we determined that a significant amount of material was lost due to the soupy nature of the core, which led to an inaccurate seafloor depth. This hole was planned as a dedicated microbiology hole to consist of three cores; however, because the recovery was only 0.69 m in Core 355-U1456B-1H, we decided to take an additional core. APC coring continued through Core 4H to 29.1 mbsf, where the hole was terminated. The bit was pulled clear of the seafloor at 2355 h on 13 April, ending Hole U1456B and beginning Hole U1456C.

We spent 0.3 days in Hole U1456B, which consisted of 4 APC cores recovering 28.79 m of core over 29.1 m of penetration (99% recovery). The total depth of Hole U1456B was 29.1 mbsf.

Hole U1456C

The ship was offset 15 m north of the original site coordinates, with the bit positioned at 3647 mbrf. Hole U1456C was started at 0050 h on 14 April. The seafloor depth for this hole was established based upon APC core recovery as 3649.2 mbrf (3638.4 mbsl). Oriented APC coring continued through Core 355-U1456C-17H to 134.3 mbsf. Core 18H was a partial stroke advancing only to 137.0 mbsf with limited recovery of 2.72 m, apparently hitting a significant sand layer. The bit was advanced by recovery, and the coring system was changed to the HLAPC. Cores 19F through 36F were recovered to 221.6 mbsf with Core 36F on deck at 1155 h on 15 April. During HLAPC coring, each interval was advanced 4.7 m regardless of recovery. After Core 36F was retrieved, coring was suspended, and an XCB center bit assembly deployed to drill to 408.0 mbsf. Drilling of the 186.4 m interval required 12.25 h to complete. We suspect that bit balling of the PDC bit in the soft clay formation slowed the drilling. In addition, hard layers were occasionally encountered, requiring a longer amount of time to penetrate because of the limited weight-on-bit that could be applied due to the presence of the XCB center bit. The net rate of penetration (ROP) achieved (including connection time, mud sweeps, etc.) was 15.2 m/h. Thirty-barrel sea gel mud sweeps were pumped every 30 m to proactively avoid sand build-up in the annulus and to hopefully prevent any recurrences of the stuck wireline barrels that occurred in Hole U1456A.

After reaching 408.0 mbsf, the center bit was recovered, an XCB core barrel deployed, and at 0230 h on 16 April, coring resumed in Hole U1456C. Cores 38X and 39X were cut and recovered to 418.0 mbsf. Core 39X was on deck at 0745 h. While Core 39X was being recovered, a notification came from the bridge (at ~0700 h) that they were observing an unknown vessel located ~3.5 nmi away from the drill site. Soon after, the bridge instructed the drill floor to suspend coring operations and begin to pull out of the hole to near the seafloor when the vessel began to approach. The vessel began deploying fishing line in the vicinity of the *JOIDES Resolution* and also motioned to personnel onboard that they wanted food. After being instructed that we were a research vessel and that they needed to standoff a minimum of 3 nmi from our drilling location, the vessel departed. At 0845 h, the drill crew began tripping pipe back to the bottom of the hole and XCB coring resumed, with Cores 40X through 46X cut and recovered to 465.2 mbsf. At this point we determined that this depth would make a reasonable casing point and that the material being cored was recoverable with the RCB. Coring operations were terminated in Hole U1456C, and we began to prepare the hole for wireline logging operations.

A 40 bbl sea gel mud sweep was circulated out of the hole, and at 0215 h on 17 April, a wiper trip was conducted to 56.3 mbsf. The driller detected no overpull, excessive drag, or fill on the bottom. At 0645 h on 17 April, the lockable float valve go-devil was deployed, another 40 bbl sea gel mud sweep was pumped, and after chasing the sweep with 500 strokes of seawater, the hole was displaced with 171 bbl of 10.5 lb/gal heavy mud. The drill string was then positioned with the end-of-pipe at a logging depth of 81.1 mbsf. We started assembling the first wireline logging tool string (triple combo tool string without radioactive source), and it was deployed at 1155 h on 17 April. This suite of logging tools reached the total borehole depth of 465.2 mbsf, and after an uplog was collected, the tool string was retrieved to the rig floor at 1740 h. The second suite of tools, the FMS-sonic tool string, was deployed at 1810 h and also was able to reach bottom. Two up-passes were collected with the FMS-sonic tool string, and the tool string was retrieved to the surface at 0315 h on 18 April. The third and final logging run was made with the triple combo tool suite, this time with the source, after the hole was determined to be in good condition. The tool string was deployed at 0445 h, reached the total depth of the hole, and was retrieved to the rig floor at 1150 h on 18 April. After rigging down from logging, the subsea camera was deployed, and the drill string was pulled out of the hole, clearing the seafloor at 1440 h on 18 April. The vessel was offset in dynamic positioning mode to 15 m south of the original site coordinates. A drill string tag of the seafloor was observed on the subsea camera, establishing a seafloor depth adjusted to the rig floor dual elevator stool of 3648.0 mbrf for Hole U1456D. The subsea camera was then returned to the surface while we began to trip the drill string back to the vessel. We completed the pipe trip out of Hole U1456C, racked the drill collars

back in the derrick, and laid out the seal bore and nonmagnetic collars to the forward pipe rack. The bit cleared the rig floor at 0220 h on 19 April 2015, officially ending Hole U1456C and beginning Hole U1456D.

Hole U1456C consisted of 15 APC cores recovering 126.94 m of core over 133.5 m of penetration (95.1% recovery), 18 HLAPC cores recovering 71.33 m of core over 84.6 m of penetration (84.3% recovery), and 9 XCB cores recovering 16.73 m of core over 57.2 m of penetration (29.2% recovery). The total depth of the hole was 465.2 mbsf. Total time spent on Hole U1456C was 5.1 days.

Hole U1456D

The vessel was offset 15 m south of the original site coordinates, and the seafloor tag depth of 3648.0 mbrf used as the official seafloor depth for the hole. After laying out the upper guide horn, preparations began for installing the reentry cone and 10¾ inch casing string. The 16 inch casing hanger assembly was made up and racked back in the derrick. We then assembled and tested the 458.83 m long drilling assembly, which consisted of the 9⅞ inch tricone drilling bit, 8 inch mud motor, and underreamer with arms set to 12¾ inches. The preassembled standard reentry cone was positioned over the moonpool doors. We began to run casing at 1200 h on 19 April. The casing string, made up of a Texas pattern casing shoe, shoe joint, 33 joints of 10¾ inch casing, a 16 inch × 10¾ inch casing crossover (swage), 16 inch casing pup joint, and a 16 inch casing hanger, totaled 455.11 m in length. This assembly was lowered into the reentry cone using the casing running tool. At 2045 h on 19 April, the driller lowered the drilling assembly into the reentry cone and latch-in was completed at 0035 h on 20 April. At 0100 h we began tripping the assembly toward the seafloor. During the pipe trip, the subsea camera was deployed and the drill pipe filled with seawater every 15 stands.

After picking up the top drive, Hole U1456D was spudded at 1035 h on 20 April. It required a total of 20.75 h to drill in the 455 m of casing. The reentry cone base landed on the seafloor at 0710 h on 21 April, positioning the casing shoe at a depth of 455.1 mbsf. The driller rotated the drill string 3½ turns to the right to release the casing running tool; however, the drilling assembly was unable to pull free of the reentry cone and casing. We attempted to free the assembly over the next 4.25 h by offsetting the ship in a grid pattern away from the hole location. After this did not free the assembly, it became clear that the running tool was released, but the underreamer arms had not fully retracted. At 1135 h on 21 April, the drilling assembly was pulled free with 15,000 lb of overpull. While pulling the drill string, the underreamer continued to drag intermittently inside the casing, predominantly when passing through casing couplings. The top drive was set back, the subsea camera retrieved to the ship, and the bit pulled clear of the seafloor at 1540 h. After tripping the assembly back to the ship, the running tool was detorqued, the drill collars racked back in the derrick, the mud motor and underreamer assemblies flushed with freshwater, and at 0140 h on 22 April, the bit cleared the rotary table. From start to finish, using a mud motor and underreamer assembly, we required only a total of 3 days to make up and install a standard reentry cone with 455 m of 10¾ inch casing in 3637 m water depth using the drill-in casing approach.

With the reentry cone and casing installed, the drill crew requested time to investigate a noise they had heard on multiple occasions that emanated from the drilling package. During operations they were unable to determine whether the source of the noise was the top drive itself or the swivel assembly. A total of 9 h of "down time" was taken to separate the swivel from the top drive and thoroughly investigate the issue. Ultimately, the gear was all reassembled without identifying the original source of the noise. Once everything was reassembled, the noise was no longer heard.

We then made up the RCB BHA and, after slipping and cutting the drilling line, began tripping toward the seafloor. The subsea camera was deployed during the pipe trip; however, after a problem with the video feed was detected, the camera was brought back on board, repaired, and redeployed. At 0245 h on 23 April we reentered Hole U1456D after maneuvering the ship for only 20 min. The drill string was lowered into the casing string to a depth of 416.0 mbsf (39.1 m above the casing shoe) when soft fill was tagged. We picked up the top drive, deployed a wash barrel, and began to slowly circulate. The fill was cleared by 0800 h on 23 April. A 40 bbl sea gel mud sweep was circulated out and the wash barrel recovered. At 1000 h on 23 April, a core barrel was deployed and continuous RCB coring using nonmagnetic core barrels initiated. RCB coring continued with 30 bbl sea gel mud sweeps pumped every third core. Although we encountered no fill on bottom between cores, rapid penetration rates, low recovery, and evidence of sand in the recovered core material indicated there was still some sand in the formation. We therefore initiated preventative measures in order to preserve the integrity of the hole as much as possible.

RCB coring continued without incident through Core 355-U1456D-43R to 866.2 mbsf. Hole conditioning consisted of pumping 40 bbl sea gel mud sweeps every third core. While cutting Core 44R, the driller noted erratic changes in pump pressure and excessive torque. After pumping a 40 bbl mud sweep, the core barrel landed with a 200 psi pressure loss. After advancing 2.0 m, the lost pressure was regained; however, after advancing another 1.0 m the hole apparently began to collapse around the drill string. Pump pressure increased by 600 psi, top drive torque increased by 200 A, and there was a 20,000 lb weight loss. We spent 2.25 h circulating and working the pipe back to 821.0 mbsf. We then recovered Core 44R and completed a wiper trip to just inside the 10¾ inch casing shoe at 442.6 mbsf. The wiper trip was uneventful, with no apparent issues with the upper portion of the hole. After taking a short period of time to service the rig and grease the traveling block, the pipe was tripped back in the hole. The pipe was lowered to 821.0 mbsf, with the driller noting 10,000–15,000 lb of drag from 722.0 to 753.0 mbsf. We picked up the top drive at 0930 h on 27 April, and after beginning circulation we noted a 400 psi pump pressure excess, indicating that the annulus of the hole was filled with drill cuttings. We pulled the pipe back to 791.9 mbsf and deployed a wash barrel. At 1100 h, the pipe was washed/reamed back to the original total depth of 869.2 mbsf, encountering 12 m of fill at the bottom of the hole. We circulated a 50 bbl sea gel mud sweep and then spent an additional 2.5 h circulating a series of mud sweeps (two 50 bbl sweeps at 110 viscosity, a 50 bbl sweep at 120 viscosity, and a 60 bbl sweep at 130 viscosity) before regaining normal drilling parameters.

With the hole stabilized, we recovered the wash barrel and deployed an RCB core barrel. At 1830 h on 27 April, RCB coring recommenced. As a preventative measure, the drillers pumped 50 bbl high-viscosity mud sweeps every other core to help prevent any recurrence of cuttings build-up in the hole annulus. Coring continued without incident through Core 54R to 966.2 mbsf. While cutting Core 55R, an abrupt drop in the ROP to 2.9 m/h occurred at ~970 mbsf. We recovered Core 55R after only a 6.0 m advance and found that the core barrel had been jammed, resulting in poor recovery (3%). We recovered Core 56R after a 6.0 m advance (125 min at 2.9 m/h) due to concerns that the barrel may have jammed again; however, the core barrel was full (111% recovery) and the slow ROP was

due to the hard sandstone lithology. We picked up a knobby drilling joint for cutting Core 57R to 987.4 mbsf. This 9.2 m advance required 270 min of rotating time (2.0 m/h). At this point, hole conditions became problematic with high torque (600 A) and pump pressure elevated by 400 psi. We spent >8 h working the pipe, circulating multiple 50 bbl high-viscosity mud sweeps, and conditioning the hole before coring could resume. At 1830 h on 29 April, we resumed coring. Core 58R was cut to 996.6 mbsf (9.2 m advance) in 160 min at 3.5 m/h. After recovering this core and deploying the next core barrel, hole conditions again deteriorated. Top drive torque increased, and when the core barrel landed, the driller noted that he had lost the ability to rotate the pipe. The pipe was freed in <1 h; however, this required 900 A of top drive torque and 55,000 lb of overpull. Core 59R was cut to 1005.8 mbsf with a slightly higher ROP. Coring continued through Core 61R to 1024.4 mbsf at an average ROP of 6.0 m/h. Because of the accumulated bit rotating hours plus the intangible unrecorded reaming hours, we decided to cut one additional core and then round trip the drill string for a bit change. When the core barrel landed for the final core, the WKM valve on the top drive failed and would not seal properly. Since replacing the valve required tripping the pipe up inside the casing shoe at 455 mbsf, we decided instead to recover the entire drill string to change the bit and also repair the WKM valve.

We displaced the hole with heavy mud, recovered the empty core barrel, and the drill string was pulled clear of the seafloor at 1900 h on 30 April. We offset the vessel 50 m from the reentry cone, serviced the rig, and removed the WKM valve to expedite the required repairs. The drill string was recovered back to the surface, with the bit clearing the rotary table at 0355 h on 1 May. We checked all outer core barrel subs, inspected the RCB latch sleeve, and prepared a new CC-4 RCB bit. The BHA was reassembled, and by 1045 h the drill string was deployed to 3274.4 mbrf when the 5½ inch pipe racker developed a problem. We spent 45 min troubleshooting and fixing the pipe racker. The pipe trip resumed to 3624 mbrf, and then the subsea camera was deployed and lowered toward the seafloor for reentry. While the camera was being deployed, the spare WKM valve was installed on the top drive in preparation for coring operations. We began maneuvering the ship at 1440 h on 1 May and reentered Hole U1456D in 35 min. We recovered the subsea camera to the ship, and continued tripping the pipe inside the 10¾ inch casing to 442.6 mbsf, where we encountered unexpected resistance. We pulled back the pipe, deployed a wash barrel, and picked up the top drive. Using very slow rotation and minimal pump pressure, the bit was lowered through the obstructed area with no discernible indication of resistance. We lowered the drill string below the casing shoe to 529.9 mbsf, recovered the wash barrel, and racked back the top drive.

We continued to lower the drill string without incident to a tag depth of 995.8 mbsf with a maximum drag of 10,000 lb. We picked up the drill string to 966.6 mbsf and picked up the top drive. At 0100 h on 2 May, the driller attempted to break circulation and realized that he could not rotate the string or circulate fluid. The driller picked up the drill string to 937.5 mbsf with no overpull. We picked up a knobby joint and the top drive and worked the drill string for 2.75 h. Circulation was reestablished; however, 900 A of maximum torque and 150,000 lb of overpull failed to free the drill string. At 0600 h on 2 May, we offset the ship 185 m (5% of water depth) to the south to set a drill pipe tool joint at the rig floor. The sinker bars were installed with a core barrel attached, and this assembly was lowered into the drill string to determine if there were any mechanical issues with the integrity of the drill string or if hole instability and stuck pipe was the sole issue. The core barrel would not pass a depth approximately equal to the seafloor depth (hard tag at ~3668 mbrf), indicating that there were other issues in addition to hole conditions. The vessel was offset to allow recovery of the wireline assembly, the upper guide horn was pulled, and the subsea camera was deployed to determine if there was a problem at the seafloor. The subsea camera showed that the reentry cone was buried in cuttings; however, the drill pipe appeared to be extending straight up from the reentry cone/cuttings pile. We observed no identifiable problem with the drill pipe or the seafloor installation. We recovered the subsea camera on deck at 1240 h on 2 May.

At this point we decided to sever the drill string and abandon Hole U1456D. We hoped to sever in the first joint of 5½ inch drill pipe (transition joint) above the tapered drill collar (TDC) at the top of the BHA; however, there was some concern that (1) the wireline severing tool may not be able to pass the seafloor and (2) if the pipe was severed above the BHA the drill pipe above may still remain firmly stuck in the hole. We held a safety meeting at the rig floor, and preparations began for rigging up the Schlumberger wireline drill pipe severing tool. After securing radio silence and shutting down all wireless devices, the severing tool was deployed at 1800 h on 2 May. There was no problem passing through the transition zone at the seafloor, and the tools reached all the way to the bit. The system was then recovered and positioned at the approximate midpoint (~4.5 m) of the first joint of 5½ inch drill pipe above the TDC. We applied a slight amount of torque and overpull to the drill string before the charge was fired; however, no voltage was sent. The Schlumberger computer used to control the system was rebooted and the second attempt to fire the charge was successful. The driller was then able to pull the drill string back to the next tool joint and rotate, indicating that the string was successfully severed at the location desired and freed from the formation.

While pulling the Schlumberger wireline severing tools the Schlumberger engineer indicated that a weak link on the Schlumberger cable head had failed and the severing tool assembly was lost in the hole. With the top drive in, the drill string was pulled back to 756.6 mbsf. Overpull was 10,000–15,000 lb. The top drive was set back, and the drill string was pulled clear of the seafloor at 0425 h on 3 May. When the drill string reached 753.9 mbrf it became apparent why the core barrel deployed earlier via wireline would not pass the seafloor depth. Several joints of 5 inch drill pipe that had extended from just below the seafloor and deeper into the hole were recovered severely bent. The next 13 h were spent removing the joints from the drill string and laying them out via the pipe racker to the portside inboard bay of the riser hold. In total, there were 39 joints (~377 m) of bent 5 inch drill pipe. The four-stand RCB BHA that was lost in the hole included 11 control length drill collars (CLDC), 1 TDC, a new CC-4 RCB core bit, a complete mechanical bit release assembly (MBR), two modified head subs, and one modified top sub. A detailed list of lost hardware was prepared along with an incident report. The remainder of the drill string was intact, and the severed end of the last joint of 5 inch drill pipe cleared the rig floor at 2200 h on 3 May. This officially ended Hole U1456D and began Hole U1456E.

Hole U1456D consisted of 60 RCB cores recovering 319.18 m of core over 656.6 m of penetration (57% recovery). Including the initial drilled interval, the total depth of the hole was 1024.4 mbsf. Total time spent on Hole U1456D was 14.8 days.

Hole U1456E

Because we had not achieved our objectives at Site U1456, we decided to install a new casing string to ~750 mbsf to stabilize the unconsolidated sands above this depth. The drill crew cleared the rig floor of all remnants of the bent pipe recovery (cut-off tool joints, etc.) and serviced the rig. At 2245 h on 3 May the drill crew began picking up the 11 additional CLDCs and TDC required to make up the BHA for drilling operations in Hole U1456E. The drill collars were made up into stands and racked back in the derrick. The upper guide horn was laid out to the forward main deck pipe rack, and the casing running tools, subs, and equipment were picked up. At 0700 h on 4 May, we began to assemble the drilling stinger. This included a 9⅞ inch R2 tricone drill bit, a bit sub with float valve, an underreamer with the mill tooth arms/cutters set to 12¾ inch diameter, and a positive displacement mud motor. This assembly was deck tested with the motor beginning rotation at ~25 strokes/min of the mud pumps, with the underreamer arms fully opening at 30–35 strokes/min. After testing, the assembly was laid out on the pipe racker. The Hole U1456E reentry cone was moved over the center of the moonpool doors and a 16 inch casing hanger with pup joint was lowered and latched into the reentry cone using the 16 inch casing running tool. A 10¾ inch casing hanger assembly was made up with the 10¾ inch casing running tool, and the power tongs and casing running equipment were rigged up. At 1430 h on 4 May, we began making up the 10¾ inch casing string. The first 5 joints were welded together, and the casing hanger was also welded to the last casing collar. Including the shoe joint, 55 joints of casing were made up in 8.5 h, and by 2400 h on 4 May the 10¾ inch casing hanger was landed and latched into the reentry cone assembly. The drilling stinger assembly was then picked up, along with 23 stands and 1 single of 5 inch drill pipe and run inside the casing string, and the casing running tool was attached to the 10¾ inch casing hanger. Three hours were spent working on the 5½ inch pipe racker jacking assembly before beginning the pipe trip toward the seafloor.

At 0700 h on 5 May, with the drilling stinger assembly (bit) extending 4.82 m ahead of the casing shoe, the reentry cone, casing, and drilling stinger assembly were deployed. This space out placed the underreamer arms 2.61 m below the 10¾ inch casing shoe. While lowering the casing toward the seafloor, the pipe was filled with seawater every 15 stands, the drilling line was slip and cut, and the subsea camera was deployed. The drilling assembly reached the seafloor by 2045 h on 5 May. We then picked up the top drive, and the drill string was spaced out. At 2130 h, Hole U1456E was spudded. We spent the next day drilling in the casing to 743.4 mbsf. The reentry cone landed at the seafloor (3648 mbrf) at 0100 h on 7 May. We then released the casing string and retracted the underreamer assembly back up inside the casing. After setting back the top drive, the subsea camera and drill string were recovered back to the ship. After the drilling assembly cleared the seafloor at 0410 h on 7 May, the vessel was offset 50 m east of the reentry installation as a precaution. After spending 1 h repairing a ruptured hose on the iron roughneck, the pipe trip was completed by 1415 h. We then washed and laid out the mud motor/underreamer assembly.

At 1615 h on 7 May, we began making up the new RCB drilling/coring BHA. The drill string was once again tripped to the seafloor and the subsea camera deployed. After maneuvering the ship for 36 min, we reentered Hole U1456E. The subsea camera was recovered, the pipe advanced to 706.1 mbsf (still inside the casing string), the top drive picked up, and then a RCB core barrel dressed with a center bit was deployed. The bit was advanced to 748.2 mbsf before tagging the bottom of the hole. This was the depth the drilling "stinger" assembly reached when drilling in the 10¾ inch casing shoe, indicating that there was no fill at the bottom of the hole. We pumped a 30 bbl high-viscosity mud sweep, and at 0830 h on 8 May, we began drilling without coring with the RCB center bit. A total of 26.5 h was required to advance the 9⅞ inch diameter hole to 970.0 mbsf, and at 1100 h on 9 May, the drill ahead was completed. The overall average ROP for the 221.8 m interval drilled was 10.9 m/h. We pumped a 40 bbl mud sweep and recovered the RCB center bit; however, before a core barrel could be dropped the driller noted that he had 4 m of fill on bottom. Therefore, instead of dropping a RCB core barrel, we deployed a wash barrel and pumped two 50 bbl high-viscosity mud sweeps out of the hole at a circulating rate of 130 strokes/min. Once the hole was considered to be clean, the wash barrel was recovered, and at 1545 h on 9 May, we deployed a core barrel and coring initiated in Hole U1456E from 970.0 mbsf. For reference, it required 5.6 days to drill in a new reentry cone and 10¾ inch casing assembly to 743.4 mbsf and then drill a 9⅞ inch hole to 970.0 mbsf. Prior to that, another 1.8 days had been spent severing the drill string and recovering the bent string of drill pipe. Total lost time due to the loss of Hole U1456D was 7.4 days.

We continued RCB coring in Hole U1456E through Core 19R to 1109.4 mbsf with the ROP varying between 2.9 and 7.0 m/h. To enhance hole cleaning, the drillers pumped 40 bbl high-viscosity mud sweeps after each core. These were pumped at high annular velocity all the way to the surface prior to recovering the core barrel so that the cuttings from the entire cored interval would be flushed from the hole. After recovering Core 19R, we decided to recover the drill string, inspect the outer core barrel assembly, and change the bit because the present bit was approaching 60 h of use. We pumped a final mud sweep from the total depth of the hole and then displaced the open hole section with 125 bbl of heavy mud. We began to pull out of the hole but had to wait until the drill bit was inside the 10¾ inch casing shoe at 735.2 mbsf before we could set back the top drive, indicating that the formation was beginning to impinge on the open hole below the casing. Once the top drive was set back, the drill string was pulled up to 36.6 mbsf, the circulating head picked up, and the reentry cone thoroughly flushed with seawater to remove any remnant cuttings or drilling mud that might inhibit the reentry attempt. The drill bit cleared the seafloor at 2330 h on 12 May, and the remaining drill string was recovered back to the ship. The BHA was racked back in the derrick and the MBR and coring bit were removed, clearing the rotary table at 0740 h on 13 May.

Coincident with the decision to trip the drill string for a bit change, we were approached and contacted by an Indian Navy vessel, which informed us that we would have to move because the Indian military was planning to conduct a live fire weapons exercise the following morning (13 May) between 0800 and 1200 h. We informed the boarding officer (1) that we were in international waters conducting scientific research under IODP in collaboration with the Indian government, and (2) that our drill string was more than 1100 m below the seafloor and that it would take many hours to recover our drill string and prepare to get under way, making it impossible for us to vacate the zone of operation before their deadline. After a number of shore-based entities were contacted (Siem, IODP management, and Indian Ministry of Earth Sciences), the situation was ultimately resolved when the military moved the prohibited zone away from our location.

On 13 May, we prepared a new RCB CC-4 core bit and new MBR and deployed the new BHA. We lowered the drill string to 3597.6 mbrf and deployed the subsea camera for reentry. Shortly after deployment, the camera had to be recovered due to a network

communication problem. The issue was resolved quickly, and at 1630 h the camera was again deployed. While running to bottom, the drilling line was slipped and cut and the RigWatch drawworks encoder recalibrated. At 1900 h the ship began maneuvering for reentry. Picture quality was poor, primarily as a result of the seafloor around the reentry cone being covered with white drilling mud. The backscatter became worse as the camera got closer to the seafloor, and that, coupled with particles in the water column, created a severe glare. Attempts to reenter Hole U1456E continued for more than 18 h until 1315 h on 14 May, when the camera failed completely and had to be recovered back to the ship. During this time multiple unsuccessful stab attempts were made, which further reduced visibility. After recovering the subsea camera, we attempted to disconnect the camera iris auto-adjust feature; however, this was unsuccessful. The spare black and white camera was installed and this camera provided a better picture, although the other lighting and visibility issues remained. The subsea camera was redeployed and reached the seafloor by 1615 h on 14 May, and attempts at reentering Hole U1456E resumed. With the improved picture quality and elapsed time for some of the particles to settle out of the water column, we finally reentered Hole U1456 at 1900 h after an additional 2.75 h of maneuvering.

We positioned the bit just inside the throat of the reentry cone to thoroughly flush it with seawater in an attempt to remove the veneer of cuttings and drilling mud that masked all of the cone markings. The top drive was set back and the subsea camera recovered to the ship. At 0000 h on 15 May, we began lowering the pipe inside the casing until encountering an obstruction at 725.6 mbsf while the bit was still within the casing near the casing shoe. Just as in Hole U1456D, the obstruction was easily passed after picking up the top drive, deploying an RCB wash barrel, and circulating through the obstruction. The pipe was advanced to 822.7 mbsf with minimal rotation or weight on bit. The next 12 h was spent unsuccessfully washing and reaming the hole in an attempt to reach to the total depth of the hole (1109.4 mbsf) to resume RCB coring. The deepest the bit could be advanced was 936.0 mbsf, and several momentary episodes of stuck pipe were experienced during these attempts. We decided to abandon Hole U1456E and concentrate on achieving at least some of the remaining expedition objectives at another location. After reviewing the sites available, the collective science decision was to proceed to Site U1457 (proposed Site IND-06B), core two shallow APC holes, and then attempt to reach basement in the third hole using the RCB coring system. At 1530 h on 15 May, we began to pull the pipe out of the hole. Just as in the previous hole, the top drive was required in order to pull the bit back into the casing shoe, and drag continued even while pulling the bit up inside the casing. We speculate that this was as a result of a clay ball on the core bit being dragged into the casing from the open hole. The pipe trip into the casing was interrupted briefly (30 min) to repair a ruptured hydraulic line on the iron roughneck. Ultimately the bit was pulled clear of the seafloor at 2350 h on 15 May, and by 0800 h on 16 May, the ship was secured and under way for Site U1457.

Hole U1456E consisted of 17 RCB cores recovering 82.45 m of core over 139.4 m of penetration (59% recovery). Including the two drilled intervals, the total depth of the hole was 1109.4 mbsf. Total time spent on Hole U1456E was 12.4 days.

Transit to Site U1457

After a 62 nmi transit from Site U1456 averaging 11.3 kt, the vessel arrived at the second expedition site, U1457. During the transit, the rig crew conducted rig maintenance tasks and began preparing equipment required for the ACP/XCB BHA. The vessel stabilized over the site and switched from cruise mode to dynamic positioning at 1330 h on 16 May 2015, and the positioning beacon was deployed. The position reference was a combination of GPS signals and a single acoustic beacon.

Site U1457

Hole U1457A

We completed preparing the BHA, added the 2 stands of 5½ inch transition drill pipe, and then lowered the pipe to 3503.4 mbrf. The bit was positioned at 3521.0 mbrf, or 6.4 m above the depth determined by the precision depth recorder. The bit was positioned slightly higher than normal because at the last site 62 nmi away, the seafloor was determined to be 1.6–2.5 m shallower than the precision depth recorder depth. We prepared an APC core barrel and attempted to spud Hole U1457A. After the first attempt retrieved only water, the bit was lowered 3.0 m, and a second water core was recovered. The bit was lowered again, and the third attempt at spudding was successful, recovering 8.76 m of core and establishing a seafloor depth of 3534.3 mbrf (3523.11 mbsl). Coring in Hole U1457A started at 0045 h on 17 May 2015.

Oriented APC coring using nonmagnetic core barrels continued in Hole U1457A through Core 355-U1457A-12H to 111.2 mbsf. Core 12H had an incomplete stroke and upon recovery was found to have a shattered core liner that required pumping out. We continued coring using the HLAPC through Core 19F to 144.8 mbsf for Hole U1457A. To advance the hole more quickly, we used the technique employed during IODP Expedition 354, during which a 4.7 m HLAPC-cored interval was followed by a 4.7 m drilled interval. At 1900 h on 17 May, we terminated Hole U1457A in the interest of time. The drill string was tripped to the seafloor with the top drive in place, and the bit cleared the seafloor at 2015 h, ending Hole U1457A and beginning Hole U1457B.

Hole U1457A consisted of 12 APC cores recovering 103.93 m of core over 111.2 m of penetration (94% recovery) and 5 HLAPC cores recovering 18.83 m of core over 19.2 m of penetration (98% recovery). The total depth of the hole was 144.8 mbsf. Total time spent on Hole U1457A was 1.3 days.

Hole U1457B

The ship was offset 15 m west of Hole U1457A, and the bit was positioned at 3528.5 mbrf. Hole U1457B was started at 2140 h on 17 May. The first core recovered 3.22 m, establishing a seafloor depth of 3534.8 mbrf. We continued APC coring with nonmagnetic core barrels and core orientation through Core 355-U1457B-13H to 110.7 mbsf. Cores 10H and 12H required pumping out and we also drilled ahead without coring over a 3 m interval (88.7–91.7 mbsf) to realign the core breaks for optimized stratigraphic correlation. We continued coring with the HLAPC system from Core 14F through 33F to 204.7 mbsf, where the hole was terminated in the interest of time. The drill string was pulled back to 181.2 mbsf with the top drive in place, and after racking the top drive, the pipe trip continued with the bit clearing the seafloor at 2250 h on 18 May. We had recovered the drill string to 2108.0 mbrf when a hydraulic hose on the starboard pipe racker ruptured. This caused a stand of drill pipe to drop into the pipe racker, damaging the center chain shock absorber and also causing the chain to jump off the sprocket. The damage was repaired in 1 h, and the pipe trip resumed with the bit clearing the rig floor at 0810 h on 19 May. This ended Hole U1457B, and marked the beginning of Hole U1457C.

Hole U1457B consisted of 12 APC cores recovering 98.80 m of core over 107.7 m of penetration (92% recovery) and 11 HLAPC

cores recovering 52.39 m of core over 51.7 m of penetration (101% recovery). The total depth of the hole was 204.7 mbsf and total time spent on the hole was 1.5 days.

Hole U1457C

The ship was offset 15 m east of Hole U1457B, and we assembled a 4-stand RCB BHA. The drill string was lowered to 199.0 mbrf when another repair on the starboard pipe racker was required. It was fixed in 1 h, and at 1100 h on 19 May, the pipe trip resumed. The top drive was picked up when the drill string reached 3509.6 mbrf, the pipe spaced out for spudding, and an RCB wash barrel deployed. Hole U1457C was started at 1830 h on 19 May. The seafloor depth was established by tagging the seafloor at 3534.0 mbsf (3522.71 mbsl). We drilled without coring to 191.6 mbsf in 5.5 h. The interval was drilled at a rate of 95.8 m/h. The wash barrel was recovered, and at 0030 h on 20 May we began to RCB core using nonmagnetic core barrels. Core recovery in the first few cores was very poor (<0.5 m), most likely due to the formation being washed away by the RCB bit jets. As the material became more lithified the recovery improved.

RCB coring continued without incident through Core 355-U1457C-95R to 1090.1 mbsf at 1610 h on 28 May. The drillers frequently pumped high-viscosity mud sweeps to maintain good hole conditions. Initially, we pumped 30 bbl sweeps every third connection, later increasing to 35 bbl sweeps every other core and occasionally every core. Care and time were taken to fully pump the sweeps out of the hole at the seafloor before attempting to deploy the sinker bars and recover the core barrel. This technique worked and excellent hole conditions prevailed, despite the presence of unconsolidated sands over some intervals of the borehole.

While cutting Core 96R, ROP slowed dramatically at ~1098 mbsf (~1.4 m from the end of the advance). Upon recovery, we discovered igneous rock in the core catcher and bottom portion of the core, indicating that we had reached our basement target. Given the short amount of time remaining for coring operations, we decided to cut two or three half-length RCB cores with the remaining time to improve recovery of the basement rock. Cores 97R and 98R were cut to 1108.6 mbsf at an average ROP of 1.9 m/h, with an average recovery of 91.7%. Coring operations ended with the retrieval of Core 98R.

The wireline was coated on the last core retrieval, and a 50 bbl mud sweep was pumped at the total depth of 1108.6 mbsf to help mitigate problems that might occur while pulling the drill string out of the hole. The top drive was used to pull the pipe to 995.1 mbsf while laying out the 30 ft knobby drilling joints from the drill string to the forward pipe rack. Per protocol, the hole was displaced with 380 bbl of 10.5 lb/gal heavy mud, and the top drive was set back. We then continued retrieving the drill string, with the bit clearing the seafloor at 1050 h on 29 May. We recovered the positioning beacon at 1723 h while retrieving the drill string. The drill collars were broken down and stored in the forward main deck pipe rack. The bit cleared the rotary table at 2115 h, and the RCB coring bit, MBR, and outer core barrel subs were broken down and the rig floor was cleared of all handling equipment. The rig floor was secured for transit, all thrusters/hydrophones were raised, and at 2300 h on 29 May, we began the sea passage to Mumbai, India. This officially ended operations at Site U1457.

Hole U1457C consisted of 97 RCB cores recovering 436.96 m of core over 917.0 m of penetration (48% recovery). The total depth of the hole was 1108.6 mbsf. Total time spent on Hole U1457C was 10.6 days.

Transit to Mumbai, India

The 315 nmi transit to Mumbai was completed at an average speed of 8.7 kt. The pilot boarded the ship at 1026 h on 31 May 2015, and at 1112 h the ship dropped anchor in the Mumbai harbor anchorage, officially ending Expedition 355.

References

Aitchison, J.C., Ali, J.R., and Davis, A.M., 2007. When and where did India and Asia collide? *Journal of Geophysical Research: Solid Earth,* 112(B5):B05423. **http://dx.doi.org/10.1029/2006JB004706**

Ali, K.F. and de Boer, D.H., 2008. Factors controlling specific sediment yield in the upper Indus River basin, northern Pakistan. *Hydrological Processes,* 22(16):3102–3114. **http://dx.doi.org/10.1002/hyp.6896**

Alizai, A., Carter, A., Clift, P.D., VanLaningham, S., Williams, J.C., and Kumar, R., 2011. Sediment provenance, reworking and transport processes in the Indus River by U-Pb dating of detrital zircon grains. *Global and Planetary Change,* 76(1–2):33–55. **http://dx.doi.org/10.1016/j.gloplacha.2010.11.008**

An, Z., Kutzbach, J.E., Prell, W.L., and Porter, S.C., 2001. Evolution of Asian monsoons and phased uplift of the Himalaya–Tibetan Plateau since late Miocene times. *Nature,* 411(6833):62–66. **http://dx.doi.org/10.1038/35075035**

Anczkiewicz, R., Burg, J.P., Villa, I.M., and Meier, M., 2000. Late Cretaceous blueschist metamorphism in the Indus Suture Zone, Shangla region, Pakistan Himalaya. *Tectonophysics,* 324(1–2):111–134. **http://dx.doi.org/10.1016/S0040-1951(00)00110-4**

Baksi, A.K., 1994. Geochronological studies on whole-rock basalts, Deccan Traps, India: evaluation of the timing of volcanism relative to the K-T boundary. *Earth and Planetary Science Letters,* 121(1–2):43–56. **http://dx.doi.org/10.1016/0012-821X(94)90030-2**

Beaumont, C., Jamieson, R.A., Nguyen, M.H., and Lee, B., 2001. Himalayan tectonics explained by extrusion of a low-viscosity crustal channel coupled to focused surface denudation. *Nature,* 414(6865):738–742. **http://dx.doi.org/10.1038/414738a**

Beck, R.A., Burbank, D.W., Sercombe, W.J., Riley, G.W., Barndt, J.K., Berry, J.R., Afzal, J., Khan, A.M., Jurgen, H., Metje, J., Cheema, A., Shafique, N.A., Lawrence, R.D., and Khan, M.A., 1995. Stratigraphic evidence for an early collision between northwest India and Asia. *Nature,* 373(6509):55–58. **http://dx.doi.org/10.1038/373055a0**

Bernard, A., and Munschy, M., 2000. Were the Mascarene and Laxmi Basins (western Indian Ocean) formed at the same spreading centre? *Comptes Rendus de l'Academie des Sciences, Serie IIa: Sciences de la Terre et des Planetes,* 330(11):777–783. [French with English abstract] **http://dx.doi.org/10.1016/S1251-8050(00)00221-4**

Berner, R.A., Lasaga, A.C., and Garrels, R.M., 1983. The carbonate-silicate geochemical cycle and its effect on atmospheric carbon dioxide over the past 100 million years. *American Journal of Science,* 283(7):641–683. **http://dx.doi.org/10.2475/ajs.283.7.641**

Berner, R.A., and Raiswell, R., 1983. Burial of organic carbon and pyrite sulfur in sediments over Phanerozoic time: a new theory. *Geochimica et Cosmochimica Acta,* 47(5):855–862. **http://dx.doi.org/10.1016/0016-7037(83)90151-5**

Bernet, M., van der Beek, P., Pik, R., Huyghe, P., Mugnier, J.-L., Labrin, E., and Szulc, A., 2006. Miocene to recent exhumation of the central Himalaya determined from combined detrital zircon fission-track and U/Pb analysis of Siwalik sediments, western Nepal. *Basin Research,* 18(4):393–412. **http://dx.doi.org/10.1111/j.1365-2117.2006.00303.x**

Besse, J., and Courtillot, V., 2002. Apparent and true polar wander and the geometry of the geomagnetic field over the last 200 Myr. *Journal of Geophysical Research: Solid Earth,* 107(B11):2300. **http://dx.doi.org/10.1029/2000JB000050**

Bhattacharya, G.C., Chaubey, A.K., Murty, G.P.S., Srinivas, K., Sarma, K.V.L.N.S., Subrahmanyam, V., and Krishna, K.S., 1994. Evidence for seafloor spreading in the Laxmi Basin, northeastern Arabian Sea. *Earth and*

Planetary Science Letters, 125(1–4):211–220. **http://dx.doi.org/10.1016/0012-821X(94)90216-X**

Bhattacharyya, R., Verma, P.K., and Majumdar, T.J., 2009. High resolution satellite geoids/gravity over the western Indian offshore for tectonics and hydrocarbon exploration. *Indian Journal of Geo-Marine Sciences,* 38(1):116–125. **http://nopr.niscair.res.in/bitstream/123456789/4252/4/IJMS 38(1) 116-125.pdf**

Bhushan, R., Dutta, K., and Somayajulu, B.L.K., 2001. Concentrations and burial fluxes of organic and inorganic carbon on the eastern margins of the Arabian Sea. *Marine Geology,* 178(1–4):95–113. **http://dx.doi.org/10.1016/S0025-3227(01)00179-7**

Biswas, S.K., 1987. Regional tectonic framework, structure and evolution of the western marginal basins of India. *Tectonophysics,* 135(4):307–327. **http://dx.doi.org/10.1016/0040-1951(87)90115-6**

Biswas, S.K., and Singh, N.K., 1988. Western continental margin of India and hydrocarbon potential of deep-sea basins. *Proceedings of the 7th Offshore Southeast Asia (SEAPEX) Conference:* Singapore (Southeast Asia Petroleum Exploration Society), 170–181.

Blöthe, J.H., Munack, H., Korup, O., Fülling, A., Garzanti, E., Resentini, A., and Kubik, P.W., 2014. Late Quaternary valley infill and dissection in the Indus River, western Tibetan Plateau margin. *Quaternary Science Reviews,* 94:102–119. **http://dx.doi.org/10.1016/j.quascirev.2014.04.011**

Boillot, G., Beslier, M.O., Krawczyk, C.M., Rappin, D., and Reston, T.J., 1995. The formation of passive margins: constraints from the crustal structure and segmentation of the deep Galicia margin, Spain. *In* Scrutton, R.A., Stoker, M.S., Shimmield, G.B., and Tudhope, A.W. (Eds.), *The Tectonics, Sedimentation and Palaeoceanography of the North Atlantic Region.* Geological Society Special Publication, 90(1):71–91. **http://dx.doi.org/10.1144/GSL.SP.1995.090.01.04**

Bollinger, L., Avouac, J.P., Beyssac, O., Catlos, E.J., Harrison, T.M., Grove, M., Goffé, B., and Sapkota, S., 2004. Thermal structure and exhumation history of the Lesser Himalaya in central Nepal. *Tectonics,* 23(5):TC5015. **http://dx.doi.org/10.1029/2003TC001564**

Bookhagen, B., Thiede, R.C., and Strecker, M.R., 2005. Late Quaternary intensified monsoon phases control landscape evolution in the northwest Himalaya. *Geology,* 33(2):149–152. **http://dx.doi.org/10.1130/G20982.1**

Boos, W.R., and Kuang, Z., 2010. Dominant control of the South Asian monsoon by orographic insulation versus plateau heating. *Nature,* 463(7278):218–222. **http://dx.doi.org/10.1038/nature08707**

Bovis, M.J., 2003. Mass movement. *In* Middleton, G.V., Church, M.J., Coniglio, M., Hardie, L.A., and Longstaffe, F.J. (Eds.), *Encylopedia of Sediments and Sedimentary Rocks* (Encyclopedia of Earth Sciences Series): Amsterdam (Springer), 692–695. **http://dx.doi.org/10.1007/978-1-4020-3609-5_131**

Bryn, P., Solheim, A., Berg, K., Lien, R., Forsberg, C.F., Haflidason, H., Ottesen, D., and Rise, L., 2003. The Storegga slide complex: repeated large scale sliding in response to climatic cyclicity. *In* Locat, J., Mienert, J., and Boisvert, L. (Eds.), *Advances in Natural and Technological Hazards Research* (Vol. 19): *Submarine Mass Movements and Their Consequences:* Dordrecht, The Netherlands (Kluwer), 215–222. **http://dx.doi.org/10.1007/978-94-010-0093-2_24**

Budziak, D., Schneider, R.R., Rostek, F., Müller, P.J., Bard, E., and Wefer, G., 2000. Late Quaternary insolation forcing on total organic carbon and C_{37} alkenone variations in the Arabian Sea. *Paleoceanography,* 15(3):307–322. **http://dx.doi.org/10.1029/1999PA000433**

Bugge, T., Belderson, R.H., and Kenyon, N.H., 1988. The Storegga slide. *Philosophical Transactions of the Royal Society, A: Mathematical, Physical & Engineering Sciences,* 325(1586):357–388. **http://dx.doi.org/10.1098/rsta.1988.0055**

Bünz, S., Mienert, J., and Berndt, C., 2003. Geological controls on the Storegga gas-hydrate system of the mid-Norwegian continental margin. *Earth and Planetary Science Letters,* 209(3–4):291–307. **http://dx.doi.org/10.1016/S0012-821X(03)00097-9**

Calvès, G., Clift, P.D., and Inam, A., 2008. Anomalous subsidence on the rifted volcanic margin of Pakistan: no influence from Deccan plume. *Earth and Planetary Science Letters,* 272(1–2):231–239. **http://dx.doi.org/10.1016/j.epsl.2008.04.042**

Calvès, G., Huuse, M., Clift, P.D. and Brusset, S., submitted. Giant fossil mass wasting off the coast of West India: the Nataraja submarine slide. *Earth and Planetary Science Letters*.

Calvès, G., Schwab, A.M., Huuse, M., Clift, P.D., and Inam, A., 2010. Thermal regime of the northwest Indian rifted margin–comparison with predictions. *Marine and Petroleum Geology,* 27(5):1133–1147. **http://dx.doi.org/10.1016/j.marpetgeo.2010.02.010**

Cane, M.A., and Molnar, P., 2001. Closing of the Indonesian Seaway as a precursor to East African aridification around 3–4 million years ago. *Nature,* 411(6834):157–162. **http://dx.doi.org/10.1038/35075500**

Catlos, E.J., Harrison, T.M., Kohn, M.J., Grove, M., Ryerson, F.J., Manning, C.E., and Upreti, B.N., 2001. Geochronologic and thermobarometric constraints on the evolution of the Main Central Thrust, central Nepal Himalaya. *Journal of Geophysical Research: Solid Earth,* 106(B8):16177–16204. **http://dx.doi.org/10.1029/2000JB900375**

Channell, J.E.T., Mazaud, A., Sullivan, P., Turner, S., and Raymo, M.E., 2002. Geomagnetic excursions and paleointensities in the Matuyama Chron at Ocean Drilling Program Sites 983 and 984 (Iceland Basin). *Journal of Geophysical Research: Solid Earth,* 107(B6):2114–2127. **http://dx.doi.org/10.1029/2001JB000491**

Chatterjee, N., and Ghose, N.C., 2010. Metamorphic evolution of the Naga Hills eclogite and blueschist, northeast India: implications for early subduction of the Indian plate under the Burma microplate. *Journal of Metamorphic Geology,* 28(2):209–225. **http://dx.doi.org/10.1111/j.1525-1314.2009.00861.x**

Chatterjee, S., Goswami, A., and Scotese, C.R., 2013. The longest voyage: tectonic, magmatic, and paleoclimatic evolution of the Indian plate during its northward flight from Gondwana to Asia. *Gondwana Research,* 23(1):238–267. **http://dx.doi.org/10.1016/j.gr.2012.07.001**

Chaubey, A.K., Bhattacharya, G.C., Murty, G.P.S., Srinivas, K., Ramprasad, T., and Gopala Rao, D., 1998. Early Tertiary seafloor spreading magnetic anomalies and paleo-propagators in the northern Arabian Sea. *Earth and Planetary Science Letters,* 154(1–4):41–52. **http://dx.doi.org/10.1016/S0012-821X(97)00178-7**

Chaubey, A.K., Dyment, J., Bhattacharya, G.C., Royer, J.-Y., Srinivas, K., and Yatheesh, V., 2002. Paleogene magnetic isochrons and palaeo-propagators in the Arabian and Eastern Somali basins, NW Indian Ocean. *In* Clift, P.D., Kroon, D., Gaedicke, C., and Craig, J. (Eds.), *The Tectonic and Climatic Evolution of the Arabian Sea Region.* Geological Society Special Publication, 195(1):71–85. **http://dx.doi.org/10.1144/GSL.SP.2002.195.01.05**

Chenet, A.-L., Fluteau, F., Courtillot, V., Gérard, M., and Subbarao, K.V., 2008. Determination of rapid Deccan eruptions across the Cretaceous-Tertiary boundary using paleomagnetic secular variation: results from a 1200-m-thick section in the Mahabaleshwar escarpment. *Journal of Geophysical Research: Solid Earth,* 113(B4):B04101. **http://dx.doi.org/10.1029/2006JB004635**

Clemens, S.C., and Prell, W.L., 2003. A 350,000 year summer-monsoon multiproxy stack from the Owen Ridge, northern Arabian Sea. *Marine Geology,* 201(1–3):35–51. **http://dx.doi.org/10.1016/S0025-3227(03)00207-X**

Clift, P., Gaedicke, C., Edwards, R., Lee, J., II, Hildebrand, P., Amjad, S., White, R.S. and Schlueter, H.-U., 2002. The stratigraphic evolution of the Indus Fan and the history of sedimentation in the Arabian Sea. *Mar. Geophys. Res.*, 23(3):223-245.

Clift, P.D., 2006. Controls on the erosion of Cenozoic Asia and the flux of clastic sediment to the ocean. *Earth and Planetary Science Letters,* 241(3–4):571–580. **http://dx.doi.org/10.1016/j.epsl.2005.11.028**

Clift, P.D., and Blusztajn, J., 2005. Reorganization of the western Himalayan river system after five million years ago. *Nature,* 438(7070):1001–1003. **http://dx.doi.org/10.1038/nature04379**

Clift, P.D., Campbell, I.H., Pringle, M.S., Carter, A., Zhang, X., Hodges, K.V., Khan, A.A., and Allen, C.M., 2004. Thermochronology of the modern Indus River bedload; new insight into the controls on the marine stratigraphic record. *Tectonics,* 23(5):TC5013. **http://dx.doi.org/10.1029/2003TC001559**

Clift, P.D., Giosan, L., Carter, A., Garzanti, E., Galy, V., Tabrez, A.R., Pringle, M., Campbell, I.H., France-Lanord, C., Blusztajn, J., Allen, C., Alizai, A., Lückge, A., Danish, M., and Rabbani, M.M., 2010. Monsoon control over erosion patterns in the western Himalaya: possible feed-back into the tectonic evolution. *In* Clift, P.D., Tada, R., and Zheng, H. (Eds.), *Monsoon Evolution and Tectonics–Climate Linkage in Asia.* Geological Society Special Publication, 342(1):185–218. **http://dx.doi.org/10.1144/SP342.12**

Clift, P.D., Giosan, L., Henstock, T.J., and Tabrez, A.R., 2014. Sediment storage and reworking on the shelf and in the canyon of the Indus River-Fan system since the Last Glacial Maximum. *Basin Research,* 26(1):183–202. **http://dx.doi.org/10.1111/bre.12041**

Clift, P.D., Hodges, K.V., Heslop, D., Hannigan, R., Long, H.V., and Calves, G., 2008. Correlation of Himalayan exhumation rates and Asian monsoon intensity. *Nature Geoscience,* 1(12):875–880. **http://dx.doi.org/10.1038/ngeo351**

Clift, P.D., Shimizu, N., Layne, G.D., Blusztajn, J.S., Gaedicke, C., Schlüter, H.-U., Clark, M.K., and Amjad, S., 2001. Development of the Indus Fan and its significance for the erosional history of the western Himalaya and Karakoram. *Geological Society of America Bulletin,* 113(8):1039–1051. **http://dx.doi.org/10.1130/0016-7606(2001)113<1039:DOTIFA>2.0.CO;2**

Clift, P.D., and VanLaningham, S., 2010. A climatic trigger for a major Oligo-Miocene unconformity in the Himalayan foreland basin. *Tectonics,* 29(5):TC5014. **http://dx.doi.org/10.1029/2010TC002711**

Collier, J.S., Sansom, V., Ishizuka, O., Taylor, R.N., Minshull, T.A., and Whitmarsh, R.B., 2008. Age of Seychelles–India break-up. *Earth and Planetary Science Letters,* 272(1–2):264–277. **http://dx.doi.org/10.1016/j.epsl.2008.04.045**

Courtillot, V., Féraud, G., Maluski, H., Vandamme, D., Moreau, M.G., and Besse, J., 1988. Deccan flood basalts and the Cretaceous/Tertiary boundary. *Nature,* 333(6176):843–846. **http://dx.doi.org/10.1038/333843a0**

Courtillot, V., Gallet, Y., Rocchia, R., Féraud, G., Robin, E., Hofmann, C., Bhandari, N., and Ghevariya, Z.G., 2000. Cosmic markers, $^{40}Ar/^{39}Ar$ dating and paleomagnetism of the KT sections in the Anjar area of the Deccan large igneous province. *Earth and Planetary Science Letters,* 182(2):137–156. **http://dx.doi.org/10.1016/S0012-821X(00)00238-7**

Courtillot, V., Jaupart, C., Manighetti, I., Tapponnier, P., and Besse, J., 1999. On causal links between flood basalts and continental breakup. *Earth and Planetary Science Letters,* 166(3–4):177–195. **http://dx.doi.org/10.1016/S0012-821X(98)00282-9**

DeCelles, P.G., Kapp, P., Gehrels, G.E., and Ding, L., 2014. Paleocene–Eocene foreland basin evolution in the Himalaya of southern Tibet and Nepal: implications for the age of initial India-Asia collision. *Tectonics,* 33(5):824–849. **http://dx.doi.org/10.1002/2014TC003522**

deMenocal, P., Bloemendal, J., and King, J., 1991. A rock-magnetic record of monsoonal dust deposition to the Arabian Sea: evidence for a shift in the mode of deposition at 2.4 Ma. *In* Prell, W.L., Niitsuma, N., et al., *Proceedings of the Ocean Drilling Program, Scientific Results,* 117: College Station, TX (Ocean Drilling Program), 389–407. **http://dx.doi.org/10.2973/odp.proc.sr.117.178.1991**

Dewey, J.F., Cande, S., and Pitman, W.C., III, 1989. Tectonic evolution of the India/Eurasia collision zone. *Eclogae Geologicae Helvetiae,* 82(3):717–734. **http://retro.seals.ch/digbib/view?pid=egh-001:1989:82::733**

Donaldson, D.G., Webb, A.A.G., Menold, C.A., Kylander-Clark, A.R.C., and Hacker, B.R., 2013. Petrochronology of Himalayan ultrahigh-pressure eclogite. *Geology,* 41(8):835–838. **http://dx.doi.org/10.1130/G33699.1**

Dortch, J.M., Owen, L.A., Haneberg, W.C., Caffee, M.W., Dietsch, C., and Kamp, U., 2009. Nature and timing of large landslides in the Himalaya and Transhimalaya of northern India. *Quaternary Science Reviews,* 28(11–12):1037–1054. **http://dx.doi.org/10.1016/j.quascirev.2008.05.002**

Droz, L., and Bellaiche, G., 1991. Seismic facies and geologic evolution of the central portion of the Indus Fan. *In* Weimer, P., and Link, M.H. (Eds.), *Frontiers in Sedimentary Geology* (Volume 4): *Seismic Facies and Sedimentary Processes of Submarine Fans and Turbidite Systems.* Bouma, A.H. (Series Ed.): New York (Springer-Verlag), 383–402. **http://dx.doi.org/10.1007/978-1-4684-8276-8_21**

England, P., and Houseman, G., 1986. Finite strain calculations of continental deformation: 2. Comparison with the India-Asia collision zone. *Journal of Geophysical Research: Solid Earth,* 91(B3):3664–3676. **http://dx.doi.org/10.1029/JB091iB03p03664**

Fleitmann, D., Burns, S.J., Mudelsee, M., Neff, U., Kramers, J., Mangini, A., and Matter, A., 2003. Holocene forcing of the Indian monsoon recorded in a stalagmite from southern Oman. *Science,* 300(5626):1737–1739. **http://dx.doi.org/10.1126/science.1083130**

Garzanti, E., Baud, A., and Mascle, G., 1987. Sedimentary record of the northward flight of India and its collision with Eurasia (Ladakh Himalaya, India). *Geodinamica Acta,* 1(4–5):297–312. **http://dx.doi.org/10.1080/09853111.1987.11105147**

Garzanti, E., Vezzoli, G., Andò, S., Paparella, P., and Clift, P.D., 2005. Petrology of Indus River sands: a key to interpret erosion history of the Western Himalayan syntaxis. *Earth and Planetary Science Letters,* 229(3–4):287–302. **http://dx.doi.org/10.1016/j.epsl.2004.11.008**

Giosan, L., Clift, P.D., Macklin, M.G., Fuller, D.Q., Constantinescu, S., Durcan, J.A., Stevens, T., Duller, G.A.T., Tabrez, A.R., Gangal, K., Adhikari, R., Alizai, A., Filip, F., VanLaningham, S., and Syvitski, J.P.M., 2012. Fluvial landscapes of the Harappan civilization. *Proceedings of the National Academy of Sciences of the United States of America,* 109(26):E1688–E1694. **http://dx.doi.org/10.1073/pnas.1112743109**

Godin, L., Grujic, D., Law, R.D., and Searle, M.P., 2006. Channel flow, ductile extrusion and exhumation in continental collision zones: an introduction. *In* Law, R.D, Searle, M.P., and Godin, L. (Eds.), *Channel Flow, Ductile Extrusion and Exhumation in Continental Collision Zones.* Geological Society Special Publication, 268(1):1–23. **http://dx.doi.org/10.1144/GSL.SP.2006.268.01.01**

Gombos, A.M., Jr., Powell, W.G., and Norton, I.O., 1995. The tectonic evolution of western India and its impact on hydrocarbon occurrences: an overview. *Sedimentary Geology,* 96(1–2):119–129. **http://dx.doi.org/10.1016/0037-0738(94)00129-I**

Goswami, V., Singh, S.K., Bhushan, R., and Rai, V.K., 2012. Temporal variations in $^{87}Sr/^{86}Sr$ and ε_{Nd} in sediments of the southeastern Arabian Sea: impact of monsoon and surface water circulation. *Geochemistry, Geophysics, Geosystems,* 13(1):Q01001. **http://dx.doi.org/10.1029/2011GC003802**

Gupta, A.K., Mohan, K., Sarkar, S., Clemens, S.C., Ravindra, R., and Uttam, R.K., 2011. East–west similarities and differences in the surface and deep northern Arabian Sea records during the past 21 Kyr. *Palaeogeography, Palaeoclimatology, Palaeoecology,* 301(1–4):75–85. **http://dx.doi.org/10.1016/j.palaeo.2010.12.027**

Harris, N., 2007. Channel flow and the Himalayan-Tibetan orogen: a critical review. *Journal of the Geological Society,* 164(3):511–523. **http://dx.doi.org/10.1144/0016-76492006-133**

Hartog Jager, D.D., Giles, M.R., and Griffiths, G.R., 1993. Evolution of Paleogene submarine fans of the North Sea in space and time. In Parker, J.R. (Ed.), *Petroleum Geology of Northwest Europe: Proceedings of the 4th Conference,* Geological Society, London, 4:59–71. **http://dx.doi.org/10.1144/0040059**

Haug, G.H., and Tiedemann, R., 1998. Effect of the formation of the Isthmus of Panama on Atlantic Ocean thermohaline circulation. *Nature,* 393(6686):673–676. **http://dx.doi.org/10.1038/31447**

Heine, C., Müller, R.D., and Gaina, C., 2004. Reconstructing the lost eastern Tethys ocean basin: convergence history of the SE Asian margin and marine gateways. *In* Clift, P., Kuhnt, W., Wang, P., and Hayes, D. (Eds.), *Continent-Ocean Interactions within East Asian Marginal Seas.* Geophysical Monograph, 37–54. **http://dx.doi.org/10.1029/149GM03**

Hodges, K.V., 2006. A synthesis of the channel flow-extrusion hypothesis as developed for the Himalayan-Tibetan orogenic system. *In* Law, R.D, Searle, M.P., and Godin, L. (Eds.), *Channel Flow, Ductile Extrusion and Exhumation in Continental Collision Zones.* Geological Society Special Publication, 268(1):71–90. **http://dx.doi.org/10.1144/GSL.SP.2006.268.01.04**

Hopper, J.R., Dahl-Jensen, T., Holbrook, W.S., Larsen, H.C., Lizarralde, D., Korenaga, J., Kent, G.M., and Kelemen, P.B., 2003. Structure of the SE

Greenland margin from seismic reflection and refraction data: implications for nascent spreading center subsidence and asymmetric crustal accretion during North Atlantic opening. *Journal of Geophysical Research: Solid Earth,* 108(B5):2269. **http://dx.doi.org/10.1029/2002JB001996**

Huber, M., and Goldner, A., 2012. Eocene monsoons. *Journal of Asian Earth Sciences,* 44:3–23. **http://dx.doi.org/10.1016/j.jseaes.2011.09.014**

Huyghe, P., Galy, A., Mugnier, J.-L., and France-Lanord, C., 2001. Propagation of the thrust system and erosion in the Lesser Himalaya: geochemical and sedimentological evidence. *Geology,* 29(11):1007–1010. **http://dx.doi.org/10.1130/0091-7613(2001)029<1007:POTTSA>2.0.CO;2**

Jaeger, J.-J., Courtillot, V., and Tapponnier, P., 1989. Paleontological view of the ages of the Deccan Traps, the Cretaceous/Tertiary boundary, and the India-Asia collision. *Geology,* 17(4):316–319. **http://dx.doi.org/10.1130/0091-7613(1989)017<0316:PVOTAO>2.3.CO;2**

Karisiddaiah, S.M., and Iyer, S.D., 1991. Petrology of rift-releated basalts at Bombay High waters, Arabian Sea. *Indian Journal of Marine Sciences* 20:208–211.

Karlapati, S., 2004. Seismic reflection and bathymetric study over deep offshore regions off the central west coast of India. [Ph.D. thesis], University of Goa, India.

Kenyon, N.H., Amir, A., and Cramp, A., 1995. Geometry of the younger sediment bodies of the Indus Fan. *In* Pickering, K.T., Hiscott, R.N., Kenyon, N.H., Ricci Lucchi, F., and Smith, R.D.A. (Eds.), *Atlas of Deep Water Environments: Architectural Style in Turbidite Systems*: London (Chapman & Hall), 89–93. **http://dx.doi.org/10.1007/978-94-011-1234-5_16**

Kolla, V., and Coumes, F., 1984. Morpho-acoustic and sedimentologic characteristics of the Indus Fan. *Geo-Marine Letters,* 3(2–4):133–139. **http://dx.doi.org/10.1007/BF02462458**

Kolla, V., and Coumes, F., 1987. Morphology, internal structure, seismic stratigraphy, and sedimentation of Indus Fan. *AAPG Bulletin,* 71(6):650–677. **http://archives.datapages.com/data/bulletns/1986-87/images/pg/00710006/0650/06500.pdf**

Kolla, V., and Coumes, F., 1990. Extension of structural and tectonic trends from the Indian subcontinent into the eastern Arabian Sea. *Marine and Petroleum Geology,* 7(2):188–196. **http://dx.doi.org/10.1016/0264-8172(90)90041-E**

Krishna, K.S., Gopala Rao, D., and Sar, D., 2006. Nature of the crust in the Laxmi Basin (14°–20°N), western continental margin of India. *Tectonics,* 25(1):TC1006. **http://dx.doi.org/10.1029/2004TC001747**

Kroon, D., Steens, T., and Troelstra, S.R., 1991. Onset of monsoonal related upwelling in the western Arabian Sea as revealed by planktonic foraminifers. *In* Prell, W.L., Niitsuma, N., et al., *Proceedings of the Ocean Drilling Program, Scientific Results,* 117: College Station, TX (Ocean Drilling Program), 257–263. **http://dx.doi.org/10.2973/odp.proc.sr.117.126.1991**

Licht, A., van Cappelle, M., Abels, H.A., Ladant, J.-B., Trabucho-Alexandre, J., France-Lanord, C., Donnadieu, Y., Vandenberghe, J., Rigaudier, T., Lécuyer, C., Terry, D., Jr., Adriaens, R., Boura, A., Guo, Z., Soe, A.N., Quade, J., Dupont-Nivet, G., and Jaeger, J.-J., 2014. Asian monsoons in a late Eocene greenhouse world. *Nature*, 513(7519):501–506. **http://dx.doi.org/10.1038/nature13704**

Malod, J.A., Droz, L., Mustafa Kemal, B., and Patriat, B., 1997. Early spreading and continental to oceanic basement transition beneath the Indus deep-sea fan: northeastern Arabian Sea. *Marine Geology,* 141(1–4):221–235. **http://dx.doi.org/10.1016/S0025-3227(97)00074-1**

McCaffrey, W.D., Gupta, S., and Brunt, R., 2002. Repeated cycles of submarine channel incision, infill and transition to sheet sandstone development in the Alpine Foreland Basin, SE France. *Sedimentology,* 49(3):623–635. **http://dx.doi.org/10.1046/j.1365-3091.2002.00477.x**

McKenzie, D., 1978. Some remarks on the development of sedimentary basins. *Earth and Planetary Science Letters,* 40(1):25–32. **http://dx.doi.org/10.1016/0012-821X(78)90071-7**

McKenzie, D., and Bickle, M.J., 1988. The volume and composition of melt generated by extension of the lithosphere. *Journal of Petrology,* 29(3):625–679. **http://dx.doi.org/10.1093/petrology/29.3.625**

Métivier, F., Gaudemer, Y., Tapponnier, P., and Klein, M., 1999. Mass accumulation rates in Asia during the Cenozoic. *Geophysical Journal International,* 137(2):280–318. **http://dx.doi.org/10.1046/j.1365-246X.1999.00802.x**

Meyers, P.A., 1990. Impacts of late Quaternary fluctuations in water level on the accumulation of sedimentary organic matter in Walker Lake, Nevada. *Palaeogeography, Palaeoclimatology, Palaeoecology,* 78(3–4):229–240. **http://dx.doi.org/10.1016/0031-0182(90)90216-T**

Meyers, P.A., 1997. Organic geochemical proxies of paleoceanographic, paleolimnologic, and paleoclimatic processes. *Organic Geochemistry,* 27(5–6):213–250. **http://dx.doi.org/10.1016/S0146-6380(97)00049-1**

Miles, P.R., Munschy, M., and Ségoufin, J., 1998. Structure and early evolution of the Arabian Sea and East Somali Basin. *Geophysical Journal International,* 134(3):876–888. **http://dx.doi.org/10.1046/j.1365-246x.1998.00625.x**

Miles, P.R., and Roest, W.R., 1993. Earliest sea-floor spreading magnetic anomalies in the north Arabian Sea and the ocean–continent transition. *Geophysical Journal International,* 115(3):1025–1031. **http://dx.doi.org/10.1111/j.1365-246X.1993.tb01507.x**

Milliman, J.D., and Syvitski, J.P.M., 1992. Geomorphic/tectonic control of sediment discharge to the ocean: the importance of small mountainous rivers. *The Journal of Geology,* 100(5):525–544. **http://dx.doi.org/10.1086/629606**

Minshull, T.A., Lane, C.I., Collier, J.S., and Whitmarsh, R.B., 2008. The relationship between rifting and magmatism in the northeastern Arabian Sea. *Nature Geoscience,* 1(7):463–467. **http://dx.doi.org/10.1038/ngeo228**

Mishra, R., Pandey, D.K., Ramesh, P., and Shipboard Scientific Party SK-306, 2015. Active channel system in the middle Indus fan: results from high-resolution bathymetry surveys. *Current Science*, 108(3):409–412.

Mishra, V., Smoliak, B.V., Lettenmaier, D.P., and Wallace, J.M., 2012. A prominent pattern of year-to-year variability in Indian summer monsoon rainfall. *Proceedings of the National Academy of Sciences of the United States of America,* 109(19):7213–7217. **http://dx.doi.org/10.1073/pnas.1119150109**

Misra, A.A., Sinha, N., and Mukherjee, S., 2015. Repeat ridge jumps and microcontinent separation: insights from NE Arabian Sea. *Marine and Petroleum Geology,* 59:406–428. **http://dx.doi.org/10.1016/j.marpetgeo.2014.08.019**

Miyashiro, A., 1994. *Metamorphic Petrology:* New York (Oxford University Press).

Molnar, P., England, P., and Martinod, J., 1993. Mantle dynamics, uplift of the Tibetan Plateau, and the Indian monsoon. *Reviews of Geophysics,* 31(4):357–396. **http://dx.doi.org/10.1029/93RG02030**

Molnar, P., and Tapponnier, P., 1975. Cenozoic tectonics of Asia: effects of a continental collision: features of recent continental tectonics in Asia can be interpreted as results of the India-Eurasia collision. *Science,* 189(4201):419–426. **http://dx.doi.org/10.1126/science.189.4201.419**

Moore, J.G., 1970. Water content of basalt erupted on the ocean floor. *Contributions to Mineralogy and Petrology,* 28(4):272–279. **http://dx.doi.org/10.1007/BF00388949**

Müller, A., and Mathesius, U., 1999. The palaeoenvironments of coastal lagoons in the southern Baltic Sea, I. The application of sedimentary C_{org}/N ratios as source indicators of organic matter. *Palaeogeography, Palaeoclimatology, Palaeoecology,* 145(1–3):1–16. **http://dx.doi.org/10.1016/S0031-0182(98)00094-7**

Mutti, E., 1977. Distinctive thin-bedded turbidite facies and related depositional environments in the Eocene Hecho Group (south-central Pyrenees, Spain). *Sedimentology,* 24(1):107–132. **http://dx.doi.org/10.1111/j.1365-3091.1977.tb00122.x**

Mutti, E., 1992. *Turbidite Sandstones:* Milan (Agip S.p.A., S. Donato Milanese).

Naini, B.R., 1980. Geological and geophysical study of the continental margin of western India, and the adjoining Arabian Sea including the Indus cone [Ph.D. Thesis]. Columbia University.

Naini, B.R., and Talwani, M., 1982. Structural framework and the evolutionary history of the continental margin of Western India. *In* Watkins, J.S., and Drake, C.L. (Eds.), *Studies in Continental Margin Geology.* AAPG Memoir, 167–191.

Najman, Y., 2006. The detrital record of orogenesis: a review of approaches and techniques used in the Himalayan sedimentary basins. *Earth-Science Reviews,* 74(1–2):1–72. **http://dx.doi.org/10.1016/j.earscirev.2005.04.004**

Najman, Y., Appel, E., Boudagher-Fadel, M., Bown, P., Carter, A., Garzanti, E., Godin, L., Han, J., Liebke, U., Oliver, G., Parrish, R., and Vezzoli, G., 2010. Timing of India-Asia collision: geological, biostratigraphic, and palaeomagnetic constraints. *Journal of Geophysical Research: Solid Earth,* 115(B12):B12416. **http://dx.doi.org/10.1029/2010JB007673**

Normark, W.R., Piper, D.J.W., and Hess, G.R., 1979. Distributary channels, sand lobes, and mesotopography of Navy submarine fan, California Borderland, with applications to ancient fan sediments. *Sedimentology,* 26(6):749–774. **http://dx.doi.org/10.1111/j.1365-3091.1979.tb00971.x**

Norton, I.O., and Sclater, J.G., 1979. A model for the evolution of the Indian Ocean and the breakup of Gondwanaland. *Journal of Geophysical Research: Solid Earth,* 84(B12):6803–6830. **http://dx.doi.org/10.1029/JB084iB12p06803**

Pandey, D.K., Rajan, S., and Pandey, A., 2010. Seismic imaging of Paleogene sediments of Kachchh Shelf, (western Indian margin) and their correlation with sea-level fluctuations. *Marine and Petroleum Research,* 27(6):1166–1174. **http://dx.doi.org/10.1016/j.marpetgeo.2010.02.002**

Pandey, D.K., Pandey, A., and Rajan, S., 2011. Offshore extension of Deccan Traps in Kachchh, central western India: implications for geological sequestration studies. *Natural Resources Research,* 20(1):33–43. **http://dx.doi.org/10.1007/s11053-010-9133-x**

Pandey, O.P., Agrawal, P.K., and Negi, J.G., 1995. Lithospheric structure beneath Laxmi Ridge and Late Cretaceous geodynamic events. *Geo-Marine Letters,* 15(2):85–91. **http://dx.doi.org/10.1007/BF01275411**

Ponton, C., Giosan, L., Eglinton, T.I., Fuller, D.Q., Johnson, J.E., Kumar, P., and Collett, T.S., 2012. Holocene aridification of India. *Geophysical Research Letters,* 39(3):L3407. **http://dx.doi.org/10.1029/2011GL050722**

Prell, W.L., and Kutzbach, J.E., 1992. Sensitivity of the Indian monsoon to forcing parameters and implications for its evolution. *Nature,* 360(6405):647–652. **http://dx.doi.org/10.1038/360647a0**

Prell, W.L., Murray, D.W., Clemens, S.C., and Anderson, D.M., 1992. Evolution and variability of the Indian Ocean summer monsoon: evidence from the western Arabian Sea drilling program. *In* Duncan, R.A., Rea, D.K., Kidd, R.B., von Rad, U., and Weissel, J.K. (Eds.), *Synthesis of Results from Scientific Drilling in the Indian Ocean.* Geophysical Monograph, 70:447–469. **http://dx.doi.org/10.1029/GM070p0447**

Prins, M.A., Postma, G., Cleveringa, J., Cramp, A., and Kenyon, N.H., 2000. Controls on terrigenous sediment supply to the Arabian Sea during the late Quaternary: the Indus Fan. *Marine Geology,* 169(3–4):327–349. **http://dx.doi.org/10.1016/S0025-3227(00)00086-4**

Radha Krishna, M., Verma, R.K., and Purushotham, A.K., 2002. Lithospheric structure below the eastern Arabian Sea and adjoining west coast of India based on integrated analysis of gravity and seismic data. *Marine Geophysical Research,* 23(1):25–42. **http://dx.doi.org/10.1023/A:1021288003781**

Ramstein, G., Fluteau, F., Besse, J., and Joussaume, S., 1997. Effect of orogeny, plate motion and land–sea distribution on Eurasian climate change over the past 30 million years. *Nature,* 386(6627):788–795. **http://dx.doi.org/10.1038/386788a0**

Rao, V.P., and Wagle, B.G., 1997. Geomorphology and surficial geology of the western continental shelf and slope of India: a review. *Current Science*, 73(4):330–340. **http://www.currentscience.ac.in/Downloads/article_id_073_04_0330_0350_0.pdf**

Rea, D.K., 1992. Delivery of Himalayan sediment to the northern Indian Ocean and its relation to global climate, sea level, uplift, and seawater strontium. *In* Duncan, R.A., Rea, D.K., Kidd, R.B., von Rad, U., and Weissel, J.K. (Eds.), *Synthesis of Results from Scientific Drilling in the Indian Ocean.* Geophysical Monograph, 70:387–402. **http://dx.doi.org/10.1029/GM070p0387**

Reading, H.G., and Richards, M., 1994. Turbidite systems in deep-water basin margins classified by grain size and feeder system. *AAPG Bulletin,* 78(5):792–822. **http://aapgbull.geoscienceworld.org/cgi/content/abstract/78/5/792**

Replumaz, A., and Tapponnier, P., 2003. Reconstruction of the deformed collision zone between India and Asia by backward motion of lithospheric blocks. *Journal of Geophysical Research: Solid Earth,* 108(B6):2285. **http://dx.doi.org/10.1029/2001JB000661**

Robinson, D.M., DeCelles, P.G., and Copeland, P., 2006. Tectonic evolution of the Himalayan thrust belt in western Nepal: implications for channel flow models. *Geological Society of America Bulletin,* 118(7–8):865–885. **http://dx.doi.org/10.1130/B25911.1**

Rowley, D.B., 1996. Age of initiation of collision between India and Asia: a review of stratigraphic data. *Earth and Planetary Science Letters,* 145(1–4):1–13. **http://dx.doi.org/10.1016/S0012-821X(96)00201-4**

Royer, J.-Y., Chaubey, A.K., Dyment, J., Bhattacharya, G.C., Srinivas, K., Yatheesh, V., and Ramprasad, T., 2002. Paleogene plate tectonic evolution of the Arabian and eastern Somali basins. *In* Clift, P.D., Kroon, D., Gaedicke, C., and Craig, J. (Eds.), *The Tectonic and Climatic Evolution of the Arabian Sea Region.* Geological Society Special Publication, 195(1):7–23. **http://dx.doi.org/10.1144/GSL.SP.2002.195.01.02**

Ryan, W.B.F., Carbotte, S.M., Coplan, J.O., O'Hara, S., Melkonian, A., Arko, R., Weissel, R.A., Ferrini, V., Goodwillie, A., Nitsche, F., Bonczkowski, J., and Zemsky, R., 2009. Global multi-resolution topography synthesis. *Geochemistry, Geophysics, Geosystems,* 10(3):Q03014. **http://dx.doi.org/10.1029/2008GC002332**

Self, S., Blake, S., Sharma, K., Widdowson, M., and Sephton, S., 2008. Sulfur and chlorine in Late Cretaceous Deccan magmas and eruptive gas release. *Science,* 319(5870):1654–1657. **http://dx.doi.org/10.1126/science.1152830**

Shipboard Scientific Party, 1974. Site 221. With contribution by R.E. Coleman and N. Hamilton. *In* Whitmarsh, R.B., Weser, O.E., Ross, D.A., et al., *Initial Reports of the Deep Sea Drilling Project,* 23: Washington (U.S. Government Printing Office), 167–210. **http://dx.doi.org/10.2973/dsdp.proc.23.105.1974**

Singh, A., Singh, C., and Kennett, B.L.N., 2015. A review of crust and upper mantle structure beneath the Indian subcontinent. *Tectonophysics*, 644–645:1–21. **http://dx.doi.org/10.1016/j.tecto.2015.01.007**

Singh, A.D., Jung, S.J.A., Darling, K., Ganeshram, R., Ivanochko, T., and Kroon, D., 2011. Productivity collapses in the Arabian Sea during glacial cold phases. *Paleoceanography,* 26(3):PA3210. **http://dx.doi.org/10.1029/2009PA001923**

Singh, A.P., 1999. The deep crustal accretion beneath the Laxmi Ridge in the northeastern Arabian Sea: the plume model again. *Journal of Geodynamics,* 27(4–5):609–622. **http://dx.doi.org/10.1016/S0264-3707(98)00019-2**

Sinha-Roy, S., and Mohanty, M., 1988. Blueschist facies metamorphism in the ophiolitic mélange of the late Proterozoic Delhi fold belt, Rajasthan, India. *Precambrian Research,* 42(1–2):97–105. **http://dx.doi.org/10.1016/0301-9268(88)90012-5**

Skogseid, J., Planke, S., Faleide, J.I., Pedersen, T., Eldholm, O., and Neverdal, F., 2000. NE Atlantic continental rifting and volcanic margin formation. *In* Nøttvedt, A. (Ed.), *Dynamics of the Norwegian Margin.* Geological Society Special Publication, 167(1):295–326. **http://dx.doi.org/10.1144/GSL.SP.2000.167.01.12**

Stein, C.A., and Stein, S., 1992. A model for the global variation in oceanic depth and heat flow with lithospheric age. *Nature,* 359(6391):123–129. **http://dx.doi.org/10.1038/359123a0**

Stein, R., Boucsein, B., and Meyer, H., 2006. Anoxia and high primary production in the Paleogene Central Arctic Ocean: first detailed records from Lomonosov Ridge. *Geophysical Research Letters,* 33(18):L18606. **http://dx.doi.org/10.1029/2006GL026776**

Stein, R. and Macdonald, R.W., 2004. Geochemical proxies used for organic carbon source identification in Arctic Ocean sediments. In *Chapter 1: The Arctic Ocean: boundary conditions and background information* in Stein, R., and MacDonald, R.W. (Eds.), *The Organic Carbon Cycle in the Arctic Ocean:* Berlin (Springer), 24–32. **http://dx.doi.org/10.1007/978-3-642-18912-8_1**

Storey, M., Mahoney, J.J., Saunders, A.D., Duncan, R.A., Kelley, S.P., and Coffin, M.F., 1995. Timing of hot spot—related volcanism and the breakup of Madagascar and India. *Science,* 267(5199):852–855. **http://dx.doi.org/10.1126/science.267.5199.852**

Szulc, A.G., Najman, Y., Sinclair, H.D., Pringle, M., Bickle, M., Chapman, H., Garzanti, E., Andò, S., Huyghe, P., Mugnier, J.-L., Ojha, T., and DeCelles, P., 2006. Tectonic evolution of the Himalaya constrained by detrital ^{40}Ar–^{39}Ar, Sm–Nd and petrographic data from the Siwalik foreland basin succession, SW Nepal. *Basin Research,* 18(4):375–391. **http://dx.doi.org/10.1111/j.1365-2117.2006.00307.x**

Talwani, M., and Reif, C., 1998. Laxmi Ridge—a continental sliver in the Arabian Sea. *Marine Geophysical Research,* 20(4):259–271. **http://dx.doi.org/10.1023/A:1004674909280**

Twichell, S.C., Meyers, P.A., and Diester-Haass, L., 2002. Significance of high C/N ratios in organic-carbon-rich Neogene sediments under the Benguela Current upwelling system. *Organic Geochemistry,* 33(7):715–722. **http://dx.doi.org/10.1016/S0146-6380(02)00042-6**

Tobgay, T., McQuarrie, N., Long, S., Kohn, M.J., and Corrie, S.L., 2012. The age and rate of displacement along the Main Central Thrust in the western Bhutan Himalaya. *Earth and Planetary Science Letters,* 319–320:146–158. **http://dx.doi.org/10.1016/j.epsl.2011.12.005**

Todal, A., and Edholm, O., 1998. Continental margin off western India and Deccan Large Igneous Province. *Marine and Geophysical Research,* 20(4):273–291. **http://dx.doi.org/10.1023/A:1004640508371**

Tonarini, S., Villa, I.M., Oberli, F., Meier, M., Spencer, D.A., Pognante, U., and Ramsay, J.G., 1993. Eocene age of eclogite metamorphism in Pakistan Himalaya: implications for India-Eurasia collision. *Terra Nova,* 5(1):13–20. **http://dx.doi.org/10.1111/j.1365-3121.1993.tb00221.x**

Villinger, H., Grevemeyer, I., Kaul, N., Hauschild, J., and Pfender, M., 2002. Hydrothermal heat flux through aged oceanic crust: where does the heat escape? *Earth and Planetary Science Letters,* 202(1):159–170. **http://dx.doi.org/10.1016/S0012-821X(02)00759-8**

von der Heydt, A., and Dijkstra, H.A., 2006. Effect of ocean gateways on the global ocean circulation in the late Oligocene and early Miocene. *Paleoceanography,* 21(1):PA1011. **http://dx.doi.org/10.1029/2005PA001149**

Walker, R.G., 1978. Deep-water sandstone facies and ancient submarine fans: models for exploration of stratigraphic traps. *AAPG Bulletin,* 62:932–966.

Whipple, K.X., 2009. The influence of climate on the tectonic evolution of mountain belts. *Nature Geoscience,* 2:97–104. **http://dx.doi.org/10.1038/ngeo413**

White, N.M., Pringle, M., Garzanti, E., Bickle, M., Najman, Y., Chapman, H., and Friend, P., 2002. Constraints on the exhumation and erosion of the High Himalayan Slab, NW India, from foreland basin deposits. *Earth and Planetary Science Letters,* 195(1–2):29–44. **http://dx.doi.org/10.1016/S0012-821X(01)00565-9**

Whiting, B.M., Karner, G.D., and Driscoll, N.W., 1994. Flexural and stratigraphic development of the west Indian continental margin. *Journal of Geophysical Research: Solid Earth,* 99(B7):13791–13812. **http://dx.doi.org/10.1029/94JB00502**

Whitmarsh, R.B., Manatschal, G., and Minshull, T.A., 2001. Evolution of magma-poor continental margins from rifting to seafloor spreading. *Nature,* 413(6852):150–154. **http://dx.doi.org/10.1038/35093085**

Willett, S.D., 1999. Orogeny and orography: the effects of erosion on the structure of mountain belts. *Journal of Geophysical Research: Solid Earth,* 104(B12):28957–28981. **http://dx.doi.org/10.1029/1999JB900248**

Wu, F.-Y., Ji, W.-Q., Wang, J.-G., Liu, C.-Z., Chung, S.-L., and Clift, P.D., 2014. Zircon U–Pb and Hf isotopic constraints on the onset time of India-Asia collision. *American Journal of Science,* 314(2):548–579. **http://dx.doi.org/10.2475/02.2014.04**

Yatheesh, V., Bhattacharya, G.C., and Dyment, J., 2009. Early oceanic opening off western India–Pakistan margin: the Gop Basin revisited. *Earth and Planetary Science Letters,* 284(3–4):399–408. **http://dx.doi.org/10.1016/j.epsl.2009.04.044**

Zhang, P., Molnar, P., and Downs, W.R., 2001. Increased sedimentation rates and grain sizes 2–4 Myr ago due to the influence of climate change on erosion rates. *Nature,* 410(6831):891–897. **http://dx.doi.org/10.1038/35073504**

Table T1. Operations summary, Expedition 355. DSF = drilled depth below seafloor. APC = advanced piston corer, HLAPC = half-length advanced piston corer, XCB = extended core barrel, RCB = rotary core barrel. **Download table in .csv format.**

Hole	Latitude	Longitude	Water depth (m)	Penetration (m DSF)	Cored interval (m)	Recovered length (m)	Recovery (%)	Drilled interval (m)	Drilled interval (*N*)	Total cores (*N*)	APC cores (*N*)	HLAPC cores (*N*)	XCB cores (*N*)	RCB cores (*N*)
355-														
U1456A	16°37.2855′N	68°50.3272′E	3639.2	426.6	426.6	365.25	86	0.0	0	74	16	54	4	0
U1456B	16°37.2851′N	68°50.3454′E	3645.0	29.1	29.1	28.79	99	0.0	0	4	4	0	0	0
U1456C	16°37.2940′N	68°50.3366′E	3638.4	465.2	275.3	215.00	78	189.9	4	42	15	18	9	0
U1456D	16°37.2766′N	68°50.3365′E	3637.1	1024.4	565.6	319.18	56	458.8	1	60	0	0	0	60
U1456E	16°37.2857′N	68°50.3541′E	3636.9	1109.4	139.4	82.45	59	970.0	2	17	0	0	0	17
U1457A	17°90.9487′N	67°55.8037′E	3523.1	144.8	130.4	122.76	94	14.4	3	16	12	4	0	0
U1457B	17°90.9485′N	67°55.7955′E	3523.5	204.7	159.4	151.19	95	45.3	10	23	12	11	0	0
U1457C	17°90.9486′N	67°55.8121′E	3522.7	1108.6	917.0	436.96	48	191.6	1	97	0	0	0	97
			Expedition 355 totals:		2642.8	1721.58		1870.0	21	333	59	87	13	174

Hole	Start		End		Time on hole (days)
	Date (2015)	Time UTC (h)	Date (2015)	Time UTC (h)	
355-					
U1456A	9 April	0525	13 April	1235	4.30
U1456B	13 April	1235	13 April	1825	0.24
U1456C	13 April	1825	18 April	2050	5.10
U1456D	18 April	2050	3 May	1630	14.82
U1456E	3 May	1630	16 May	0230	12.42
U1457A	16 May	800	17 May	1445	1.28
U1457B	17 May	1445	19 May	0240	1.50
U1457C	19 May	0240	29 May	1730	10.62

Figure F1. Bathymetric map of the Arabian Sea and surrounding landmasses from GeoMapApp (Ryan et al., 2009). Yellow circles = Expedition 355 sites, white lines = major rivers and tributaries, red stars = earlier scientific drilling sites that have sampled the Indus Fan, pink line = approximate extent of the fan after Kolla and Coumes (1987), yellow dashed lines = speculated location of the continent/ocean boundary, depending on whether Laxmi Basin is oceanic or continental, gray lines with numbers = magnetic anomalies from Royer et al. (2002), white box = location of detailed map in Figure **F2**.

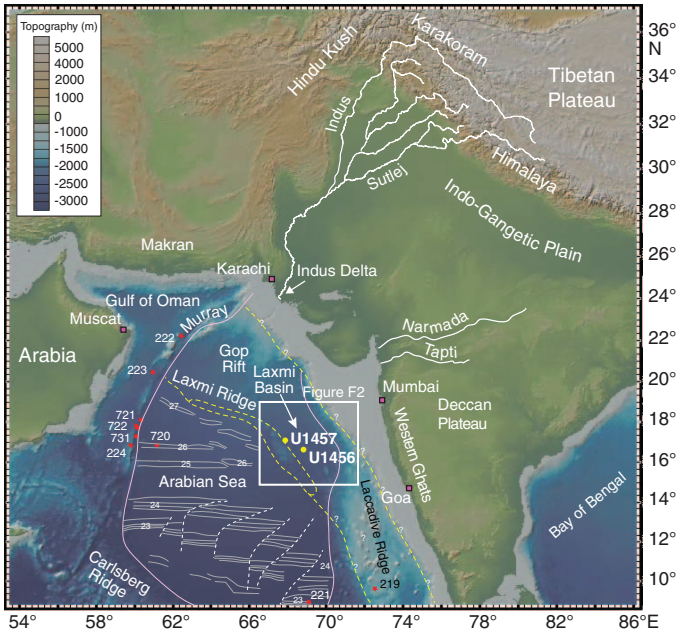

Figure F2. Bathymetric map of the region around Laxmi Basin showing the location of Expedition 355 sites in relation to other major bathymetric features, especially Laxmi Ridge. White dashed lines = possible locations of the continent/ocean boundary, depending upon whether the crust in Laxmi Basin has continental or oceanic affinity. Magnetic anomalies (yellow lines) from the Arabian Basin are from Miles et al. (1998), whereas those in Laxmi Basin (green lines) are from Bhattacharya et al. (1994). Contours (black lines) are in meters below sea level. Bathymetric data from GeoMapApp (Ryan et al., 2009).

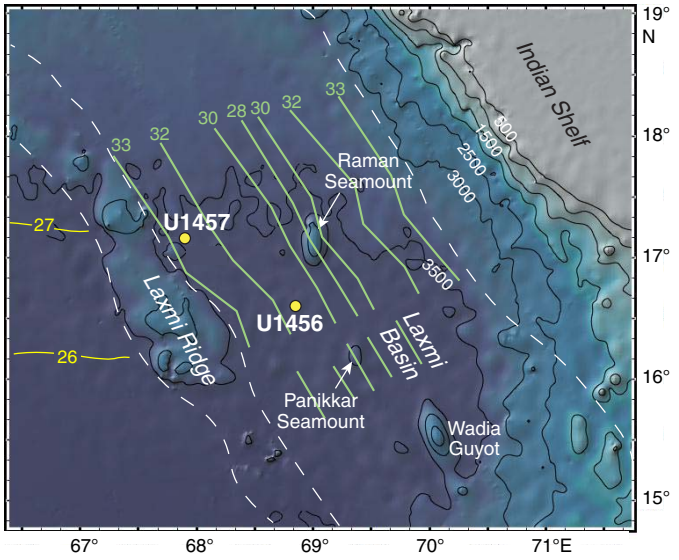

Figure F3. Uninterpreted seismic reflection profile Line W06 (top) and interpreted (bottom) seismic sections with location of Site U1456 (see Figure **F5** for seismic line locations). Orange bar = proposed penetration at Site U1456, white box = actual penetration. TWT = two-way traveltime.

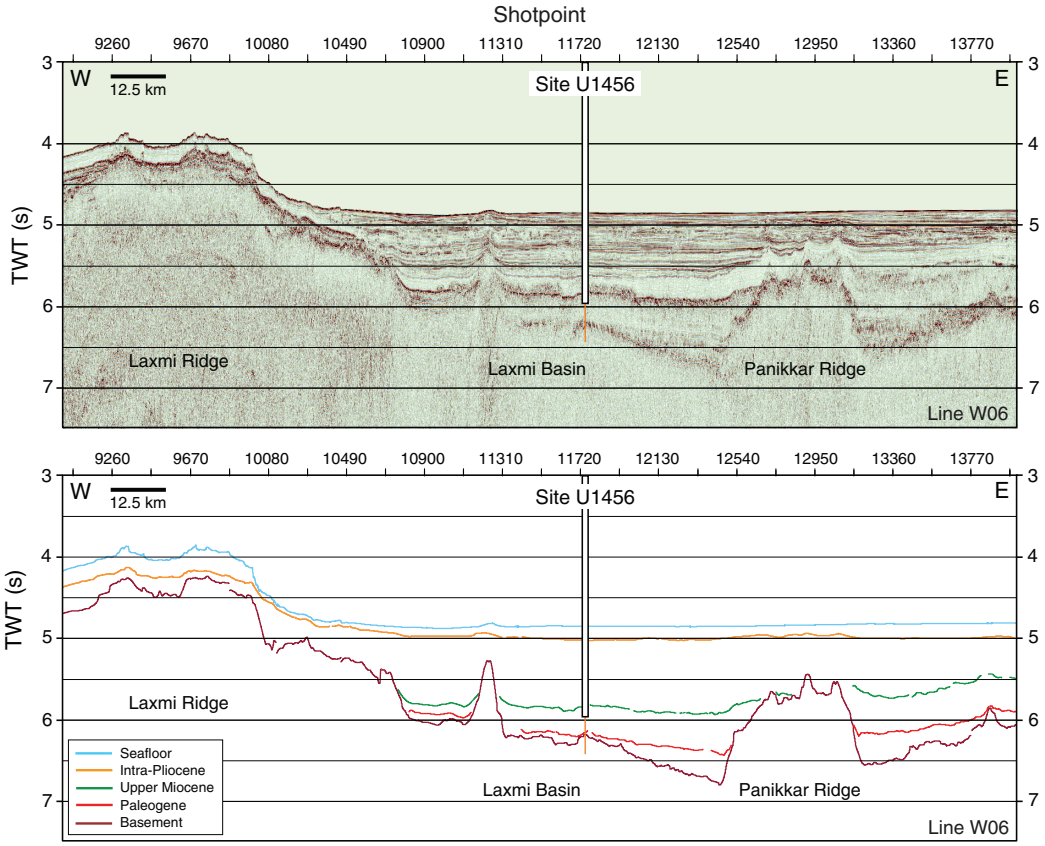

Figure F4. Uninterpreted seismic reflection profile Line IODP-04 (top) and interpreted (bottom) seismic sections with location of Site U1457 (see Figure **F5** for seismic line locations). TWT = two-way traveltime

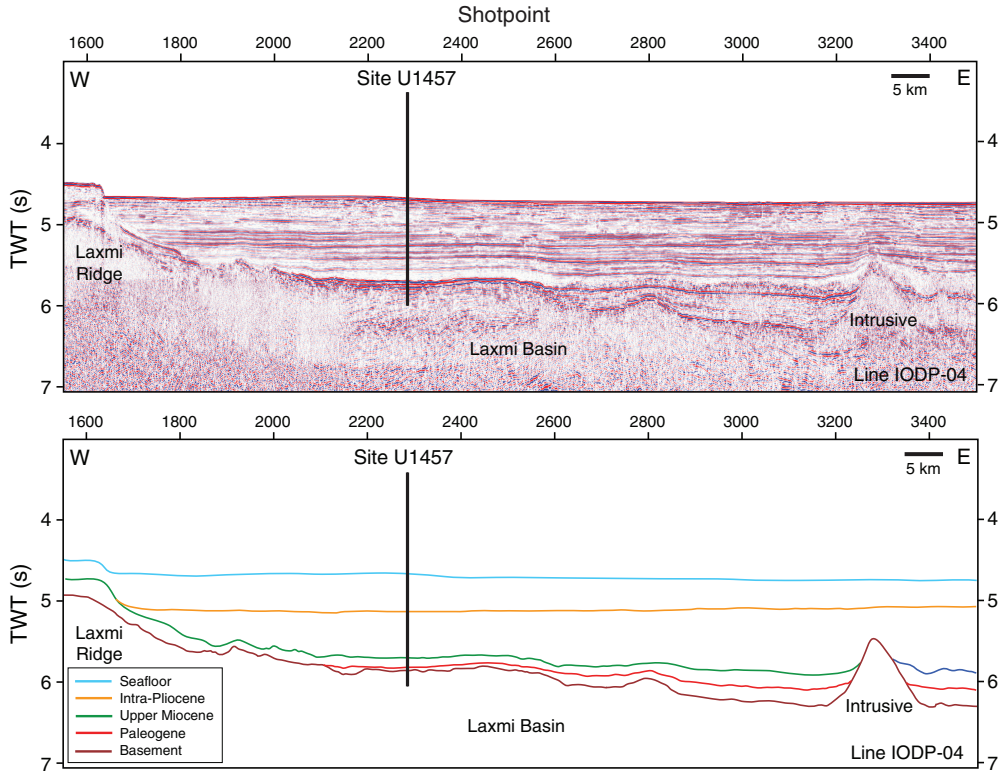

Figure F5. Multichannel seismic grid (orange and red lines) in the eastern Arabian Sea. Blue squares = industry wells, green stars = locations of existing shallow cores. Cores with published data include Core ABP-25 (Gupta et al., 2011); Cores 2491, J7, 2506, and 3268G5 (Bhushan et al., 2001); and Core SK17/MD76-131 (Singh et al., 2011). Red stars = Expedition 355 sites, blue shaded area = area surveyed by high-resolution multibeam bathymetry (see Figure **F7**). RS = Raman Seamount, PS = Panikkar Seamount, WG = Wadia Guyot.

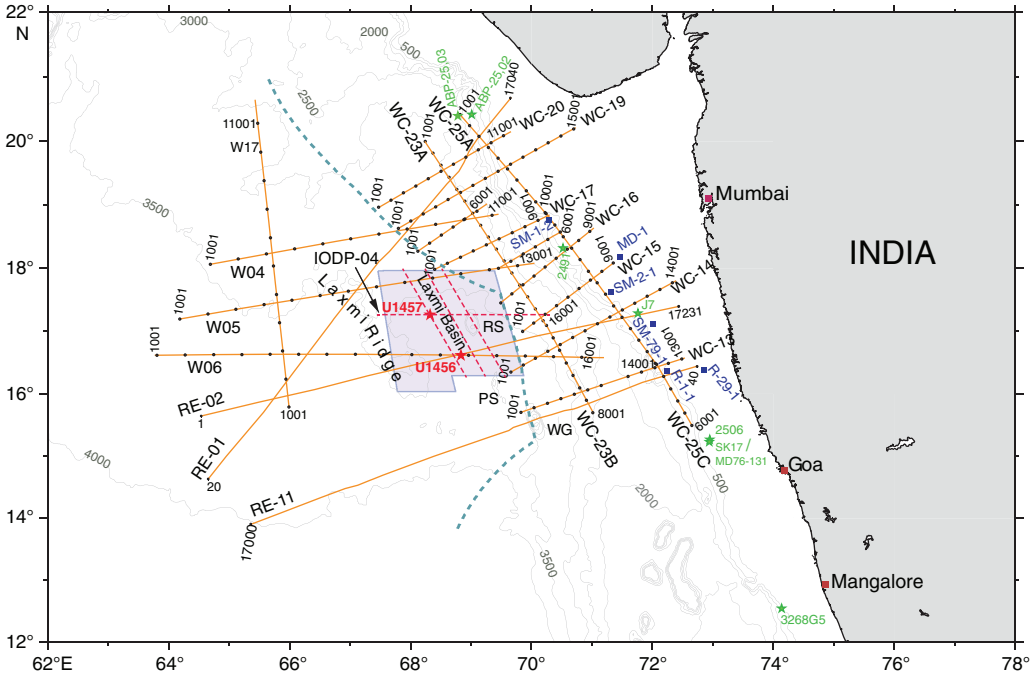

Figure F6. Locations of all seismic profiles (black and white lines) acquired by the Ministry of Earth Sciences, Government of India, in the Arabian Sea. Site U1456 is located on Line W06 and Site U1457 is located on Line IODP-04 (not shown).

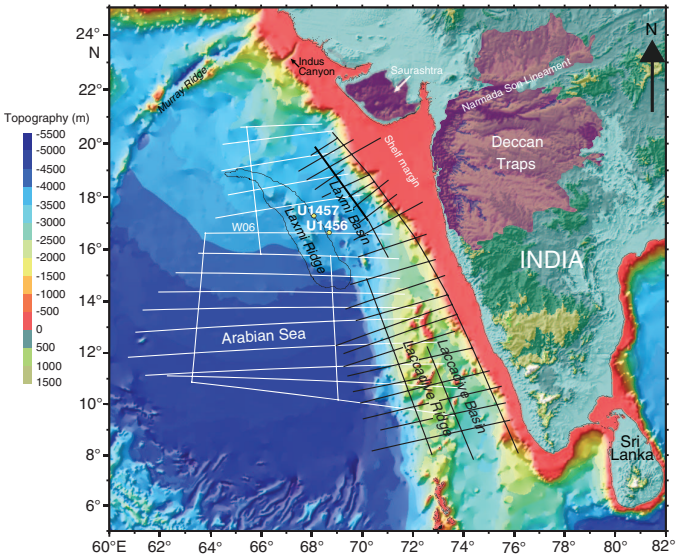

Figure F7. High-resolution multibeam bathymetry data acquired around the Expedition 355 drill sites. Contours (white lines) are in meters below sea level. Black lines are seismic lines with shotpoint numbers around site locations shown in white.

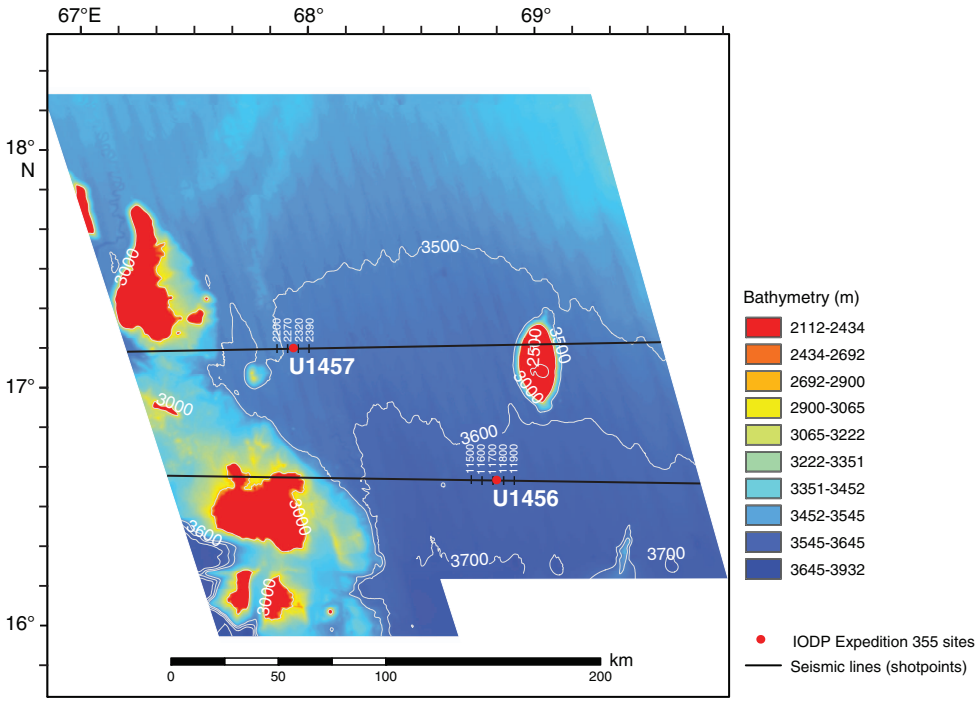

Figure F8. Depiction of the channel flow model, as described by Beaumont et al. (2001), in which surface processes in the form of erosion driven by focused precipitation along the mountain front allows deep-buried rocks from within the partial melt zone under southern Tibet to be brought to the surface in the Greater Himalaya. Uplift of the Indian foreland is expected to accompany enhanced erosion of the Himalaya, resulting in inversion of the foreland basin and loss of the erosion record onshore during this critical time (Clift and VanLaningham, 2010). STD = South Tibet Detachment, MCT = Main Central Thrust, MBT = Main Boundary Thrust.

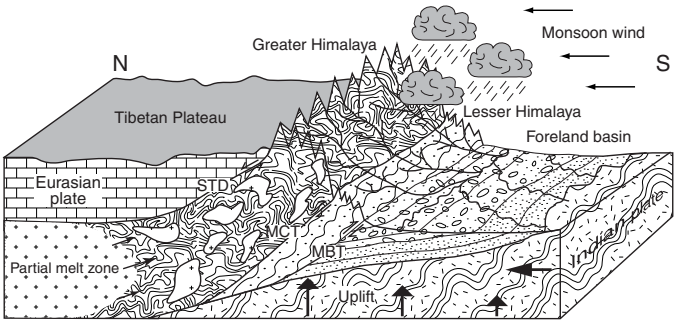

Figure F9. Lithostratigraphic and physical properties (Holes U1456A and U1456C–U1456E) summary for cored section, Site U1456. Downhole measurements are from Hole U1456C. WRMSL core data (dots): green = GRA bulk density, blue = magnetic susceptibility, purple = *P*-wave velocity. Red dots = core logger NGR. Black dots = discrete MAD bulk density and *P*-wave caliper (*x*-axis) on section halves. Gray lines = downhole measurements from end of pipe at ~82 mbsf. Natural gamma ray (in gAPI) plotted from downhole measurements continuously from open hole, through pipe to seafloor.

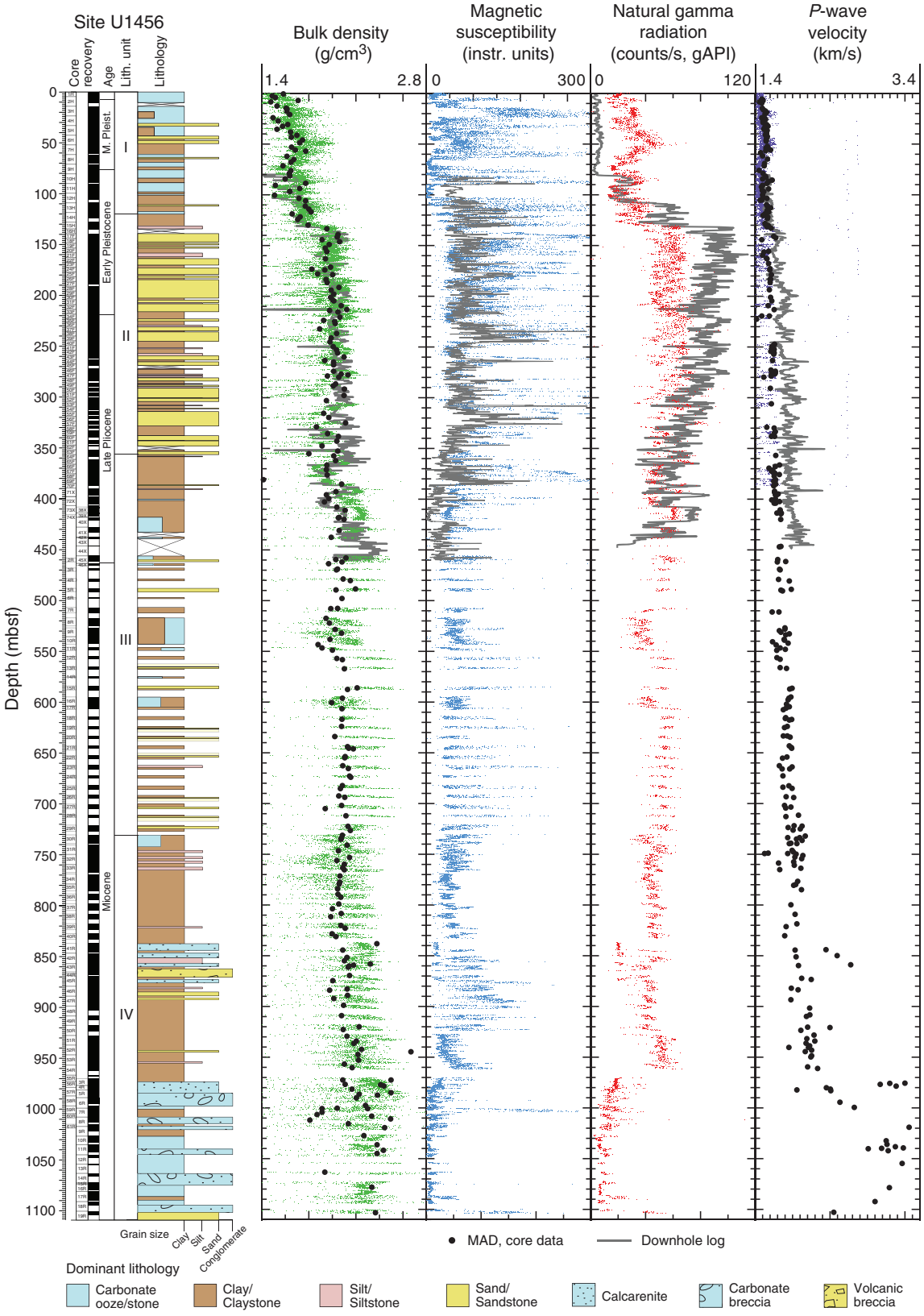

Figure F10. Age-depth model for Site U1456 created by synthesizing nannofossil and foraminifer bioevents with magnetic chron assignments. Top = last occurrence, base = first occurrence.

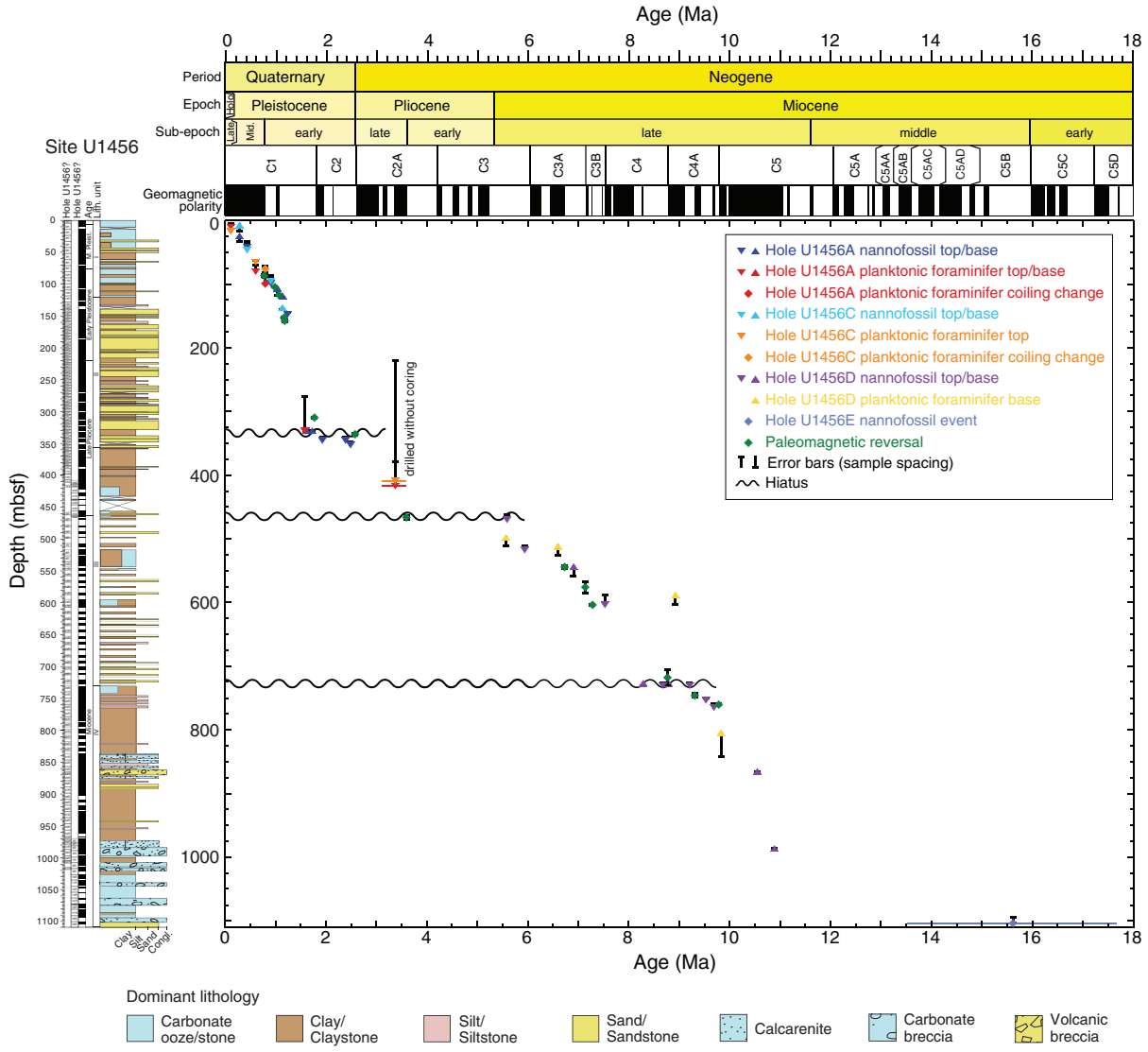

Figure F11. Lithostratigraphic and physical properties (Holes U1457A–U1457C) summary for the cored section at Site U1457. WRMSL core data (dots): green = GRA bulk density, blue = magnetic susceptibility. Red dots = core logger NGR. Black dots = discrete MAD bulk density and *P*-wave caliper (*x*-axis) on section halves. Note log scale for magnetic susceptibility.

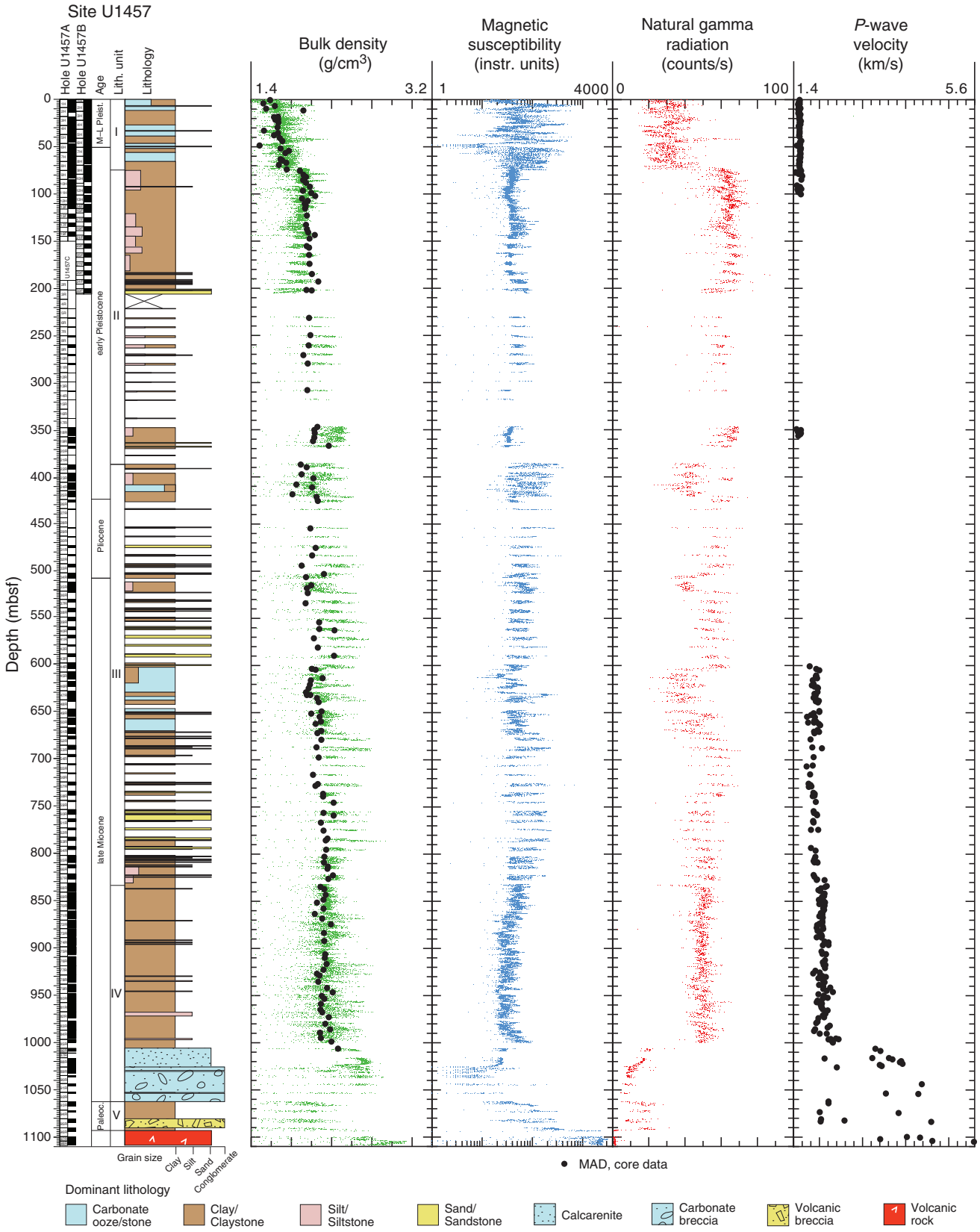

Figure F12. Age-depth model for Site U1457 created by synthesizing nannofossil and foraminifer bioevents with magnetic chron assignments. Note that the age depth model only extends to 1000 mbsf due to a long hiatus near the base of the cored section, with the top of lithologic Unit V at ~1062 mbsf dated to the early Paleocene. Top = last occurrence, base = first occurrence.

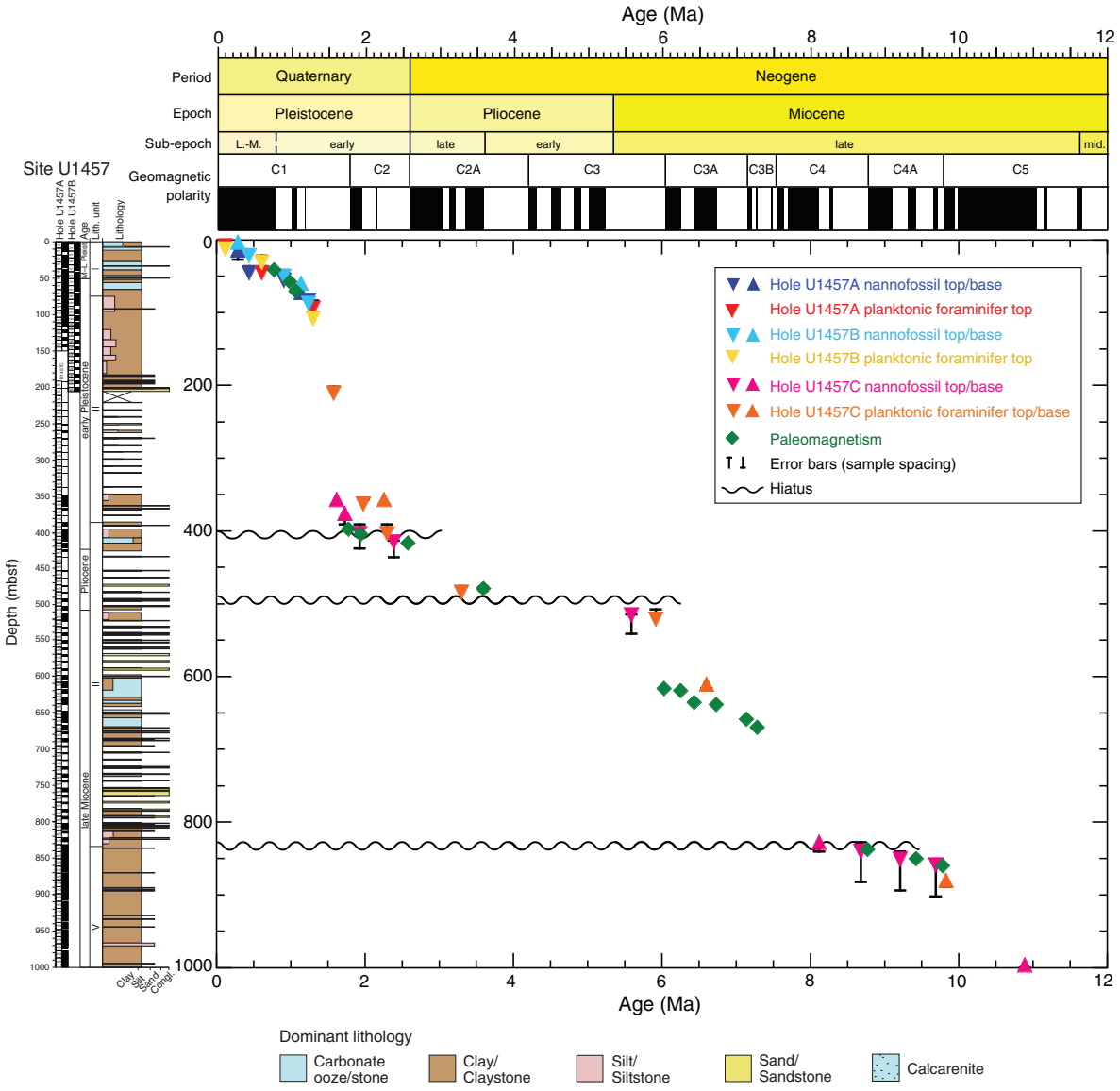

Figure F13. Heat flow map of the Arabian Sea from the compilation of GeoMapApp, together with the two new measurements derived from Expedition 355.

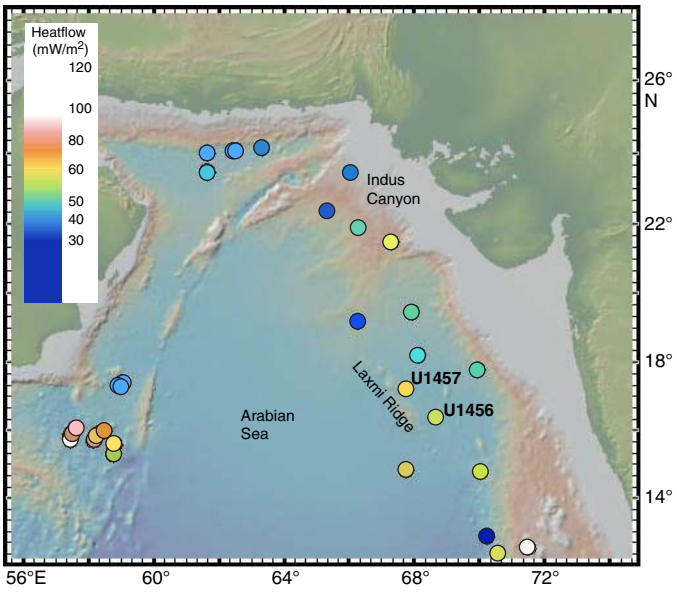

Figure F14. Close-up (left) and interpretation (right) of seismic Profile W06 showing the location of Site U1456 and the major seismic units identified. Note in particular the major cut-and-fill channels and the body of strong chaotic reflectors in the mass transport deposit (MTD) that the drill site intersects.

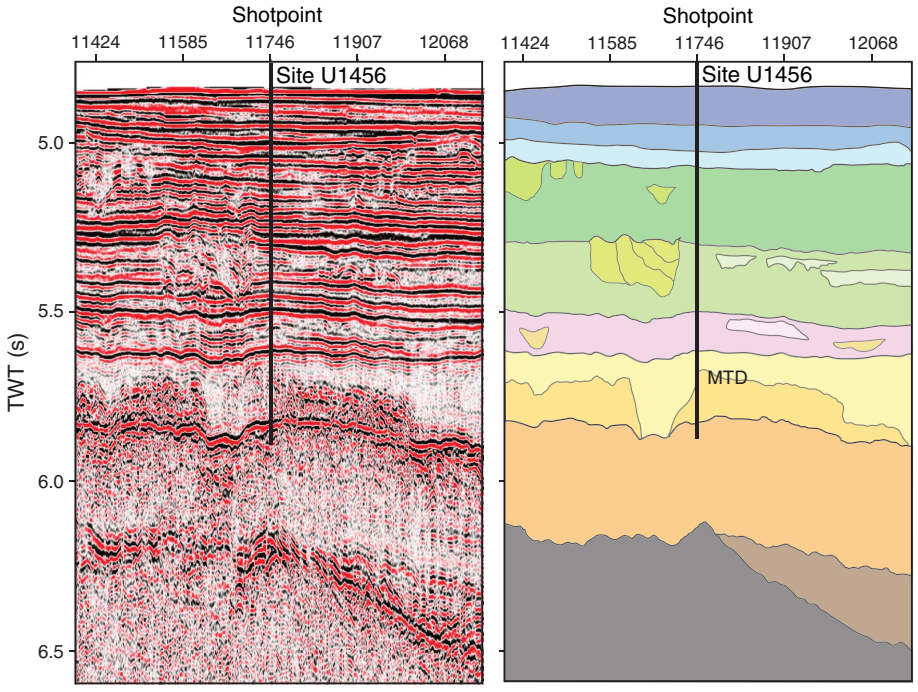

Figure F15. Close-up (left) and interpretation (right) of seismic Profile IODP-04 showing the location of Site U1457 and the major seismic units identified. Note that the mass transport deposit (MTD) is much thinner at this location compared to Site U1456. The drill site appears to cut the edge of one of the large channels in the Pleistocene section.

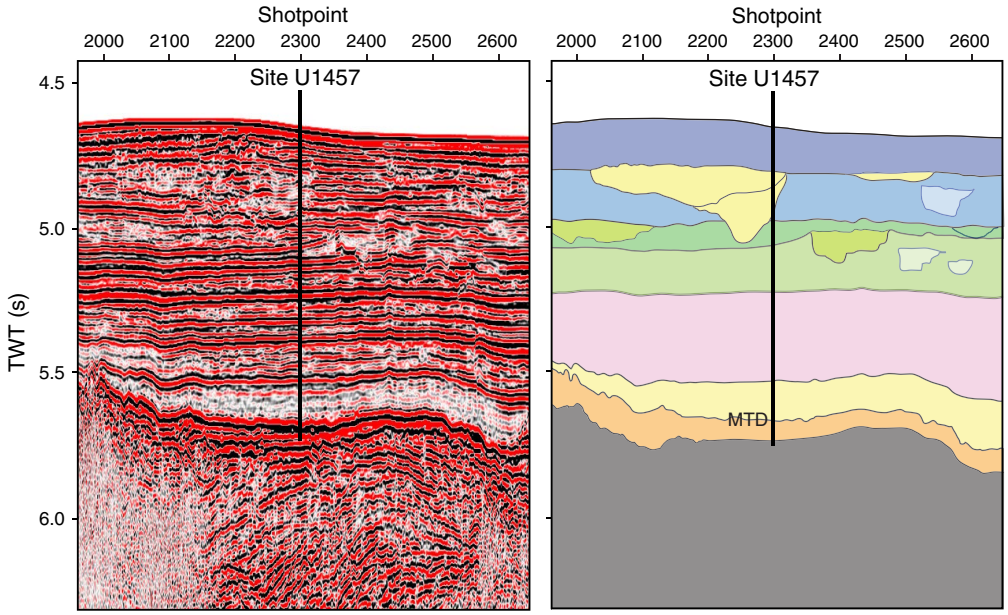

Figure F16. Heavy minerals from Site U1456. A. Augite (U1456A-11H-7A, 20 cm). B. Tourmaline (U1456A-8H-4A, 35 cm). C. Epidote (U1456A-51F-3A, 60 cm). D. Glaucophane (U1456A-50F-1A, 70 cm). E. Kyanite (U1456A-56F-1A, 30 cm). F. Hypersthene (U1456A-60F-1A, 40 cm). G. Spinel (U1456D-30R-1A, 16 cm). H. Hornblende (U1456E-19R-3A, 70 cm). Scale bars = 100 µm.